Title
THE MESON MASS RATIO AND ENERGY BALANCE IN PI-MU DECAY

Author
Birnbaum, Wallace.

Publication Date
1954-03-01

UCRL 2522

UNIVERSITY OF
CALIFORNIA

Radiation Laboratory

BERKELEY, CALIFORNIA

DISCLAIMER

UCRL-2522

UNIVERSITY OF CALIFORNIA
Radiation Laboratory
Contract No. W-7405-eng-48

THE MESON MASS RATIO AND ENERGY BALANCE IN PI-MU DECAY

Wallace Birnbaum
(Thesis)

March, 1954

Berkeley, California

THE MESON MASS RATIO AND ENERGY BALANCE IN PI-MU DECAY

TABLE OF CONTENTS

ABSTRACT 5

I. INTRODUCTION 6

A. History and Background

1. Cosmic Rays 6
2. The Artificial Production of Mesons 8

B. The Mass-Ratio Method 10

II. THEORY OF MASS NORMALIZATION 12

III. THE PARTICLE MOMENTUM 16

A. Orbit Calculations 16

B. Effects of the Finite Size of Target and of Detector 20

IV. THE PARTICLE RANGE 23

A. Energy Loss Processes

1. Energy Loss by Radiation 23
2. Energy Loss to Nuclei 24
3. Energy Loss to Electrons 26

B. The Range-Energy Relation 26

C. Range Straggling 27

1. Bohr Straggling 27
2. Heterogeneity Straggling. 29
3. Effect of Finite Grain Spacing and Grain Size. . . 30
4. Effect of Shrinkage Factor. 30

D. The Normalized Range Distribution Function. 32

V. STATISTICAL CALCULATION OF MASS RATIOS 34

VI. THE DYNAMICS OF PION-MUON DECAY 38
A. Absolute Meson Masses and Related Quantities. 38
B. The Absolute Muon Decay Momentum 40

VII. EXPERIMENTAL TECHNIQUES 44
A. Geometrical Arrangement
1. Exposures within the Cyclotron 44
2. Target and Detector Assembly. 45
B. Photographic Development Procedures 48
C. Microscope Scanning Procedures 48
D. Magnetic Measurements. 50

VIII. ANALYSIS OF EXPERIMENTAL DATA 53
A. Range Straggling of Mu-Completes 53
B. The Normalized Range Distribution Functions, Rp^{-q} . . 54
C. Derived Experimental Values
1. The Pi-Mu Mass Ratio 57
2. The Absolute Decay Momentum of the Muon . . . 58
3. The Pi-Mu Mass Difference 59
4. The Masses of the Positive Pion and Muon 59
5. The Absolute Kinetic Energy of the Muon. 59
6. The Mass of the Neutrino. 60

IX. CONCLUSIONS 61

APPENDICES 62
A. Correction for the Motion of a Particle out of the Median Plane of the Magnetic Field 62
B. Effects of the Finite Size of the Target and of the Detector in the Momentum Calculation 64
C. Statistical Calculation of the Mass Ratio 69
D. Dynamics of π-μ Decay 75
E. Correction to the Mean Range of the Mu-Completes 79
F. The Propagation of Errors 82

ACKNOWLEDGMENTS 91

TABLES 92

FIGURES 112

REFERENCES 132

THE MESON MASS RATIO AND ENERGY BALANCE IN PI-MU DECAY

Wallace Birnbaum
(Thesis)
Radiation Laboratory, Department of Physics
University of California, Berkeley, California

ABSTRACT

The mass-normalization method of measuring meson masses is extended to a determination of the positive pion-muon mass ratio. Ranges and momenta of the comparison particles produced in the 184-inch cyclotron are measured, employing the nuclear emulsion technique.

The different energy-loss processes in nuclear emulsion are considered, and various range-straggling effects are evaluated and studied experimentally.

The energetics of the $\pi \rightarrow \mu + \nu$ decay scheme are also studied in detail. From precise determinations of the absolute decay momentum p_o of the muon and the π/μ mass ratio, various meson mass and related experimental values are obtained: $m_{\pi^+}/m_{\mu^+} = 1.321 \pm 0.002$; $p_o = 29.80 \pm 0.07$ Mev/c; a new probable upper limit to the mass, m_ν, of the neutral decay particle of ≈ 6 to $7\ m_o$; and a muon center-of-mass kinetic energy of 4.12 ± 0.02 Mev. With the positive-pion mass value found by Smith, the m_{π^+}/m_{μ^+} ratio yields $m_{\mu^+} = 206.9 \pm 0.4\ m_o$. The following values in parenthesis are insensitive to m_ν and have been determined assuming $m_\nu = o$: $m_{\pi^+} - m_{\mu^+} = (66.41 \pm 0.07\ m_o)$; $m_{\mu^+} = (206.9 \pm 0.2\ m_o)$ from the Smith pion value and the mass difference reported here; $m_{\pi^+} = (273.5 \pm 1.2\ m_o)$ and $m_{\mu^+} = (207.1 \pm 1.1\ m_o)$ derived solely from the pion-muon mass ratio and mass difference.

A summary of many of the important pion and muon mass determinations by other researchers is compiled and presented for comparison.

THE MESON MASS RATIO AND ENERGY BALANCE IN PI-MU DECAY

Wallace Birnbaum
(Thesis)
Radiation Laboratory, Department of Physics
University of California, Berkeley, California

March, 1954

I. INTRODUCTION

A. History and Background

1. Cosmic Rays

The scalar meson field theory was introduced by Yukawa[1] in 1935 in an attempt to explain the nature of nuclear forces. The usual inverse-square Couloumb forces are repulsive and could not account for nuclear stabilities. Furthermore, it was known from accurate mass determinations that the binding energy per nucleon within nuclei did not vary greatly as a function of mass number. This saturation property indicated the short-range character of the nuclear force field. Developing his theory in a procedure analogous to that of the quantization of the electromagnetic field, Yukawa predicted that a quantum of finite rest mass might exist. This particle, later to be termed a "meson," then would play a role in the theory of nuclear forces similar to that of the zero-rest-mass photon in the electromagnetic theory. The range of nuclear forces, λ, could then be identified with the Compton wave length of this meson of mass m:

$$\lambda = \frac{\hbar}{mc} \quad . \tag{1}$$

This gave a value for the rest mass of this new quantum of approximately 200 electron masses, depending upon the value chosen for the range of nuclear forces.

Early absorption experiments with cosmic rays indicated the possibility that they might contain particles of mass intermediate between those of the electron and the proton. In 1937, direct experimental proof of the existence of the meson was obtained by Neddermeyer and Anderson,[2] and independently by Street and Stevenson,[3] from cloud chamber measurements of momentum, momentum loss, and specific ionization. Soon thereafter, other experimenters[4, 5, 6] were reporting mass values of this

penetrating component of cosmic rays. The values obtained appeared to be centered about 200 m_o (electron masses), with fairly wide fluctuations due to the preliminary nature of the experiments.

Shortly after the war Fretter,[7] utilizing a cloud chamber technique and employing momentum-range relations,[6] obtained the first of the more accurate mass determinations. Brode and co-workers[8-11] further developed and refined this method, producing a series of mass measurements. Their values, and those obtained from the subsequent cosmic-ray experiments to be surveyed briefly in this introduction, are listed in Table I.

Although Yukawa's prediction of the existence of a particle of intermediate mass seemed to have been substantiated, a serious difficulty arose as to its exact relation to nuclear forces. Indeed, if one expected these mesons to be the quanta of the nuclear field, strong meson interactions with nuclei should have been observed. However, the experiment of Conversi et al.[12] gave strong indication that the cross sections for these mesons were of the order of 10^{12} times too small to account for nuclear forces.

In an attempt to resolve this paradox, it was suggested that there might be two types of mesons, one of which would be strongly interacting with nuclei.[13, 14, 15] Shortly thereafter, Lattes et al.[16] provided experimental evidence for the existence of two species. It was found that approximately 10% of the mesons that came to rest within nuclear emulsions exposed at high altitudes decayed into another kind of meson of lighter mass. The mesons were identified by the grain densities and deviations in the tracks caused by multiple Couloumb scattering. The ranges of these secondary particles appeared to be constant except for the usual range straggling, indicating a two-body decay process, the other secondary being of neutral charge. Furthermore, it was observed that some of the heavier mesons, upon reaching the ends of their ranges, produced nuclear disintegrations with the emission of heavy particles such as protons and alphas.

Lattes et al.[16] suggested that the heavier mesons (now called π-mesons or pions) were to be associated with nuclear forces. Within the emulsion, positive pions -- unable to interact with nuclei at low velocities because of repulsion of like charges -- decay into secondary lighter mesons (μ-mesons or muons). On the other hand, there is high probability that the negative pions will be captured before decay, giving rise to the observed

nuclear disintegrations. The pions were presumed to have been created in the upper atmosphere. Because of their short mean lifetime ($\sim 2.5 \times 10^{-8}$ sec), most of these pions decay in flight before reaching sea level, thus the mesons that had for some time been known to be associated with the penetrating component of cosmic rays can be accounted for.

Lattes et al.[17] made the first measurements of the mass of the π-meson by the correlation of grain density with residual range, obtaining a value for the ratio m_π/m_μ.

Subsequent mass determinations with cosmic rays,[18] using relations of scattering angle vs. range, grain density vs. range, momentum vs. range, and grain density vs. scattering angle, are tabulated in Table I.

2. The Artificial Production of Mesons

With the availability of high-energy accelerators as a means for producing mesons,[19] controlled experiments with higher meson intensities have yielded better values for the meson masses.

The Film Program group at University of California Radiation Laboratory have been the pioneers in the "direct" measurement of the masses of the artificially produced pions and muons. The early experiments of Gardner, Lattes, and Barkas and collaborators[19-22] applied a method similar in principle to the cosmic-ray experiments of Brode and his group. The mass of the meson was evaluated by the simultaneous measurement of the momentum of the particle, as determined by its magnetic rigidity $H\rho$ in the magnetic field of the 184-inch cyclotron, and its range in the nuclear-emulsion detector. The detailed discussion of the range-momentum relation employed in their work is discussed more fully in a later section. The results of these experiments, as well as of other mass determinations using artificial sources, are listed in Table II. This emulsion technique is limited to positive and negative pions and to positive muons, owing to the high probability of capture of negative pions before decay.

Lederman et al.[23] obtained the negative pion-muon mass difference by studying the decay in flight of the π^- in a cloud chamber with an associated magnetic field. Determination of the momenta of the two particles and the angle between the trajectories gives the desired mass difference upon application of the relativisitic energy and momentum equations.

Parallel to the development of the so-called direct measurements of meson masses, certain indirect methods have also yielded accurate values. These methods for the most part employ the conservation laws in reactions involving either the creation or the decay of the several types of mesons.

Panofsky et al.,[24] and later Crowe,[25] have analyzed the gamma-ray spectra associated with the π^- capture in hydrogen. This work has yielded a very accurate determination of the mass. Use has been made of the following reactions:

$$\pi^- + p \rightarrow n^* \rightarrow n + \gamma,$$
$$\pi^- + p \rightarrow \pi^o + n \rightarrow 2\gamma + n. \qquad (1.2)$$

The mass difference between the negative and neutral pions has been calculated from the Doppler-shift spectrum originating from the decay of the π^o into two gammas of $\approx$ 70 Mev each. Carlson et al.,[26] using cosmic rays, have performed a similar analysis in deriving a value for the neutral pion.

The mass of the positive muon has been calculated from the value of the end point of the positron energy spectrum arising from its natural decay,[27-32]

$$\mu^+ \rightarrow e^+ + 2\nu \quad .$$

However, the breadth of the various experimental resolution curves introduced a fair amount of uncertainty in the determinations of the maximum positron energy.

Cartwright[33] and Peterson et al.[34] independently have investigated the proton-proton production of π^+-mesons with the nuclear-emulsion technique. Here one applies the conservation laws to the reaction,

$$p + p \rightarrow d + \pi + Q, \qquad (1.3)$$

and having measured Q from a determination of the kinetic energies of the pion and that of the incident proton, one then obtains a value for the mass of the π^+.

An experiment has recently been reported by Rainwater[35] which may yield still another independent estimate of the mass of the negative muon. This is accomplished by the determination with crystal detectors of the energies of mesonic atom x-ray transitions.

The very fact that these indirect methods have yielded masses consistent with the more direct measurements confirms the validity of the postulated processes.

At this point it may be well to summarize the basic pion-muon decay schemes as they are presumed at present to exist.

In vacuo:

$$\pi^{\pm} \rightarrow \mu^{\pm} + \nu \qquad (1.4a)$$

$$\mu^{\pm} \rightarrow e^{\pm} + 2\nu \qquad (1.4b)$$

$$\pi^{o} \rightarrow 2\gamma \qquad (1.4c)$$

$$\hookrightarrow \gamma + e^{+} + e^{-} \quad .$$

In an absorbing medium:

$$\pi^{+} \rightarrow \mu^{+} + \nu, \qquad (1.5a)$$

$$\pi^{-} + Z^{A} \rightarrow (Z-1)^{A^{*}} \text{ (excited)}, \qquad (1.5b)$$

(or) $$\pi^{-} + p \rightarrow n + \pi^{o}, \qquad (1.5c)$$

$$\mu^{\pm} \rightarrow e^{\pm} + 2\nu, \qquad (1.5d)$$

(or) $$\mu^{-} + p \rightarrow n + \nu, \qquad (1.5e)$$

where ν represents the neutrino, and n is the neutron.

B. The Mass-Ratio Method

The early experiments of the University of California Radiation Laboratory Film Group, briefly discussed above, contained several systematic uncertainties that limited the accuracy of the final results. The chief sources of possible error were the following: uncertainty in the range-energy relation for protons in emulsions; variation of the stopping power of the emulsion from plate to plate; and uncertainties in the absolute value of the cyclotron magnetic field.

Fortunately, it can be shown that certain experimentally measurable quantities can be normalized by the mass of a particle.[36] This in effect eliminates the need for absolute measurements; relative measurements are all that are required. For particles of the same charge the momentum, the energy, the range, the range variance, the reciprocal of the mean scattering angle, and the total ionization when divided by the mass become functions only of velocity. The nuclear-emulsion technique offers two more such quantities: the total number of developed grains and their "integrated emptiness."[37,38]

In the Lattes et al.[17] experiment mentioned previously, this normalizable property was employed in the comparison of the number of developed grains as a function of residual range for both the π- and μ-mesons. A mass ratio for the two particles was thereby derived. However, large systematic errors were involved. Later experiments indicate that this value was too high.

In 1949, Barkas[39] suggested the use of the proton as a comparison particle with which to determine the meson mass. The ratio of the momenta of the proton and of the meson was chosen to be equal to the ratio of the respective mean ranges of the two particles, thus requiring their velocities to be equal. Consequently, the meson-to-proton mass ratio could be calculated directly from the first two ratios. Preliminary results of the pion-proton mass matio have been published by Barkas, Smith and Gardner.[40] At this writing the final analysis of this experiment has just been completed.[41, 42] The latest mass values are quoted in Table II.

* * *

The experiment discussed in this paper is a logical extension of the "proton comparison" method. The theoretical basis of the experiment has been discussed by Barkas,[43] and we shall follow his analysis closely in subsequent sections. The positive pion and the positive muon have been chosen as comparison particles and the π/μ meson mass ratio is determined. At the same time, a critical quantitative analysis has been made of the energetics of the decay scheme. All the mass and kinetic-energy relations connected with the dynamics of the decay involve functions of the mass ratio and the center-of-mass momentum acquired by the muon at the time of its creation. This phase of the work has yielded a new value for the mass difference between positive pion-and-muon, and a new estimate of the upper limit of the mass of the neutral particle (presumably a neutrino) that is involved in the two-body decay.[44]

II. THEORY OF MASS NORMALIZATION

As a particle at low energy passes through matter, it loses energy principally by the excitation and ionization of the absorber atoms. Losses due to other interactions such as bremsstrahlung and nuclear collisions may be neglected, as is shown later. The theory of energy loss by a particle of mass much greater than that of the electron, aside from very small corrections, leads to the expression[45]

$$-\frac{dT}{dx} = \frac{4\pi e^4 z^2 N}{m_o v^2} Z\left[\left\{\ln \frac{2m_o v^2}{I} - \ln (1-\beta^2) - \beta^2\right\} - C_k\right] \qquad (2.1)$$

where $\frac{dT}{dx}$ is the kinetic energy loss per unit distance traversed, ze is the electric charge of the incident particle, m_o is the electron mass, v is the velocity of the particle, N is the number of atoms of stopping material per unit volume, I is the effective ionization potential of the stopping material, Z is the atomic number of the absorber, $\beta = v/c$ where c is the velocity of light, and C_k is a correction term for low velocities depending only upon v and the particular absorbing medium.

Equation (2.1) can then be written in the functional manner

$$\frac{dT}{dx} = z^2 f(\beta), \qquad (2.2)$$

where $f(\beta)$ is a function only of velocity.

Since the kinetic energy T is equal to the mass m of the incident particle times a function of velocity, the above expression may be integrated,

$$\frac{R}{m} = \frac{1}{z^2} g(\beta), \qquad (2.3)$$

where R is the residual range of the particle in the absorber, and $g(\beta)$ is another function dependent on the velocity.

One may now introduce the momentum p which, when divided by the mass, also becomes a function only of velocity. Therefore, we can express the relation:

$$\frac{R}{m} = \frac{1}{z^2} F\left(\frac{p}{m}\right) . \qquad (2.4)$$

In this study, the ranges and momenta of the positive pion and muon are compared. Since, to the best of our knowledge, the charges of both mesons are equal to unity,[22, 46, 47] we may drop the $\frac{1}{z^2}$ factor and write

$$\frac{R_\pi}{m_\pi} = F\left(\frac{p_\pi}{m_\pi}\right) ; \frac{R_\mu}{m_\mu} = F\left(\frac{p_\mu}{m_\mu}\right) \tag{2.5}$$

Bradner et al.[48] have measured the ranges of protons of energies up to 40 Mev in Ilford C-2 nuclear emulsions, and have obtained a range-energy relation which can be expressed as a simple power law

$$T_p = KR_p^n, \tag{2.6}$$

where $K = 0.251$, $n = 0.581$, are empirically determined numbers remaining remarkably constant in the 25-to-40-Mev region, R_p is the residual range of the proton expressed in microns, and T_p is the kinetic energy expressed in Mev.

Equation (2.6) may easily be transformed to the range-momentum relation

$$R_p = Cp_p^q, \tag{2.7}$$

where $q \approx {}^2/_n$ and C is a constant.

Employing the mass-normalization properties of Eq. (2.5), one can write, in the case of equal velocities,

$$\frac{R_\pi}{R_p} = \frac{m_\pi}{m_p} = \frac{p_\pi}{p_p} ; \frac{R_\mu}{R_p} = \frac{m_\mu}{m_p} = \frac{p_\mu}{p_p} . \tag{2.8}$$

Hence, one obtains

$$R_\pi = C\left(\frac{m_\pi}{m_p}\right)^{q-1} p_\pi^q ; R_\mu = C\left(\frac{m_\mu}{m_p}\right)^{q-1} p_\mu^q . \tag{2.9}$$

Dividing,

$$\frac{R_\pi}{R_\mu} = \left(\frac{m_\mu}{m_\pi}\right)^{q-1} \left(\frac{p_\pi}{p_\mu}\right)^q \quad . \tag{2.10}$$

Or, solving for the mass ratio,

$$\frac{m_\pi}{m_\mu} = \left(\frac{R_\pi}{R_\mu}\right)^{\frac{1}{1-q}} \left(\frac{p_\pi}{p_\mu}\right)^{\frac{-q}{1-q}} \quad . \tag{2.11}$$

Two important features are to be noted. Firstly, when the ratio of the momenta is equal to the ratio of the ranges, the true m_π/m_μ mass ratio can be found regardless of the value chosen for q, since the sum of the exponents on the right-hand side of the equation is exactly equal to unity. This ideal situation is attained when the velocities of the two particles being compared are exactly equal. Because the value of the mass ratio, as a function of q, is relatively insensitive to small changes in q we can apply the method of "successive approximations."* The momenta of the two particles selected for study were chosen to give approximately equal velocities based upon the best previous experimental estimate of the value of the mass ratio. Theoretically, one could repeat this procedure several times, each successive analysis converging closer to the condition of equal velocities. In this experiment, the initial momentum intervals chosen were such that the uncertainty in the value of q had an essentially negligible effect in the final determination of the mass ratio. Hence, further narrowing of the momentum intervals was unnecessary. This is shown in a later section. The mass-ratio method is then limited principally by the inherent range straggling of the particles in the absorbing medium.

Secondly, in Eq. (2.11) one has an expression in which only ratios of ranges and momenta appear. The ranges of the two types of mesons were measured in the same body of nuclear emulsion and their momenta were measured in the same magnetic field. Neither the absolute intensity of the magnetic field nor the absolute stopping power of the emulsion then entered into the calculation of the mass ratio.

---

* The application of the concept of "successive approximations" to this study was first suggested by E. Gardner.[49]

Equation (2.11) may be rewritten in the following manner:

$$\frac{m_\pi}{m_\mu}^{1-q} = \frac{R_\pi p_\pi^{-q}}{R_\mu p_\mu^{-q}} \quad . \tag{2.12}$$

For the statistical treatment of the data, we chose to study the distributions of the quantity R_p^{-q}. Experimental conditions attained were such that this quantity had an essentially normal distribution with calculable moments about the mean value.

III. THE PARTICLE MOMENTUM

A. Orbit Calculations

The dynamical problem of the motion of a charged particle moving through an axially symmetric nonuniform magnetic field has been treated by Barkas.[50,43] We shall follow his general solution for the equations of motion and apply it to our more specific case.

In this situation we used nuclear emulsions to detect the particles emitted from a thin target bombarded by the internal proton beam of the cyclotron. The position with respect to the target of the entrance point of the meson at the surface of the nuclear plate and the projected angle of entrance of the meson could then be determined easily at a later time. This entrance angle will later be referred to as θ. Accordingly, if the shape of the relative magnetic field intensity as a function of cyclotron radius is known, one can calculate the relative momenta of the two comparison particles.

The motion of the meson is best described by use of the cylindrical coordinates r, ϕ, z coaxial with the field of the cyclotron. The problem of median-plane orbit will be treated first. In this case, H is a function only of the radius r, the radial distance from the center of the cyclotron. Empirical measurements have shown that an assumption of axial symmetry is valid over the small region of the magnetic field used to define our meson trajectories. In the median plane of this slowly varying nonuniform field, the mesons with small momentum described trochoidal paths[51] as shown in Fig. 1, reaching minimum and maximum radii of R_1 and R_2, respectively (the libration limits). We define (r_1, ϕ_1) to be at the target, and (r_2, ϕ_2) to be at the point of detection. The Lagrangian of the particle motion is

$$L = -mc^2\left(1 - \frac{\dot{r}^2 + r^2\dot{\phi}^2}{c^2}\right)^{1/2} + \frac{e}{c}\dot{\phi}\int_0^r rH(r)\,dr \qquad (3.1)$$

where $r^2 + r^2\dot{\phi}^2 = \beta^2c^2$ is a constant of the motion.

Since ϕ is a cyclic or ignorable coordinate, $\frac{d}{dt}\left(\frac{\partial L}{\partial \dot{\phi}}\right) = 0$, and

$$\frac{mr^2\dot{\phi}}{(1-\beta^2)^{1/2}} + \frac{e}{c}\int_{r_1}^r rH\,dr \qquad (3.2)$$

is also a constant of the motion. If we further define $\tan\lambda \equiv \frac{1}{r}\frac{dr}{d\phi}$, and let

the momentum, $m\beta c\,(1-\beta^2)^{-1/2}\left(=\frac{eH\rho}{c}\right)$, be expressed as eK/c, we obtain for the median plane

$$K=\frac{\int_{r_1}^{r_2} rH\,dr}{r_1\cos\lambda_1 - r_2\cos\lambda_2}, \tag{3.3}$$

where the point of detection lies on the orbit.

In the above equation, the angle λ_1 represents the angle of emission of the particle from the target, and thus it is not directly measurable. All other parameters are observable, thereby reducing the problem to an analytic determination of λ_1.

The equation of the orbit is

$$\phi = \int_{R_1}^{r} \frac{\cot\lambda}{r}\,dr \quad . \tag{3.4}$$

The integration is carried out by the introduction of the parameter τ, given by

$$\cos\tau = \frac{R_2^2 + R_1^2 - 2r^2}{R_2^2 - R_1^2} \quad . \tag{3.5}$$

The integrated form of the orbit becomes

$$\phi = \arcsin\left(\frac{\rho_o \sin\tau}{r}\right) + a_o\tau + \sum_{n=1}^{\infty} a_n \sin n\tau, \tag{3.6}$$

where the a_n and ρ_o are defined below.

The cyclotron magnetic field may be expanded in powers of r. From the integrated form of Maxwell's equations, it is easily shown that such an expansion is represented by an even polynomial:

$$H(r) = H_o\left(1 + h_o + h_2 r^2 + h_4 r^4 + \cdots h_{2n} r^{2n} + \cdots\right) \quad . \tag{3.7}$$

Therefore

$$\frac{H(r) - H_o}{H_o} = h_o + h_2 r^2 + h_4 r^4 + \cdots h_{2n} r^{2n} \equiv h(r) \quad . \tag{3.8}$$

When $H_o = \frac{2}{R_2^2 - R_1^2}\int_{R_1}^{R_2} rH(r)\,dr$, we have $\int_{R_1}^{R_2} rh(r)\,dr = 0$.

Now, let us define $\rho_o \equiv \frac{R_2 - R_1}{2}$; $H_o\rho_o \equiv K$, and $R \equiv \frac{R_1 + R_2}{2}$.

The various a_n may now be evaluated in terms of the quantities ρ_o, R and the h_{2n}. For example:

$$a_o = \rho_o^2 \left[h_2 + 2h_4 (R^2 + \rho_o^2) + 3h_6 (R^4 + 3R^2 \rho_o^2 + \rho_o^4) \right. \qquad (3.9)$$
$$\left. - 3\rho_o^2 h_2^2 - h_2 h_4 (7R^2\rho o^2 + 6\rho_o^4) + \text{---} \right]$$

Equation (3.6) describes the trochoidal path of the particle as the sum of three terms. The first simply represents a circle; the second superimposes a precession around the axis of symmetry; and the third is a Fourier sum which adds an harmonic perturbation to the precessing orbit. As shown in Fig. (1), the orbit is periodically tangent to the libration circles of radii R_1 and R_2.

In our experiment, the mesons accepted by the momentum-defining channel underwent approximately 180^o bending. As illustrated in Fig. (1), this represents the situation where $\phi_1 = \phi_2 \approx 0$. In this case, a simple geometrical analysis shows that

$$\lambda_1 \approx \frac{R\tau_1}{r_1} , \quad \pi - \lambda_2 \approx \frac{R\left(\pi - \tau_2\right)}{r_2}, \qquad (3.10)$$

where τ_1 is the value of τ at the target position, and τ_2 is at the detection point. If the magnetic field were uniform, λ_1 would be equal to $\pi - \lambda_2$ when $\phi_1 = \phi_2$. Because of the nonuniformity, we define the small correction angle λ_o, such that $\lambda_1 = \pi - \lambda_2 + \lambda_o$. For the 180^o trajectory, $\lambda_1 = \lambda_o \approx \frac{R\tau_1}{r_1}$ From the integrated orbit Eq.(3.6) $\lambda_o \approx R\rho_o \pi h_2$.

Finally, therefore,

$$\lambda_o \approx \frac{\pi}{2} \frac{H(r_2) - H(r_1)}{H(r_2) + H(r_1)} \qquad (3.11)$$

Substituting, we obtain

$$K = \frac{\int_{r_1}^{r_2} rH\, dr}{r_1 \cos(\pi - \lambda_2 + \lambda_o) + r_2 \cos(\pi - \lambda_2)} \qquad (3.12)$$

In Eq. (3.12) all quantities necessary for the determination of the momentum are measurable. Bending of 180^{o} enables one to measure momenta with the minimum error, for if $\lambda_2 \approx \pi$ and $\lambda_1 \approx 0$, the calculated value of K becomes quite insensitive to the observed angle λ_2.

To further simplify the momentum calculation, rectangular coordinates are introduced with the x-axis along a radial line of the cyclotron, and the z-axis parallel to the direction of the magnetic field. In the experimental setup, the center of the target and the center of the detector plate were made to lie in the x-z plane. One measures the angle θ, which is the angle to the y-axis in the xy plane at which the orbit enters the emulsion. The x and y coordinates (x', y') at this point are also recorded. The trajectory is now extended mathematically so that it crosses the x-axis at the point $x = x_o$ at an angle θ' with respect to the y-axis. Since the magnetic field is nearly uniform in this region, the extrapolation of the orbit is accomplished by assuming that this very small increment of the total trajectory is circular. The error introduced by this mathematical assumption is completely negligible, since the calculation of the momentum up to the point $x = x'$, $y = y'$ takes into account the slow variation of the magnetic field. Figure 3 shows the simple geometrical relation between θ and θ', and x_o as a function of (x', y', θ). Furthermore, θ' is defined so that it is positive when the orbit has not yet reached the outer libration limit, R_2, and negative beyond that point. The entire apparatus was placed in the slowly varying region of the field. Consequently λ_o is quite small ($\lambda_o = 10'$) and may be neglected in the calculation.

For a particle starting at the center of the target with its orbit confined to the median plane, we finally arrive at the expression:

$$K = \frac{\sec \theta' \int_{r_1}^{r_1 + x_o} rH\, dr}{2r_1 + x_o} \quad . \tag{3.13}$$

In Eq. (3.13), r_1 is the radial distance from the center of the cyclotron to the center of the target. If the actual orbit for a particle leaving the center of the target is inclined at the nominal angle of γ_o with the median or xy-plane, the total momentum becomes

$$p = \frac{eK}{c} \sec \gamma_o = \frac{e}{c} \sec \gamma_o \sec \theta' \frac{\int_{r_1}^{r_1 + x_o} rH\, dr}{2r_1 + x_o} \tag{3.14}$$

For convenience, the quantity

$$\sec \gamma_o \int_{r_1}^{r_1 + x_o} rH\, dr \quad (\equiv A \sec \gamma_o)$$

was numerically integrated (Tables III and IV) and plotted graphically (Fig. 4) as a function of x_o. To a high degree of approximation a straight line could be fitted to represent this function, somewhat simplifying the lengthy momentum calculations.

It is important to examine the validity of the use of the factor $\sec \gamma_o$ in Eq. (3.14). We have assumed that the z-component of the velocity is small, and the composition of it with the median-plane velocity can be accomplished by multiplying by a constant $\sec \gamma_o$. However, it must be shown that the z-component remains essentially constant over the entire orbit.

In Appendix A, the following relation is derived:

$$\left|\frac{\Delta \dot{z}}{\dot{z}_1}\right| \approx \left(\pi/2 - 1\right) \rho_o\, n/R, \tag{3.15}$$

where $\Delta \dot{z}$ is the maximum change in the velocity in the vertical direction, $\dot{z}_1$ is the initial velocity at the target point, and $n = -\frac{r}{H}\frac{\partial H_z}{\partial r}$. In this experiment, $\rho_o/R \approx \frac{1}{20}$ and $n \approx 0.07$. The maximum relative change in the component of the velocity parallel to the z-axis is $\approx 2.0 \times 10^{-3}$. Consequently, the two velocity components may be treated as independent of each other, and therefore the use of the $\sec \gamma_o$ factor in Eq. (3.14) seems justified.

B. Effects of Finite Size of Target and of Detector

Employing Eq. (3.14), we calculate the apparent momentum of a particle, assuming that it came from the center of the target and that its orbit crossed the xz plane at a definite value $z = z_o$ with $\gamma = \gamma_o$. In actuality, however, the target used in this particular study was in the shape of a rectangular parallelopiped of dimensions 2a, 2b, and 2c in the x, y, and z directions, respectively. Furthermore, the area of the nuclear emulsion scanned under the microscope was obviously finite, being distributed symmetrically about the x-axis. Mesons were accepted for measurement if

θ' lay within a certain angular interval centered about $\theta' = 0$. Consequently, particles with a distribution of true momenta p_1 contribute to the group with apparent momentum p. We must study the distribution function $U(p_1, p)$, which gives the probability $U(p_1, p)\, dp_1$ that the true momentum lies between p_1 and $p_1 + dp_1$ when the apparent momentum is p. It is important in the general analysis of these "finite effects" to calculate

$$\langle p_1{}^{\eta} \rangle = \int p_1{}^{\eta}\, U(p_1, p)\, dp_1 \equiv p^{\eta}(1 + \omega_{\eta}) \quad . \tag{3.16}$$

It is desirable to keep ω_{η} as small as possible, and yet maintain adequate statistics.

The evaluation of ω_{η} is carried out in detail in Appendix B. The origin of our rectangular coordinate system is placed at the target center. The detector plate, which in the experiment was inclined at a slight angle with respect to the xy plane, is assumed to lie in the plane $z = -z_o - \epsilon y'$, with $x_o \gg z_o$, and $\epsilon \ll 1$.

The orbit is assumed to begin at some point (x, y, z) and to cross the x-axis at $x = x_o$, making an angle θ' with the y-axis. The particle is observed to enter the emulsion at the point (x', y') in the xy-plane. We also define $x > o$ in the direction of increasing cyclotron radius.

Expanding to the third order of small quantities, we obtain:

$$\omega_{\eta} = -\eta \frac{\langle x \rangle}{x_o} + \eta \frac{(\eta - 1)\langle x^2 \rangle}{2x_o^2} + \frac{\eta \langle yz \rangle}{x_o^2} + \eta \frac{\langle y\theta' \rangle}{x_o}$$

$$+ \frac{4\eta z_o}{\pi^2} \frac{\langle z \rangle}{x_o^2} + \frac{2\eta \langle z^2 \rangle}{\pi^2 x_o^2} + \frac{8\eta \langle (z_o + z)^2 (\theta' + y/x_o + y'/x_o) \rangle}{\pi^3 x_o^2}$$

$$+ \frac{4\eta z_o^2 \langle x \rangle}{\pi^2 x_o^3} - \frac{\eta(\eta - 1)\langle xy\theta' \rangle}{x_o^2} + \frac{4\eta z_o \epsilon \langle y' \rangle}{\pi^2 x_o^2}$$

$$+\frac{4\eta\,\epsilon\langle y'z\rangle}{\pi^2 x_o^2}-\frac{\eta(\eta-2)\langle xy^2\rangle}{x_o^3}-\frac{2\eta(\eta-2)\langle xz^2\rangle}{\pi^2 x_o^3}$$

$$-\frac{4\eta(\eta-2)z_o\langle xz\rangle}{\pi^2 x_o^3}-\frac{\eta(\eta-1)(\eta-2)\langle x^3\rangle}{6\,x_o^3}\,. \qquad (3.17)$$

The distributions of θ' and y' are observed directly, whereas the distributions of x, y, and z must be inferred from the geometry of the target. The momentum interval chosen for the μ-mesons coming from the target lay close to the full center-of-mass momentum for π-μ decay. All these selected muons are therefore assumed to have come from the decay of the pions that stopped in a very thin layer on the surface of the target. Consequently no positive values of θ' can be associated with the target surface $x = -a$, and no negative values with the surface $x = +a$. One actually observes a number N^+ with θ' positive and a number N^- with θ' negative.

For the case of the pions it is assumed that the orbits started with equal probability from anywhere in the target. The low-energy π-meson spectrum is fairly well described by stating that the number of mesons per unit range interval is approximately constant. Hence, energy losses within the target have little effect upon the apparent distribution of the starting points of the orbits. The uniform irradiation of the target is discussed in Sec. VIIA. Table V lists the various mean values required for the evaluation of ω_η. In general these finite target corrections proved to be comparatively small.

IV. THE PARTICLE RANGE

A. Energy Loss Processes

We wish to examine more closely the various processes by which charged particles lose energy during passage through matter. As mentioned previously [Eq. (2.1)], the predominant cause of energy loss is collisions with electrons (ionization). We shall discuss this effect as well as those energy losses associated with radiation and nuclear collisions.

1. Energy Loss by Radiation

As is well known, this is a most important effect at high energies. However, at the lower energies, radiation losses become quite negligible. The rate at which energy is radiated by a nonrelativistic particle of charge e, traveling through the emulsion, is:[52]

$$\left(\frac{dT}{dx}\right)_R = \frac{16}{3}\,\frac{e^2}{\hbar c}\left(\frac{e^2}{m_o c^2}\right)^2 \frac{m_o}{m} \sum_i N_i Z_i^2 \quad (\text{in } m_o c^2/\text{cm}) \tag{4.1}$$

where m is the mass of the particle, m_o the electron mass, N_i is the number of nuclei of atomic number Z_i per c.c. in the emulsion, $e^2/m_o c^2$ is the classical electron radius. Table VI lists the composition of the Ilford C-2 nuclear-track emulsion employed in the experiment. Placing the proper numerical values in the equation, one obtains

$$\left(\frac{dT}{dx}\right)_R \approx \frac{6.05 \times 10^{-2}}{m} \quad \text{Mev/cm} \,. \tag{4.2}$$

For a π-meson of $T \approx 5.2$ Mev with a range of ≈ 780 microns, or for a μ-meson of the same velocity, the energy lost by radiation in coming to rest is only $\approx 1.5 \times 10^{-5}$ Mev. At the lowest velocities, the Born approximation employed in the derivation of Eq. (4.1) no longer applies. The order of magnitude of the energy loss is not affected by the more exact calculations, however.

2. Energy Loss to Nuclei

In a manner similar to that employed in the development of the familiar ionization-loss formula Eq. (2.1) one may, by a classical description, obtain a relation estimating the energy loss due to transfer of momentum to nuclei. For a nonrelativistic particle of charge e traversing a distance ΔR through the emulsion, one has

$$\left(\frac{\Delta T}{\Delta R}\right)_n = \frac{4\pi e^4}{\beta^2 c^2} \Delta R \sum \frac{N_i Z_i^2}{M_i} \ln \frac{b_i}{a_i} \tag{4.3}$$

where N_i is the number of atoms per cc having atomic number Z_i and mass M_i in the emulsion, and b_i and a_i are the maximum and minimum impact parameters, respectively, of the i^{th} type of nucleus in the stopping material.[53]

The mean-square angle of scattering[53] due to the interaction of charged particles with the Couloumb fields of nuclei is given by (neglecting single large-angle scatters):

$$\langle \phi^2 \rangle = \frac{8\pi e^4}{m^2 c^4 \beta^4} \Delta R \sum_i N_i Z_i^2 \ln \frac{b_i}{a_i} \tag{4.4}$$

with $\langle \phi^2 \rangle$ in the units of (radians)^2. This scattering angle is observable, whereas the actual energy loss to nuclei is difficult to measure directly. The energy loss to nuclei may be related to the multiple Couloumb scattering by combining the last two equations. For convenience, one can define an effective mass $\overline{M}$, as follows:

$$\frac{1}{\overline{M}} = \frac{\sum_i \frac{N_i Z_i^2}{M_i} \ln \frac{a_i}{b_i}}{\sum_i N_i Z_i^2 \ln \frac{a_i}{b_i}} \approx \frac{\sum \frac{N_i Z_i^2}{M_i}}{\sum N_i Z_i^2} \tag{4.5}$$

Referring to Table VI one obtains $\overline{M} \approx 75\ M_p$ where M_p is the proton mass. Therefore, from Eqs. (4.3) and (4.4),

$$\frac{(\Delta T)_n}{T} \approx \frac{m}{\overline{M}} \langle \phi^2 \rangle \approx \frac{m}{75\ M_p} \langle \phi^2 \rangle \quad . \tag{4.6}$$

In order to evaluate this effect, one can employ the empirical quantity, $\langle a \rangle$, which is the mean projected angle between successive chords. From scattering experiments in emulsions,[54] then:

$$\langle a \rangle \approx \frac{25}{p\beta c} \left(\frac{\Delta R}{100} \right)^{1/2} , \tag{4.7}$$

with a in degrees, ΔR in microns, and $p\beta c$ in Mev. In the Gaussian approximation, it is easily shown that

$$\langle \phi^2 \rangle = \frac{3\pi}{2} \left(\frac{\pi}{180} \right)^2 \langle a \rangle^2 \quad . \tag{4.8}$$

Combining Eqs. (4.6) and (4.8), assuming the nonrelativistic approximation, we finally obtain

$$(\Delta T)_n \approx \frac{6.4 \times 10^{-8}}{\beta^2} \Delta R \quad \text{Mev} \quad . \tag{4.9}$$

We now have an expression for the energy loss to nuclei that is dependent only on velocity, preserving the form of Eq. (2.1). The very few tracks that appeared to suffer large-angle scattering were excluded from the final measurements.

Examination of Eq. (4.9) indicates that the actual energy loss in this type of process is certainly negligible. Assuming $T \approx \frac{469\ m\beta^2}{M_p}$, and employing the range-energy relation for protons in emulsion, $T = .25\ R^{.58}$, we obtain

$$(\Delta T)_n \approx 1.2 \times 10^{-4} \left(\frac{R}{m/M_p} \right)^{-.58} \Delta R \quad \text{Mev} \quad . \tag{4.10}$$

Integrating the above equation,

$$\frac{T_n}{m/M_p} \approx 2.8 \times 10^{-4} \left(\frac{R}{m/M_p}\right)^{.42} \text{ Mev} \quad . \tag{4.11}$$

In this experiment β was chosen to be ≈ 0.26. Therefore for a π meson, T_n amounts only to $\approx 1.5 \times 10^{-3}$ Mev.

3. Energy Loss to Electrons

Since the emulsion is a composite medium, we write our expression for the mean rate of energy loss due to ionization[45] as follows:

$$-\left\langle \frac{dT}{dx} \right\rangle = \frac{4\pi}{\beta^2} \frac{e^2}{m_o c^2} \sum_i N_i Z_i \ln \frac{2 m_o c^2 \beta^2 e^{-\beta^2}}{\overline{I}\left(1 + \frac{m_o}{m}\right)^2 \left(1 - \beta\right)^2} \quad . \tag{4.12}$$

We define $\overline{I}$ by the equation

$$\ln \overline{I} = \frac{\sum_i N_i Z_i \ln I_i}{\sum_i N_i Z_i} \quad , \tag{4.13}$$

where I_i is the effective ionization potential of the i^{th} atom. If the data of Bakker and Segrè,[55] and the assumed composition of the emulsion are used, $\overline{I} = 270$ ev .

B. The Range-Energy Relation and the Value of q.

As shown in Fig. 5, a logarithmic plot of range vs. momentum for protons gives a straight line over a fairly wide momentum interval. The slope of this line is simply the value of the parameter q, $\left(= p/R \frac{dR}{dp}\right)$ in the relation $R = Cp^q$. Barkas,[43] by integrating Eq. (4.12), analyzed the variation of q in the proton energy interval 23 to 42 Mev, and has verified that q remains quite constant passing through a very broad maximum near 33.6 Mev. In this experiment, the velocity chosen for the mesons corresponded to a proton energy of about 33 to 34 Mev.

In the actual calculations, the value chosen for q was equal to 3.44±0.03.* As is shown in the final analysis, the uncertainty introduced by the small error in q has a negligible effect in the evaluation of the mass ratio.

C. Range Straggling

1. Bohr Straggling and the Lewis Effect

The energy loss of a charged particle in matter is a statistical phenomenon, because the successive collisions giving rise to discrete transfers of energy are independent events. Thus the expected range in matter for a group of monoenergetic particles exhibits a dispersion about a mean. The magnitude of this range straggling was first calculated by Bohr.[57] For a composite medium such as the nuclear emulsion, one may express his result:

$$\beta_2 = \left\langle R - \overline{R} \right\rangle^2 = 4\pi \left(\sum_i N_i Z_i \right) e^4 \int_o^T \frac{dT}{\left(dT/dR \right)^3} \quad . \qquad (4.14)$$

In this case, in which very many individual events are combined, one can show from the central-limit theorem of statistics[58] that the distribution of the stochastic variable will tend toward a Gaussian. Recently, Lewis[59] has reanalyzed the range straggling of a nonrelativistic charged particle. He has evaluated the first five moments (β_1, β_2, β_3, β_4, β_5) of the range distribution, obtaining the familiar Bohr formula for the second moment or range variance, β_2.**

---

* Since the above stopping effects were calculated, Vigneron[56] concluded from a more elaborate study of the empirical information at lower velocities that the Bakker and Segrè potentials are too low. A better fit to the semi-empirical proton range data is obtained for q = 3.46. This small change in q, however, does not affect any of the final calculated results.

** Lindhard and Scharff[60] in a very recent article show that for a relativistic particle of velocity β a more exact expression for the second moment is given by the relation

$$\beta_2 = 4\pi \sum_i N_i Z_i \; e^4 \int_o^T \frac{1 - \beta^2/2}{1 - \beta^2} \frac{dT}{(dT/dR)^3} \quad .$$

In this study the maximum value of β is ≈ 0.26. This correction to the theoretical Eq. (4.14) is less than the uncertainty in the known value of the effective $\sum_i N_i Z_i$ in the fundamental stopping-power formula. It also turns out to be less than one-half of the experimental probable error in β_2 for 4-Mev μ-mesons.

If one employs the empirical range-energy relation

$$T = 0.251\, M^{0.419} \langle R_1 \rangle^{0.581} , \tag{2.6}$$

with T in Mev, M the mass of the particle in units of the proton mass, and R_1 the measured mean range in microns, one may integrate Eq. (4.14).

Differentiating Eq. (2.6),

$$\frac{dT}{d\langle R_1 \rangle} = 0.146\, M^{0.419} \langle R_1 \rangle^{-0.419} \tag{4.15}$$

Substituting in Eq. (4.14) and integrating,

$$\frac{\beta_2}{M} = 7.1 \times 10^{-4} \left(\frac{\langle R_1 \rangle}{M} \right)^{1.838} , \tag{4.16}$$

where β_2 is expressed in units of (microns)^2.

Two corrections to Eq. (2.1) must be considered now. The more exact Eq. (4.12) for the rate of energy loss to electrons contains the particle mass in an explicit manner. For most application in physics, one usually neglects this mass dependence for the so-called heavy particles. However, in this particular study the effect must be evaluated, as we are dealing with the intermediate-mass particles. The second correction is necessitated by the fact that, in the integration of Eq. (2.1) to obtain the range, one incorrectly assumes that the mean length traversed per unit energy loss is equal to the inverse of the mean energy loss per unit length. This inequality exists because the energy loss occurs in discrete steps during electron collisions of small impact parameters. Taking these two effects into account, Lewis[59] obtained

$$R_1 = \left(R \left[1 + \frac{3\epsilon_1}{2A} + \cdots \right] \right) \tag{4.17}$$

where

R_1 is the measured mean range; R is the range appearing in Eq. (2.3);

$$\epsilon_1 = \frac{4m_o}{m\left(1 + \frac{m_o}{m}\right)^2 - 4m_o} \approx \frac{4m_o}{m}; \text{ and } A \approx 2\,\ell n\,\frac{\epsilon_1 T}{I} - 5\epsilon_1/2 .$$

Evaluating this for the application herein,

$$\langle R_1 \rangle \approx R \left[1 + \left(\frac{1}{612\, M\, \ell n\, 3780\, \beta^2}\right)\right] . \tag{4.18}$$

2. Straggling Due to the Heterogeneous Composition of Emulsion

The emulsion is composed of silver halide bodies embedded in gelatin. Additional range straggling occurs because the stopping powers of the two materials are not the same. Barkas[43] has estimated this effect, assuming that the silver halide is present in the form of small spheres of diameter d, distributed uniformly throughout the gelatin. The detailed calculation gives for the range variance arising from the heterogeneity effect:

$$\sigma_h^2 \approx \frac{(r-1)^2 (S-1)(S+8)\, d}{12\left[1 + r(S-1)\right]^2} \langle R_1 \rangle , \tag{4.19}$$

where S is the ratio of emulsion volume to gelatin volume (approximately the shrinkage factor), r is the ratio of the ranges that would be found in gelatin and silver bromide separately, and d is the mean grain diameter. Electron microscope measurements give $d \approx 0.2$ microns.[61] Assuming $r \approx 4$ and $S \approx 2$, then

$$\sigma_h^2 \approx 0.06 \langle R_1 \rangle \quad (\text{microns})^2 \tag{4.20}$$

3. Effect of Finite Grain Spacing and Grain Size

If the particle, upon entering the emulsion detector, is of such energy that it is not strongly ionizing, the grains rendered developable may be separated by distances that are not negligible. In the usual manner, if the mean grain spacing is λ, the probability of not producing a grain in the distance x is $e^{-x/\lambda}$. This introduces a systematic shortening of the range by an amount λ, and an additional range variance of $\sigma_\lambda^2 = \lambda^2$. By the time the end of the track is reached where the grain density is high this correction is not necessary. The value of λ was determined experimentally, and for this study was found to be ≈ 0.9 microns for pions and muons coming directly from the target. This correction is not applied for μ-mesons originating from the decay at rest of π-mesons within the emulsion itself, since the track terminus of the parent meson clearly defines the beginning of the muon track.

The finite size of the grain (≈ 0.2 microns) causes an additional uncertainty in the true range of the particle. However, this effect is not systematic, and its order of magnitude is much too small to warrant further consideration.

Optical tests have been made to check the flatness of the emulsion surface, since any roughness would cause errors in the determination of the points of entry of the incoming particles. An optically flat piece of glass laid upon the surface gave widely spaced interference fringes indicating that no corrections were necessary.

4. Effect of Shrinkage Factor

When a nuclear emulsion undergoes processing, its thickness is significantly reduced owing to the removal of the silver halide that was not rendered developable. The ratio between the thickness at the time of exposure and the thickness after processing is commonly termed the "shrinkage factor," S_o. Clearly the shrinkage factor will vary with the relative humidity of the atmosphere and with the moisture content of the emulsion.

S_o has been determined experimentally in several ways. Plates were exposed at an angle 45° to the external alpha-particle beam of the 184-inch cyclotron. The ratio of the length of the particle-track segment (as measured in the plane parallel to the emulsion surface) to that of the

vertical change in depth from the beginning to the end of the track segment gives a measure of the shrinkage factor. In another measurement, x-rays were allowed to impinge on the emulsion at a 45° angle and similar measurements were carried out. Oliver[62] has made lengthy humidity-controlled measurements, determining emulsion thicknesses directly with a specially designed gauge. All three of these measurements indicate that $S_o = 2.3 \pm 0.1$ for the humidity conditions present in this study.

An incorrect choice of S_o will obviously introduce an error in the measurement of an element of range. Thus, if S_o is the true shrinkage factor and S is the incorrectly assumed value, then

$$\delta R' = \delta R \left(1 + \frac{S^2 - S_o^2}{S_o^2} \sin^2 \gamma_1 \right)^{1/2} \tag{4.21}$$

where δR is the true length of an element of path, $\delta R'$ is the calculated length, and γ_1 is the angle between the element of path and the plane of the unprocessed emulsion surface (the so-called dip angle).

Consequently one obtains for the error in an average range $\langle R_1 \rangle$, arising from an error in the shrinkage factor,

$$\frac{\Delta R}{\langle R_1 \rangle} = \frac{S - S_o}{S_o} \langle \sin^2 \gamma_1 \rangle , \tag{4.22}$$

where $\langle \sin^2 \gamma_1 \rangle$ is the mean value of $\sin^2 \gamma_1$ along the path, and is easily determined experimentally.

An incorrect choice of the shrinkage also introduces an additonal range variance. However, in this experiment, owing to the small value of γ_1, this variance σ_s^2 is quite negligible when compared to the other sources of range straggling.

$$\sigma_s^2 = \left(\frac{S - S_o}{S_o} \right)^2 \langle R_1 \rangle^2 \left[\langle \sin^4 \gamma_1 \rangle - \langle \sin^2 \gamma_1 \rangle^2 \right] \tag{4.23}$$

D. The Range Distribution Function

The topics discussed above allow one to estimate the mean range and range variance to be expected in the experiment for the different particles under study. One may summarize as follows:

(a) Let R_1 be a typical measured track after adding the small correction λ necessitated by the finite grain spacing. The actual mean value $\langle R_1 \rangle$ differs from the quantity R, which satisfies Eq. 2.3. The relation between the two is expressed as

$$R_1 = R\left(1 + \tau_1 + \tau_2\right) \equiv R\,(1 + \tau) \tag{4.24}$$

where $\tau_1 = \dfrac{1}{612\ M \ell n\ 3780\ \beta^2}$ and $\tau_2 \doteq \dfrac{S - S_o}{S_o} \left\langle \sin^2 \gamma_1 \right\rangle$.

(b) The variance of R_1 for a particle of momentum p_1 will be, in good approximation,

$$\sigma_R{}^2 = \left\langle R_1{}^2 \right\rangle - \left\langle R_1 \right\rangle^2 = \beta_2 + \sigma_h{}^2 + \sigma_\lambda{}^2 + \sigma_e{}^2 + \sigma_s{}^2 + \sigma_d{}^2 \tag{4.25}$$

where $\sigma_e{}^2$ represents the variance introduced by the personal human factor. This effect was measured for the different observers engaged in scanning the plates and found not to exceed $10^{-2} \langle R_1 \rangle$. As stated above, of the several known causes of variance β_2 is the dominant term, the other effects remaining small.

In addition, there remains a further source of variance which is difficult to estimate a priori. This has been included in Eq. (4.25) by the additive term $\sigma_d{}^2$. It represents the straggling arising from emulsion distortions introduced during development procedures. The total distortion may be considered as being comprised of these two effects:

a) Large-scale distortions from strains occurring during the drying of the emulsion. These may be directional.

b) Random, small-scale distortions arising from the dissolving out of the silver halide crystals during the fixing process, causing the gelatin to collapse into the empty volume left behind.

The large-scale distortions naturally do not lend themselves to any theoretical analysis. They are best treated by careful development of the emulsion. The small-scale distortions are an inherent result of photographic processing, and cannot be avoided. If one assumes that these individual regions of distortion are small compared to the total track length, one can deduce an expression for estimating σ_d^2. One can apply a statistical analysis analogous to that used in the derivation of the heterogeneity straggling effect Eq. (4.20), to obtain $\sigma_d^2 = K_1 \langle R_1 \rangle$, where K_1 is a constant. Since σ_h^2 and σ_d^2 are both proportional to $\langle R_1 \rangle$, they are not experimentally distinguishable.

The range straggling of the presumably monoenergetic μ-mesons originating and ending within the emulsion provided the empirical means for the study of Eq. (4.25).

V. STATISTICAL CALCULATION OF MASS RATIOS

In Eq. 2.12, $\left(m_\pi/m_\mu\right)^{1-q} = \dfrac{R_\pi p_\pi^{-q}}{R_\mu p_\mu^{-q}}$,

we have the basic relation for the determination of the pion-muon mass ratio. As has also been discussed previously, the quantity R_p^{-q} is the one used for statistical analysis. The range straggling, the finite target size, and the finite area of the detector are to be included in this normalized range-distribution function.

If one employs the observed empirical quantity $R_1 p^{-q}$ in Eq. (2.12) one obtains an apparent mass ratio α' defined by

$$\alpha' = \left(\frac{m_\pi}{m_\mu}\right) = \left[\frac{\left\langle R_{1\pi} p_\pi^{-q}\right\rangle}{\left\langle R_{1\mu} p_\mu^{-q}\right\rangle}\right]^{\frac{1}{1-q}} , \qquad (5.1)$$

where p_π and p_μ are the respective apparent momenta of the mesons, assuming the target to be a point source. The relation between the true mass ratio α and the apparent ratio α' can be derived by employing the information one has regarding the various distribution functions.

As in Section IIIB, let $U(p_1, p)\, dp_1$ be the probability that the true momentum is equal to p. Now, let $V(R_1, p_1)\, dR_1$ be the probability that the observed track length lies between R_1 and $R_1 + dR_1$, when the momentum is p_1; and let $W(p)\, dp$ be the fraction of the measured values of the apparent momentum that lie between p and $p + dp$. Then the mean values of the various powers ξ of the quantity $R_1 p^{-q}$ may be calculated in the usual manner.

$$\left\langle \left(R_1 p^{-q}\right)^\xi \right\rangle = \int_p \int_{p_1} \int_{R_1} \left(R_1 p^{-q}\right)^\xi W(p) U(p_1, p) V(R_1, p_1)\, dp\, dp_1\, dR_1$$

The integrations for $\xi = 1$ and $\xi = 2$ are carried out in detail in Appendix C. We assume that the exact expression for the ideal quantity R of Eq. (2.3) is given by the relation $R = C_o M^{1-q_o} p_1^{q_o}$, where C_o is a constant; M is the mass of the particle in units of the proton mass. Because of the Lewis Effect, q_o differs in principle from the q obtained from the proton range-energy relation by $\approx p_1 \frac{d\tau_1}{dp_1}$. In this study, this difference is much smaller than the uncertainty ($\approx 1\%$) in q caused by the uncertainty in the experimental range-energy relation. The following relations are derived:

a) The mean value of $R_1 p^{-q}$:

$$\left\langle R_1 p^{-q} \right\rangle = C_o M^{1-q_o} \left\langle p \right\rangle^{q_o - q} \left[1 + \omega_q + \tau + \frac{q - q_o}{2} \frac{\sigma_p^2}{\left\langle p \right\rangle^2} \right] \tag{5.3}$$

where ω_q and τ have previously been evaluated [Equations (3.17) and (4.24)] and are both $<< 1$. We have defined $\sigma_p^2 = \int (p - \langle p \rangle)^2 W(p)\, dp$ and $\langle p \rangle = \int p\, W(p)\, dp$. In this experiment $\sigma_p << p$. As the sign in the difference $(q_o - q)$ is unknown, we let $\langle q_o - q \rangle = 0$ with an uncertainty given by σ_q. Similarly we take $\langle S_o - S \rangle = 0$ with a standard deviation σ_s. Therefore Eq. (5.3) reduces to:

$$\left\langle R_1 p^{-q} \right\rangle = C_o M^{1-q_o} \left\langle p \right\rangle^{q_o - q} (1 + \omega_q + \tau_1) \tag{5.3a}$$

b) The variance of $R_1 p^{-q}$:

$$\sigma^2 = \left\langle R_1^2\, p^{-2q} \right\rangle - \left\langle R_1 p^{-q} \right\rangle^2 \approx \left\langle p \right\rangle^{2q} \left[\sigma_R^2 + \left\langle R_1 \right\rangle^2 (\omega_{2q} - 2\omega_q) \right] \tag{5.4}$$

The experiment is designed so that the range straggling σ_R^2 is by far the largest contributor to the total variance of $R_1 p^{-q}$.

If we define the quantity r by the equation

$$\frac{\langle p_\pi \rangle}{\langle p_\mu \rangle} \equiv a\,(1 + r)\,, \tag{5.5}$$

we obtain the following relation:

$$a = a' \left[1 + \frac{\tau_{1\pi} - \tau_{1\mu}}{q - 1} + \frac{\omega_{q\pi} - \omega_{q\mu}}{q - 1} \right] \tag{5.6}$$

Hence, if there are n_π observations of $R_{1\pi}\, p_\pi^{-q}$ and n_μ observations of $R_{1\mu}\, p_\mu^{-q}$, then the variance σ_a^2 of the calculated mass ratio is

$$\sigma_a^2 = \frac{a^2}{(q-1)^2} \left\{ \frac{\sigma_\pi^2}{n_\pi \langle R_{1\pi}\, p_\pi^{-q} \rangle^2} + \frac{\sigma_\mu^2}{n_\mu \langle R_{1\mu}\, p_\mu^{-q} \rangle^2} \right.$$

$$+ \frac{\sigma_q^2}{4} \left(\frac{\sigma_{p_\pi}^2}{\langle p_\pi \rangle^2} - \frac{\sigma_{p_\mu}^2}{\langle p_\mu \rangle^2} - 2r \right)^2$$

$$\left. + \frac{\sigma_s^2}{s^2} \left[\langle \sin^2 \gamma_{1\pi} \rangle - \langle \sin^2 \gamma_{1\mu} \rangle \right]^2 \right\} \tag{5.7}$$

Equations (5.6) and (5.7) allow one to calculate the value of the mass ratio and its statistical uncertainty. There exists a possibility of the contamination by stray mesons (i.e., those not entering the detector directly from the target, but arising from scattering off the channel walls, decay in flight, etc.); Eqs. (5.3) and (5.4) provide measures of the distributions of $R_1 p^{-q}$ which can be compared to those actually observed. In this manner, we can distinguish the small percentage of contamination from the direct target mesons. This is described in a subsequent section and distribution functions are shown (Figs. 14, 15, and 17).

In the entire discussion above, one assumes that the stopping of charged particles in an absorber is purely an electromagnetic effect, and that the absolute value of the charge of the proton, and of either kind of positive meson, is unity. Obviously, if these assumptions are not strictly valid, an error will have been made.

VI. THE DYNAMICS OF PION-MUON DECAY

A. Absolute Meson Masses and Related Quantities

A careful study of the energy and momentum balance of the assumed mode of pion decay,[44] $\pi \rightarrow \mu + \nu$, not only tests the validity of this assumption, but also yields accurate meson mass relations, in terms of certain observables. However, the process of decay involving the sudden acceleration of the newly created muon is necessarily accompanied by a continuous soft-photon spectrum. This process is the analogue of the inner bremsstrahlung accompanying nuclear beta decay.[63] Therefore, kinetic energies of the muon from zero to the full energy T_o are possible. Several authors[64-66] have obtained expressions for the probability distribution function $P(T,\epsilon)\, dT\, d\epsilon$, where ϵ refers to the energy of the photon. Thus, if one integrates with respect to ϵ, one obtains the probability, $P(T)\, dT$, of the muon's possessing a kinetic energy lying between T and T + dT. The ratio of the probability of soft-photon decay to radiationless decay for $T < 3.5$ Mev is calculated to be $\approx 1.3 - 2.0 \times 10^{-4}$. Fry,[67] examining anomalously short muon tracks that cannot be explained by a decay-in-flight analysis, has obtained an experimental value for this probability of $(3.3 \pm 1.6) \times 10^{-4}$, which is in agreement as to order of magnitude. In any event, the probability of obtaining a "low-energy" μ-meson is very small. If one calculates the mean energy of the muon arising from the presence of the complete bremsstrahlung spectrum, it is found to be but a few hundred electron volts less than the radiationless value of ≈ 4 Mev. Furthermore, as no anomalously short-range tracks are included in the present analysis, the effect of the inner bremsstrahlung process will be felt even less. The difference of a few hundred electron volts is too small to be detected in this study. Therefore, for the purposes of this discussion, the decay of the pion resolves itself into a simple two-body problem. Thus we may write the relativistic equations for the conservation of energy and momentum for a pion decaying while at rest as follows:

$$m_\pi c^2 = \sqrt{p_\mu^2 c^2 + m_\mu^2 c^4} + \sqrt{p_\nu^2 c^2 + m_\nu^2 c^4} = m_\mu c^2 + T_\mu + m_\nu c^2 + T_\nu; \tag{6.1}$$

$$p_\mu = p_\nu \tag{6.2}$$

The algebraic derivations of the following relations are presented in Appendix D. For future clarity of notation, we distinguish between the momentum p_μ of a μ-meson coming from the target and entering the emulsion, and the momentum p_o that the μ-meson acquires at the instant of decay. We shall also define

$$\alpha \equiv \frac{m_\pi}{m_\mu} \quad \text{and} \quad \beta \equiv \frac{m_\nu}{m_\mu} \quad .$$

a) Mass of Neutral Particle

$$m_\nu = m_\mu \left[\alpha^2 + 1 - 2\alpha \sqrt{1 + \frac{p_o}{m_\mu c}^2} \right]^{1/2} . \tag{6.3}$$

One cannot hope by this experiment to obtain a value of the mass of the presumed neutrino with an accuracy comparable to that obtained in the beta-decay studies.[68-69] As shown in Eq. (6.3), the mass of the neutrino is a function of a large mass value multiplied by the difference between two comparatively large numbers. Figure 6 shows the sensitivity of the derived neutrino mass to small changes in α, p_o, and the muon mass. One can merely arrive at a new upper limit to the mass of the neutral particle and note if any inconsistencies exist in the presumed mode of decay.

On the other hand, certain quantities can be derived that are very insensitive to the mass of the neutrino, if it is indeed quite small. Assuming $m_\nu = 0$, we have several important relations.

b) The Pion-Muon Mass Difference

$$\left(m_\pi - m_\mu\right) c^2 = \frac{2\alpha}{\alpha + 1} \; p_o c \quad . \tag{6.4}$$

As is shown later, in Section VIIIC and in Appendix F, very high accuracy can be obtained in the estimate of the mass difference. This difference, coupled with the value of the mass ratio α, enables one to derive absolute values of the positive pion and muon masses, independent of any other comparison particle such as the proton.

c) Mass of the Pion and Muon

$$m_\pi c^2 = \frac{2a^2}{a^2 - 1} \; p_o c \; , \tag{6.5}$$

$$m_\mu c^2 = \frac{2a}{a^2 - 1} \; p_o c \; . \tag{6.6}$$

d) Kinetic Energy of the Muon

$$T_o = \frac{a - 1}{a + 1} \; p_o c \; , \tag{6.7a}$$

$$T_o = \frac{(a - 1)^2}{2a^2} \; m_\pi c^2 \; . \tag{6.7b}$$

From the usual relativistic relations, one can also obtain a value of the kinetic energy where E_μ is the total energy of the muon, with no assumptions being made regarding the mass of the neutrino.

$$T_o = E_\mu - m_\mu c^2 = \sqrt{p_o^2 c^2 + m_\mu^2 c^4} - m_\mu c^2 \tag{6.8}$$

B. The Absolute Muon-Decay Momentum

All the mass and kinetic-energy relations connected with the dynamics of the decay scheme involve functions of the mass ratio a and the full decay momentum p_o. We have already discussed in Section V the specific details of determining a, and now concern ourselves with the evaluation of the other important parameter, p_o.

Those μ-mesons entering the detector from the target no longer have their full decay energy, owing to small losses within the target. The μ-mesons created within the emulsion, however, and expending their entire energy therein, lend themselves to this phase of the study. These mesons are referred to as μ-completes, with momentum p_o, while those muons coming from the target are termed ρ-mesons with momentum p_μ.

Once again, we utilize the range-momentum relation and the mass-normalization property. As outlined in Section II, we can write for two particles

$$\left(\frac{m_1}{m_2}\right)^{1-q} = \frac{R_1 p_1^{-q}}{R_2 p_2^{-q}} \quad . \tag{2.12}$$

Two methods, involving this fundamental equation, can be employed to determine p_o.

In the first method, the μ-completes are to be compared with the target ρ-mesons. Therefore, $m_1 = m_2 = m_\mu$. Let $p_1 = p_o$, and $p_2 = p_\mu$ with associated ranges R_o and R_μ, respectively. Solving for the absolute decay momentum, we get

$$p_o = \left[\frac{R_o}{R_\mu p_\mu^{-q}}\right]^{1/q} \quad . \tag{6.9}$$

Now, however, the determination of an absolute value for p_o requires an absolute measurement of the magnetic field of the cyclotron. As before, the velocities of the two sets of mesons are to be chosen as nearly equal as possible and still have adequate statistics for the analysis. This is desirable in order that the uncertainty in q, once again, is not a significant source of error. Thus, by determining the mean range of the μ-completes, and the absolute mean value of the normalized range $\left\langle R_{1\mu} p_\mu^{-q} \right\rangle$, and introducing the effects of the finite sizes of the target and detector (as shown in Appendix C), one obtains

$$p_o = \left[\frac{\langle R_o \rangle}{\left\langle R_{1\mu} p_\mu^{-q} \right\rangle}\right]^{1/q} \left[1 + \frac{\tau_{1\mu} - \tau_{1o}}{q} + \frac{\omega_{q\mu}}{q}\right] \tag{6.10}$$

where the various parameters have been defined previously in Sections IIIB and IVC.

If we define ϵ by the relation $\epsilon \equiv \frac{\langle p_\mu \rangle - p_o}{p_o}$, where $\langle p_\mu \rangle$ is the mean momentum of the ρ-mesons that are selected from the detector for range measurements, the uncertainty in p_o may be expressed by

$$\frac{\sigma_{p_o}^2}{p_o^2} = \frac{1}{q^2}\left\{\frac{\sigma_{R_o}^2}{n_o\langle R_o\rangle^2} + \frac{\sigma_\mu^2}{n_\mu\langle R_{1\mu}\, p_\mu^{-q}\rangle^2} + \frac{\sigma_q^2}{4}\left(\frac{\sigma_{p_\mu}^2}{p_\mu^2} + 2\epsilon\right)^2 + \frac{\sigma_S^2}{S^2}\left[\langle \sin^2\gamma_{1\mu}\rangle - \langle \sin^2\gamma_{1o}\rangle\right]^2\right\} + \frac{\sigma_H^2}{H^2} \qquad (6.11)$$

where $\sigma_{R_o}^2$ is the variance or range straggling of the μ-completes, and $\sigma_{p_\mu}^2$ is the spread in the value of the momentum of the ρ-mesons. The additional terms, $\frac{\sigma_H^2}{H^2}$, represents the uncertainty in the absolute magnitude of the magnetic field.

In the second method the mean range and momentum of the μ completes are compared with the ranges and absolute momenta of π-mesons originating at the target and entering the emulsion detector. Once again the velocities of the two particles are to be chosen approximately equal. Employing the fundamental Eq. (2.12), we solve for p_o, obtaining

$$p_o = \left[\frac{\langle R_o\rangle}{\alpha^{q-1}\langle R_{1\pi}\, p_\pi^{-q}\rangle}\right]^{1/q}\left[1 + \frac{\tau_\pi - \tau_o}{q} + \frac{\omega_{q\pi}}{q}\right]. \qquad (6.12)$$

Thus, knowing the value of mass ratio α from an independent study, we have another method of evaluating the absolute decay momentum of the muon. If we let $\frac{\langle p_\pi\rangle}{p_o} \equiv \alpha(1-\delta)$, we now express the uncertainty in p_o as follows,

$$\frac{\sigma_{p_o}^2}{p_o^2} = \frac{1}{q^2}\left\{\frac{\sigma_{R_o}^2}{n_o\langle R_o\rangle^2} + \frac{\sigma_\pi^2}{\langle R_{1\pi}\, p_\pi^{-q}\rangle^2} + (1-q)^2\,\frac{\sigma_a^2}{a^2} + \frac{\sigma_q^2}{4}\left(\frac{\sigma_{p_\pi}^2}{\langle p_\pi\rangle^2} + 2\delta\right)^2\right.$$

$$\left. + \frac{\sigma_s^2}{s^2}\left[\langle \sin^2\gamma_{1\pi}\rangle - \langle \sin^2\gamma_{1o}\rangle\right]^2 + \frac{\sigma_H^2}{H^2}\right\} \qquad (6.13)$$

where σ_a^2 is the uncertainty in the value of the $\pi/_\mu$ mass ratio.

VII. EXPERIMENTAL TECHNIQUES

A. Geometrical Arrangement

1. Exposures within the Cyclotron

The mesons under study are produced by the internal circulating proton beam of the 184-inch cyclotron. The geometrical arrangement is shown schematically in Fig. 7. The protons (≈ 290 Mev) strike a thin copper target, producing π-mesons. Those positive pions leaving the target with energies acceptable to the defining channel spiral down under the influence of the cyclotron magnetic field and enter a 200-micron thick Ilford C-2 nuclear-emulsion detector. The points of entry of the pions are distributed more or less uniformly over the entire plate.

At the same time, positive pions coming to rest within the target decay into muons. Those muons created near the surface of the target leave with only small energy losses and can be accepted by the channel if their angles of emission are "proper", entering the emulsion in a more defined region of the plate. The pions reaching the detector lose energy and stop within the emulsion, giving rise to muons, approximately 17 percent of which come to the ends of their ranges before leaving the plate. These are the μ-mesons previously referred to as "μ-completes." The target muons or "ρ-mesons" coming to rest decay into an electron plus two neutrinos. Since the C-2 emulsion is insensitive to electrons, one can quickly distinguish between a pion and a muon by simply observing whether or not another track appears at the end of the range of the particle.

The experimental apparatus is mounted on a cart and run into the main vacuum tank of the cyclotron by means of the so-called "proton probe." The cart is stopped along its track at a point that places the meson target at a cyclotron radius of 73 inches. This is the maximum allowable radius at which the trajectories of the particles under study remain within the fairly uniform region of the magnetic field. The diameters of the pion orbits are approximately 7 inches. Figure 12 gives the magnetic field intensity as a function of cyclotron radius, showing the change in slope at the 80-inch point.

2. Target and Detector Assembly

A perspective sketch showing the arrangement of the target, channel, and detector plate is given in Fig. 8. The entire apparatus is mounted and fixed upon a dural base and later placed on the proton probe cart. Considerable care is given to the establishment of a median reference line (Central Radial-Line) passing through the centers of the target and plate holder.

In the first set of exposures, Run I, the meson target of copper had the dimensions 0.041 x 1/4 x 1/2 inch, and was attached to a narrow copper stem. To increase the solid angle, the target center was located at a height of 0.44 ± 0.06 inches above the surface of the emulsion. A wedge-shaped carbon absorber was placed in the channel, effectively casting a geometrical shadow and preventing mesons that originated in the stem from reaching the detector.

In a subsequent experimental run, Run II (see Fig. 9), the mounting of the 40-mil target was improved. It was supported from a brass C-shaped holder by one-mil tungsten wires looped through small holes in the target. These wires fit into accurately milled grooves, facilitating the centering of the target. The upper set of wires was wrapped around a pin at the top of the target holder, while the bottom pair had a small lead weight attached. This arrangement proved quite satisfactory in preventing perturbation of the target position. The need for a shadow in the channel was eliminated, as the contributions from the 1-mil wires were negligible.

It was desirable to have uniform irradiation of the target to facilitate the identification of the effective geometric center of meson production. Preliminary tests were made to locate the median plane of the circulating proton beam as well as its intensity half-width in the vertical direction. Bowker,[70] employing thin polyethylene monitors, has measured the vertical profile of the beam. Readings with the aid of a Lauritsen electroscope of the β activity from the C^{12} (p, pn) C" reaction indicated that the beam intensity dropped to half-maximum in a vertical distance of 0.25 inch. The median plane of the beam was also checked by irradiating a 3-inch-long graphite cylinder of 36-mil diameter, and locating the point of maximum activity. At the 73-inch radius, it was found to be ≈ 0.25 inch below the median plane of the gap between the pole faces of the cyclotron magnet. A mock target, consisting of four 10-mil slices pressed together, was bombarded to check the relative irradiation across the target by the beam. All four sections, when separated, showed essentially the same activity.

The original philosophy regarding the channel was to have the minimum amount of shielding that appeared feasible. Background problems inside the vacuum tank of the cyclotron are rather severe and ordinarily call for considerable shielding. On the other hand, using a great deal of shielding can increase the possibility of contamination from mesons scattering off the channel walls. Preliminary runs were made with wide-open channels and comparatively little shielding. Exposures had to be limited to ten seconds to prevent the heavy neutron-proton background from completely obscuring the desired mesons; consequently, statistics were poor. Moreover, as the plates were placed in the apparatus without any outer paper wrapping, any source of light within the tank could blacken the film surfaces. Arcing from the dee and light emanating from the tungsten filament in the cyclotron ion source clearly called for some light shielding.

The final channel, therefore, represents the inevitable compromise. More shielding is employed to permit longer exposure times (30 to 45 seconds) and to decrease the ever-present light hazards. The channel is designed to accept mesons leaving the target within specified angular intervals (π-mesons with angles in the backward direction with respect to the incident proton beam of $\pm 10^{\circ}$ and ρ-mesons with angles of -15° to $+10^{\circ}$). Mesons produced in the shielding by protons, and target mesons scattered in the channel are effectively minimized. The shape for the channel was developed empirically, meson trajectories being drawn from all points of the channel. Any unwanted meson that does manage to get through will either enter the detector with the wrong angle, or will have a considerably lower or higher energy and consequently can easily be distinguished from the main distribution by its range measurement. The copper walls are lined with 1/8-inch polyethylene to lower the atomic number of the surface material and thereby possibly reduce the scattering. A certain amount of decay in flight takes place, the products of which cannot be prevented from reaching the detector. This effect, however, is small, as is seen in the ρ-meson distributions obtained.

The detector is mounted on a 1 x 3-inch plate holder having an inclination angle of 5° to the horizontal x-y plane. The plate holder is shown in Fig. 10. A glass-backed photographic film negative of a drawing of two fiducial marks is cemented on the surface of the holder. The Central Radial Line joining the centers of the fiducial marks, when extended, passes through the center of the target. By means of a small battery-operated lamp, a latent image of these fiducial lines is produced in the nuclear emulsion detector after it has been fixed in place on top of the negative by phosphor bronze clamps. These lines not only give a permanent record of the exact position of the detector at the time of exposure, but also enable the investigator to quickly locate the proper regions of the plate to be scanned under the microscope (i.e. momentum intervals which give approximately equal velocities for the pion and muon, respectively). At the time of exposure, a brass measuring bar is laid parallel to the Central Radial Line, and the distances between the target and the fiducial marks are readily determined with the aid of a low-power microscope attached to a micrometer. The brass bar contains two fiducial marks whose known distance apart is approximately equal to the target-detector distance. One measures small differences between the target and the first bar mark, and between the fiducial lines on the plate holder and the second bar mark. Figure 11 shows schematically the actual physical measurements made for Run I. The differences can be read to 0.1 mil, and the over-all distance between the center of the target and the plate fiducial mark is probably known to $\approx$ one mil. This represents a negligible contribution to the total uncertainty in the final momentum determination.

In the calculation of the momentum, it should be emphasized that the locations of the target and detector are considered with reference to two coordinate systems. The first reference frame had its origin at the center of the target. In this frame, the distance between the target and detector is known to high accuracy ($\approx$ 1 part in 10^4), and the entire target-detector assembly remains fixed on its dural base for a particular run.

The percentage error in the target-to-detector distance reflects itself directly as an equal uncertainty in the momentum. The second frame of reference has its origin at the center of the cyclotron, for the absolute value of the magnetic field is known as a function of the cyclotron radius. The proton probe cart carrying the target-detector assembly can be set at a particular radius with an accuracy of ± 1/8 inch. Since the gradient of the field in this region is ≈ 10 gauss per inch, the error in the location of the cart gives an error in the momentum of less than 1 part in 10^4. This error is an order of magnitude smaller than the over-all uncertainty in the actual measurement of the field itself (See Sec. VII D).

B. Photographic Development Procedures

Development of the 200μ Ilford C-2 emulsions consisted of these steps:

1. Immerse in distilled water - one hour
2. Immerse in cold developer at 5° C - one hour
3. Immerse in hot developer (26°C) (6 parts H_2O to one part Kodak D-19) - twenty minutes
4. Immerse in cold stopbath (1% acetic acid at 5°C.) - one hour
5. Fixer-Kodak F-5 - 5 or 6 hours under agitation
6. Wash and dry
7. Coat surface with lacquer - household cement mixture

C. Microscope Scanning Techniques

Employed in the study are standard Bausch and Lomb and Leitz binocular microscopes equipped with special research stages designed by Mr. Brower of the University of California Physics Department. Angle and range measurements are taken with magnification of ≈ 1000X. The x and y movements of the stages were checked for perpendicularity and showed no measurable deviations from 90°. A reticle placed inside one of the eyepieces in conjunction with a goniometer (protractor) mounted around the outside of the collimating tube enables one to measure track angles to an absolute accuracy of ± 1°. The 1 x 3-inch developed plate is lined up with the x and y movements of the scope by means of the

fiducial marks exposed on the emulsion just prior to its exposure within the cyclotron. The 0° angle is then defined by having the central line of the eyepiece reticle set parallel to the direction of the y-axis. The angular requirements for mesons accepted for range measurements are $\theta' = -11^{\circ}$ to $+ 11^{\circ}$ for pions, and $\theta' = -15^{\circ}$ to $+ 11^{\circ}$ for muons. As already defined, θ' is the angle a track makes with the y-axis if its orbit is extended until it crosses the x-axis (Central Radial Line).

Another criterion for acceptance by the microscope observer involves the dip angle of the track at the surface of the emulsion. The expected dip angle for a particle leaving the target is easily calculated from the geometry of the target-detector assembly. Both the dip angle and range measurements require a calibration of the fine-focus adjustment of the scope (vertical z-motion), and a knowledge of the shrinkage factor[62] S of the emulsion. The calibration is accomplished by measuring the known thickness of a thin cover glass. Because of the shrinkage factor and the rather small angles involved, accurate measurements of the dip are not possible. Since the amount of scattering of these low-energy mesons within the emulsion is large, only short track lengths in the x-y plane can be considered. The tangent of the dip angle is then determined by measuring the change in depth of the track over this short segment of length. Mesons are accepted for analysis with observed dip angles lying within a 5° to 9° interval.

Particle ranges are measured by two slightly different methods. In one case the reticle, which is divided into 100 divisions, is calibrated against a stage micrometer. Thus, the projected range in the x-y plane is measured by lining up the reticle with the track and counting the number of divisions per track length. In the other method the projected range is measured with the aid of the Brower stage, with which changes in the x and y directions can be read directly on a dial to with 0.1 of a micron. Since the mesons scatter quite freely, the total range is determined by measuring the lengths of short straight-line segments of the track:

$$R_l = \sqrt{\sum_i (\Delta X_i)^2 + (\Delta Y_i)^2 + S^2 (\Delta Z_i)^2} \quad . \qquad (7.1)$$

The accuracy of the stages was tested against a stage micrometer, and small differences were observed between true distances and the actual readings of the stages. The stages of the three microscopes used in the experiment showed a sinusoidal variation in the difference of approximately 2 to 3 microns per 100 microns. However, as this is a sinusoidal effect, not only is the percentage error over a range of 600 to 800 microns quite small, but it is effectively random in nature. This effect, then, merely represents an additional range straggling, which can be neglected when compared to some of the other sources of straggling mentioned previously. Furthermore, since the mass-normalization method involves only ratios, relative values of the ranges are all that are required. It is best to have a particular plate scanned under one microscope, and preferably by the same observer. In this manner any systematic factors affecting the absolute measurements, due either to the microscope itself or to the subjectivity of the observer, tend to cancel out.

D. Magnetic Measurements

Absolute measurements of the magnetic field are carried out with the aid of the nuclear induction technique,[71] employing the Varian Associates Nuclear Induction Meter. In the preliminary runs the proton moment head, containing the water sample and coils, was mounted directly on top of the channel, and the Larmor frequency was measured at the same time as the plate exposure. Because of certain engineering difficulties, this arrangement proved to be too cumbersome for efficient operation. The absolute values of the preliminary terminations of the magnetic field intensity (for the same excitation current) were found, on different days, to be equal to each other within a few gauss. This is not particularly surprising, as the magnet is operating near saturation; hence hysteresis effects are expected to be small. Consequently, a more efficient procedure was adopted. In Run I, exposures were made on one day, and the cyclotron field was measured the following day, the field current being carefully monitored by means of a Leeds-Northrup potentiometer. In Run II, both the exposures and the field measurements were completed in the same day, but not simultaneously. The proton moment head was inserted into the cyclotron by means of a special probe at the conclusion of the plate exposures.

Figure 12 shows a plot of several determinations of the absolute field as a function of cyclotron radius. In all cases, the magnetic field currents had been set for 5 to 6 hours. The individual values obtained all fall within ± 0.1 percent of the mean value despite the widely different dates of the measurements. The Larmor frequency, and hence the value of the field, can be located on an oscilloscope and read on a General Radio Signal Generator to ≈ 0.03% accuracy for any one determination.

Unfortunately, it was noticed during the magnetic measurements of Run II that the resonance frequency appeared to shift slightly as the proton moment probe head was rotated about its own axis inside the cyclotron. The angle of rotation vs. the frequency was recorded during the measurement. It was later discovered that a small magnetic set screw had been inadvertently placed near the borrowed probe head by unknown persons, and had acted as a magnetic dipole perturbing the main cyclotron field. Assuming the screw to be in the form of a sphere, one can derive the analytic expression

$$H_T \approx H_o \left[1 + \frac{I}{H_o r^3} \left(2 \cos^2 \theta - \sin^2 \theta\right) \right] , \qquad (7.2)$$

where H_T is the perturbed magnetic field as determined by the Larmor frequency reading, H_o is the true unperturbed magnetic field of the cyclotron, I is the total magnetic moment of the set screw, r is the distance from the center of the set screw to the center of the water sample, and θ is the angle of rotation between the vector $\vec{r}$ and the direction of $\vec{H}_o$. After the run, the probe head with the set screw was inserted in a pair spectrometer magnet whose magnetic field intensity was approximately equal to that of the cyclotron. The probe was then rotated in both directions, varying θ from -60° to $+60^\circ$. The set screw was then removed and the probe head reinserted into the magnet, thereby determining its H_o. This time, rotation of the probe head gave no frequency shift. Table VII gives the results of this test. As expected from the analytic expression, a null effect appeared for $\theta \approx 55^\circ$. Since the Larmor frequency as a function of the angle of rotation within the cyclotron was known, corrections as determined from the pair spectrometer could then be applied directly to obtain the true H_o of the cyclotron without having to determine I/r^3.

In the worst case, $\theta = 0^{\circ}$, the correction amounted to 0.25%. As a further check, the mean value of the quantity, I/r^3, was determined from the individual pair spectrometer readings, was inserted into Eq. (7.2) in conjunction with the H_{T_i} and θ_i of the cyclotron measurements, allowing one to solve for the H_o of the cyclotron field. The agreement between the two methods of determining H_o was excellent, the results being equal to within 0.03%. Compounding the various sources of possible error in the field measurements, one can conservatively estimate the uncertainty in the absolute value of the field as ± 0.1 % (standard error) for Run II, and ±0.2% (standard error) for Run I. The quoted uncertainty is larger in the first run because the magnetic measurements and plate exposures were not completed in the same day.

VIII. ANALYSIS OF EXPERIMENTAL DATA

A. The Range Straggling of the Mu-Completes

Since the main source of variance in the R_p^{-q} distribution function originates from the Bohr range straggling, this effect has been studied experimentally in some detail. Data are taken from twelve plates, adding up to a total of 558 μ-complete events.

Because the stopping power varies from one emulsion to another, different mean values of the range $\langle R_\mu \rangle$ are obtained. Table VIII gives a summary of these results. It can easily be shown that for $R_\mu > t$ (where R_μ is the range of the μ-complete and t is the thickness of the emulsion) the probability of the particle's expending its entire energy within the emulsion is approximately equal to $\frac{t}{2R_\mu}$. Therefore, the observed $\langle R_\mu \rangle_i$ will tend to have a value that is smaller than the true mean range $\langle R_o \rangle_i$, as the shorter tracks have a greater probability of remaining within the emulsion. The equation correction for this effect is derived in Appendix E,

$$\langle R_o \rangle = \langle R_\mu \rangle + \frac{\sigma_{R_\mu}^2}{\langle R_\mu \rangle} \quad , \tag{8.1}$$

where $\sigma_{R_\mu}^2$ is the observed variance of the ranges of the μ-completes.

In order to combine the data from the different plates, the various values for $\langle R_o \rangle_i$ are normalized to a range of 600 microns, and the entire distribution is plotted in Fig. 13. The percentage standard deviation of this distribution is found to be 4.5 ± 0.1.

If one now calculates the range straggling for μ-mesons from the Bohr formula, Eq. (4.14), the straggling is expected to be 4.0%. Furthermore, when the other known sources of straggling as summarized in Eq. (4.25) are introduced, the total straggling $\frac{\sigma_{R_o}}{\langle R_o \rangle}$, ($\sigma_{R_o}$ is the true straggling) adds up only to 4.1%. A statistical analysis of the method of range normalization employed in combining the data indicates that $\frac{\sigma_{R_\mu}}{\langle R_o \rangle}$ is actually less by $\approx 0.01\%$.[72] For these energies, the π-meson comes to rest in the emulsion

within $\sim 10^{-12}$ seconds, and the possibility that additional range straggling is due to decay-in-flight events is certainly ruled out. The straggling due to the inner bremsstrahlung effect discussed in Sec. VIA is found to be $\approx 0.01\%$. Hence one must conclude that distortion effects, σ_d^2, are probably the sources of the additional straggling. Such effects have also been reported by Seifert.[73] White and Fry[74] have also examined the range straggling of the completes and find it to be $= 4.86 \pm 0.12\%$. The difference between the two results may be due to different distortion effects, or perhaps to an incorrect choice of the shrinkage factor.

A chi-square test[75] for a normal-curve fit to the data gives a significance level of ≈ 0.4, indicating that the Gaussian assumption is indeed a good one. Table IX compares the actual distribution obtained with the frequency distribution to be expected for a normal curve with parameters $n_o = 588$, $\langle R_o \rangle = 600\mu$, and $\frac{\sigma_{R_o}}{\langle R_o \rangle} = 4.5\%$.

The skewness of the distribution is measured by the ratio $\beta_3 \Big/ \beta_2^{3/2}$, where β_2 and β_3 are the second and third moments of the distribution. From the Lewis calculation, one expects a slight skewness equal to ≈ -0.03. The contribution to the skewness from the inner bremsstrahlung process is < -0.001 if one includes only events that lie in the interval $\pm 3\sigma_{R_o}$ about the mean, $\langle R_o \rangle$. The skewness of the observed distribution is -0.03 ± 0.12. Obviously, because of the very slight skewness involved, the percentage error in the estimate of the skewness becomes unduly large, approaching infinity for a true Gaussian distribution. This study cannot test quantitatively the validity of the Lewis theory nor that of the theory of the inner bremsstrahlung process.

It is of interest to note that one track was found to have a range of only 268 microns. This event was excluded from the above analysis. The energy and momentum analysis of the event shows that it could as well have arisen from decay in flight of a pion of 58 Kev energy as from the inner bremsstrahlung effect.

B. The Normalized Range Distribution Functions, Rp^{-q}

The range variance obtained for the μ-completes serves as a calibration function for the various Rp^{-q} distributions being studied. For two particles having equal velocities,

$$\frac{(\beta_2)_{m_1}}{(\beta_2)_{m_2}} = \frac{m_2}{m_1} \quad \text{and} \quad \frac{\langle R \rangle_{m_1}}{\langle R \rangle_{m_2}} = \frac{m_1}{m_2} .$$

Therefore, upon application of Equations (4.25) and (5.4), one should expect for the target π-mesons, $\frac{\sigma_\pi}{\langle R_{1\pi}\, p_\pi^{-q} \rangle} \approx 4.0\,\%$, and for the ρ-mesons, $\frac{\sigma_\mu}{\langle R_{1\mu}\, p_\mu^{-q} \rangle} \approx 4.5\%$. Any significant increases over these values would indicate the presence of contamination.

Run I

In this run, the normalized ranges of the target pions and muons (ρ-mesons) are compared in order to determine the π/μ mass ratio. In addition, a value for the absolute decay momentum is obtained by comparing the normalized ranges of the ρ-mesons with the ranges of the μ-completes. The latter distributions are shown in Fig. 16.

The data for this run have been collected from five different plates. (Sample calculations of $R_1 p^{-q}$ are presented in Table X). For simplicity, the constant multiplicative factor e/c has been omitted in the calculation of p^{-q} (See 3.12 and 3.14). The π-meson and ρ-meson normalized range distributions are plotted in Figs. 14 and 15, with ρ actually representing the magnetic rigidity of the particles. In general, two distinct peaks are observed, corresponding to the two types of mesons coming from the target. A small amount of background contamination also appears to be present. Since a few of the background events run into the tails of the main distributions, the following procedure is employed:

(a) The median of the distribution is determined including all "questionable" events. The median is first chosen as a statistical measure, since it is less sensitive to spurious events than the mean, especially for small sample statistics.

(b) When the median has been determined, the theoretically expected standard deviations of

$$\frac{\sigma_\pi}{\langle R_{1\pi}\, p_\pi^{-q} \rangle} = 4.0\,\% \text{ and } \frac{\sigma_\mu}{\langle R_{1\mu}\, p_\mu^{-q} \rangle} = 4.5\%$$

are "folded" into the distributions, and any events lying outside an interval of $\pm 3\sigma$ from the median are considered as background.

(c) The mean, $\left\langle R_1 p^{-q} \right\rangle$, and its standard deviation are then calculated for the adjusted distribution as outlined in Sec. V.

Table XI includes the final $\left\langle R_1 p^{-q} \right\rangle_i$ results with the associated $\left\langle R_o \right\rangle_i$. Actually, a total of only 8 (5 π-meson and 3 p-meson) "questionable" events are excluded from the final calculations. The averages of percentage straggling of the normalized range distributions containing no "questionable" events are:

$$\frac{\overline{\sigma_\pi}}{\left\langle R_{1\pi} p_\pi^{-q} \right\rangle} = 3.8 \pm 0.2\% \text{ and } \frac{\sigma_\mu}{\left\langle R_{1\mu} p_\mu^{-q} \right\rangle} = 4.9 \pm 0.2\% \quad .$$

The deviations from the predicted values are not considered statistically significant, although there is always the possibility that a small amount of indistinguishable contamination may lie within the $\pm 3\sigma$ interval. In the few cases where some events are eliminated, the computed standard deviations of the adjusted distributions also agree with the expected values, whereas the unadjusted distributions have standard deviations that are $\approx$ 50 to 60% larger owing to the presence of the few spurious events.

The existence of the background is probably due to the presence of the carbon shadow absorber that was placed in the channel, as described in Sec. VII A. Also, with the present geometry, the p-meson distributions always have $\approx$ 5% contamination originating from pions decaying in flight.

Run II

To test the possibility of unknown experimental systematic errors, especially in the measurement of the absolute value of the magnetic field, another set of exposures within the cyclotron was made. In this run, the normalized ranges of target pions were compared with the μ-complete ranges to obtain a value for the absolute decay momentum.

As described in Sec. VII A, the target assembly was improved for this run, and the shadow absorber was also removed from the channel. The $R_{1\pi}\, p_{\pi}^{-q}$ distributions obtained are plotted in Fig. 17. One immediately observes the absence of any apparent background in the distributions. It is also of interest to note the comparative values of $\langle R_{1\pi}\, p_{\pi}^{-q} \rangle$ for the three plates. Whereas two (No. 28848 and No. 28853) are essentially equal, the third (No. 28849) is considerably higher. A comparison of the $\langle R_o \rangle$ associated with the μ-completes of the three plates shows the same trend. (Fig. 18). These results, which are also summarized in Table XI, emphasize the effectiveness of the mass normalization method, illustrating the uncertainties that are present when one employs an absolute range-energy relation. The observed standard deviations are in excellent agreement with the predicted values, further indicating the lack of contamination.

C. Derived Experimental Values

All errors to be quoted below in this section are statistical probable errors.

1. The Pi-Mu Mass Ratio.

As set forth in Sec. VI, the π/μ mass ratio α and absolute decay momentum p_o are the fundamental experimental quantities. Table XII summarizes the calculation of the mass ratio from Eqs. (5.6) and (5.7), showing the magnitudes of the target-detector and Lewis corrections and the magnitudes of the various uncertainties contributing to the total probable error in α. The weighted average over the five plates of Run I yields

$$\alpha = 1.321 \pm 0.002 \quad .$$

The statistical probable error calculated from external consistency is ± 0.0020 and from internal consistency is ± 0.0017.[76] These values give a ratio of 1.18 ± 0.22, indicating that there are no large systematic errors.

The Lewis Effect correction systematically lowered the apparent mass ratio α' by ≈ 0.0003. The target-detector corrections vary over the individual plates from -0.0025 to $+0.0015$. It is also clearly seen in Table XII that the predominant contributions to the total probable error come from the variances of the observed normalized range distributions of $R_{1\pi}\, p_{\pi}^{-q}$ and $R_{1\mu}\, p_{\mu}^{-q}$.

2. The Absolute Decay Momentum of the Muon

Tables XIII and XIV summarize the calculations of $(p_o)_I$ and $(p_o)_{II}$, employing Equations (6.10) and (6.11) for Run I, and Equations (6.12) and (6.13) for Run II, respectively.

The Lewis Effect correction is zero for Run I, as we are comparing equal-mass particles (ρ-mesons and μ-completes). The target-detector corrections vary from -0.02 to + 0.08 Mev/c over the five plates. In Run II, where one compares the μ-completes with target pions, the Lewis correction systematically lowers the apparent momentum p_o by 0.006 Mev/c, whereas the target-detector corrections vary from - 0.006 to + 0.002 Mev/c. The ratio of external to internal consistency in Run I is 1.18 ± 0.22; in Run II the ratio is 0.70 ± 0.28. In Run I, the uncertainty in the absolute value of the magnetic field (See Sec. VII D) is the dominant term in the probable error, with a smaller contribution from range straggling. In Run II, the error in the momentum calculation is determined by the uncertainty in α and the inherent range straggling, and to a lesser degree by the uncertainty in the magnetic field. The following values are obtained:

$$\text{Run I}: \quad p_o = 29.85 \text{ Mev/c};$$

$$\text{Run II}: \quad p_o = 29.77 \text{ Mev/c}.$$

The values chosen for the physical constants needed to convert from units of gauss-mm to Mev/c are taken from the latest table of Du Mond and Cohen[77]: $c = 2.99792.9 \pm 0.8 \text{ km sec}^{-1}$; $m_o c^2 = 0.510984 \pm 0.000016$ Mev.

As noted in Eq. 6.12, $(p_o)_{II}$ is a function of α, which is determined from Run I. Therefore, since the determination of a mean value for p_o from both runs involves dependent quantities, a simple averaging of the two values is no longer valid. In general, the computations of final mean values for all the other pertinent quantities given below depend upon interrelated parameters. It is necessary in the averaging procedure and in the propagation of errors to express all the equations of Sec VI A only in terms of directly observable and independent quantities. The lengthy details of these calculations are outlined in Appendix F. One thus obtains the weighted mean,

$$\langle p_o \rangle = 29.80 \pm 0.04 \text{ Mev/c}.$$

3. The Pi-Mu Mass Difference. Eq. (6.4)

Run I: $m_\pi - m_\mu = 66.53 \pm 0.10\ m_o$

Run II: $m_\pi - m_\mu = 66.32 \pm 0.10\ m_o$

Mean: $\langle m_\pi - m_\mu \rangle = 66.41 \pm 0.07\ m_o$

4. (a) The Mass of the Positive Muon. Eq. (6.6)

Run I: $m_\mu = 207.2 \pm 1.2\ m_o$

Run II: $m_\mu = 206.6 \pm 1.4\ m_o$

Mean: $\langle m_\mu \rangle = 207.1 \pm 1.1\ m_o$

4. (b) The Mass of the Positive Pion. Eq. (6.5)

Mean: $\langle m_\pi \rangle = 273.5 \pm 1.2\ m_o$

5. The Absolute Kinetic Energy of the Muon

Assuming $m_\nu = 0$,
we have from Eq. (6.7a)

Run I: $T_o = 4.126 \pm 0.017$ Mev

Run II: $T_o = 4.117 \pm 0.023$ Mev

Mean: $\langle T_o \rangle = 4.123 \pm 0.016$ Mev

The mass of the positive pion has been determined accurately and independently from Run I by Smith et al.[41, 42] and found to be $273.3 \pm 0.2\ m_o$. Substituting this value into Eq. (6.7b) along with the value for the π/μ mass ratio, one obtains another estimate for the kinetic energy,

$$T_o = 4.123 \pm 0.038 \text{ Mev} \quad .$$

One can also determine T_o from the usual relativistic energy-momentum mass relation, Eq. (6.8), with no assumptions being made about the mass of the neutrino. For the best estimate of the mass of the muon, we use the Smith pion mass value and divide by the mass ratio α. If one then employs the methods of Appendix F to calculate the weighted value for T_o with its associated probable error, we are led to an extremely cumbersome algebraic expression. The exact solution of this equation involves some rather lengthy calculations, which appear to be unwarranted in view of the magnitude of the statistical probable errors. Therefore, for simplicity, a graphical method is used to eliminate the tedious algebra. In Fig. 19, a family of curves for different values of T_o is plotted as a function of the muon mass and the absolute decay momentum. The hatched region represents the area subtended by the probable errors in p_o and α. Although this is not a rigorous mathematical treatment of the problem, one certainly obtains a good estimate of T_o. The following value is found:

$$T_o = 4.12 \pm 0.02 \text{ Mev} .$$

6. The Mass of the Neutrino (Eq. 6.3)

Here, as in the case for T_o immediately above, the methods of Appendix F lead to algebraic complications. As is readily seen in Fig. 6, the derived mass of the neutrino is extremely sensitive to slight variations in α, p_o, and m_μ. Therefore, because of the statistical uncertainties in the values of these parameters, the exact analytical solution is not attempted and a graphical method is once again applied. Higher accuracy is also achieved if one again replaces m_μ in Eq. (6.3) by the quantity m_π/α, where m_π is the Smith value for the pion mass. The graphical solution is presented in Fig. 20. A family of curves for different values of $\beta\left(\equiv \frac{m_\nu}{m_\mu}\right)$ is plotted as a function of α and the quantity $p_o/m_\pi c$. If one substitutes the final weighted means given above for these parameters into Eq. (6.3) one finds $\beta^2 = 0.0001$, but with an error of $\approx$ 400 to 500 %. Examination of Fig. 20 indicates a probable upper limit to the mass of the neutrino of 6-7 m_o.

IX. CONCLUSIONS

The chief limitation to the experiment and the largest contributor to the various probable errors has been the inherent range straggling of the particles traversing the nuclear emulsion medium.

The absolute positive-pion value of $273.5 \pm 1.2\ m_o$ derived here by assuming $m_\nu = 0$ is in excellent agreement with the value of $273.3 \pm 0.2\ m_o$ found by Smith et al.[41, 42] Employing the Smith pion value in conjunction with this study, one obtains $m_{\mu}^{+} = 206.9 \pm 0.4\ m_o$ from the π/μ mass ratio with no assumptions regarding the mass of the neutral decay particle; on the other hand, if one assumes $m_\nu = 0$, then one gets $m_{\mu}^{+} = 206.9 \pm 0.2\ m_o$ from the calculated mass difference. Finally, from the mass ratio and the mass difference alone, we obtain $m_{\mu}^{+} = 207.1 \pm 1.1\ m_o$, further indicating quantitatively that the assumed decay scheme probably involves a neutrino.

Several theories of meson masses have been advanced in the past few years by different authors.[25] Because present-day theoreticians have not come to any definite conclusions in their efforts to explain the mass spectrum and its role in the theory of nuclear forces, no attempt has been made to relate the results of this study to nuclear theory.

APPENDIX

A. Correction for the Motion of a Particle Out of the Median Plane of the Magnetic Field.

The motion in the z-direction may be described by the differential equation

$$m\ddot{z} = -\frac{e}{c}\, r\dot{\phi}\, H_r \ ,$$

which represents the vertical component of the Lorentz force, assuming no azimuthal variation in the magnetic-field-intensity function.

Integrating with respect to time, we obtain

$$\dot{z} - \dot{z}_1 \equiv \Delta\dot{z} = -\frac{e}{mc}\int_0^t r\dot{\phi}\, H_r\, dt = -\frac{e}{mc}\int_0^{\phi} H_r\, r\, d\phi \qquad (A.2)$$

where $\dot{z}_1$ is the z-component of the velocity at $r = R_1$.

Now $H_r \approx \frac{\partial H_r}{\partial z} z$, and from Maxwell's equations $\frac{\partial H_r}{\partial z} = \frac{\partial H_z}{\partial r}$.

Therefore, we can write [See Eq. 3.8]

$$H_r = \frac{\partial H_r}{\partial r} z \approx 2H_o h_2 rz \ . \qquad (A.3)$$

From Fig. 2, one obtains the approximate geometrical relation (for an assumed circular orbit),

$$r\,d\phi \approx \frac{\rho_o}{r}\,(R\cos\tau - \rho_o)\, d\tau \ . \qquad (A.4)$$

We neglect the initial value of z which at most amounts to 1/4 inch. Since $\frac{z}{\dot{z}} \approx \frac{\rho_o \tau}{\beta c}$, we let $z \approx \frac{\rho_o \tau \dot{z}_1}{\beta c}$ in order to simplify the integration.

The "a posteriori" justification of the assumption, $\dot{z} \approx \dot{z}_1$ follows below.

Substituting the various expressions in the integral, we get

$$\frac{\Delta\dot{z}}{\dot{z}_1} \approx -\frac{e}{c}\, 2h_2\, \frac{H_o \rho_o^2}{m\beta c}\int_0^{\tau}(R\cos\tau - \rho_o)\,\tau\, d\tau \ . \qquad (A.5)$$

Integrating,

$$\frac{\Delta \dot{z}}{\dot{z}_1} \approx 2h_2 \rho_o \left[R \cos \tau + R \tau \sin \tau - R - \frac{\rho_o \tau^2}{2} \right], \tag{A.6}$$

since $\frac{e}{c} H_o \rho_o = m\beta c$ (nonrelativistically). Therefore, the maximum change in the z-component of the velocity becomes

$$\left| \frac{\Delta \dot{z}}{\dot{z}_1} \right|_{max.} \approx 2h_2 \rho_o R (\pi/2 - 1). \tag{A.7}$$

We now introduce the familiar parameter n, defined as $n \equiv \frac{r}{H} \frac{\partial H_z}{\partial r} \approx 2h_2 r^2$. Substituting, assuming n to be constant over this small region, and letting $r \approx R$, we finally obtain the equation

$$\left| \frac{\Delta \dot{z}}{\dot{z}_1} \right|_{max.} = (\pi/2 - 1) \frac{n\rho_o}{R} . \tag{3.15}$$

Since $\rho_o/R \approx \frac{1}{20}$ for the π-mesons and $n \approx 0.07$, then

$$\left| \frac{\Delta \dot{z}}{\dot{z}_1} \right|_{max} \approx 2.4 \times 10^{-3} ,$$

indicating the previous assumption to be quite justified.

B. Effects of the Finite Size of the Target and of the Detector

Once again, we make use of the slow variation of the magnetic-field-intensity function to derive certain geometrical relations necessary for the determination of the magnitudes of the finite target and detector effects. Hence, we assume circular orbits for the particles under study. The magnitudes of these effects as calculated under this circular approximation are quite small. Thus, further calculations involving the true orbits -- besides being difficult -- would be mere perturbations on an already small effect.

We define a rectangular coordinate system such that the origin (0, 0, 0) is located at the target center. The unprimed coordinates (x, y, z) refer to the target and the primed coordinates (x', y', z') to the detector plate. The orbit of the particle crosses the x-axis at the point $x' = x_o$ making an angle θ' with the y-axis. In this experiment, the plate was inclined at an angle ϵ with respect to the xy-plane. Therefore, we assume the emulsion surface to lie in the plane $z' = -z_o - \epsilon y'$ with $x_o \gg z_o$ and $\epsilon \ll 1$. The positive x-direction is established in the direction of increasing cyclotron radius. The pertinent geometrical relations of the orbit are illustrated in Fig. 3.

From Eq. (3.14) we have $\rho_l = \rho_r \sec \gamma$ where ρ_l is the "total" radius or the orbit, ρ_r is the radius in the median plane, and γ is the angle the orbit makes with the median plane. Now,

$$\tan \gamma = \frac{-z_o + \epsilon y' + z}{\rho_r (\pi - 2\alpha - 2\alpha' - 2\theta')} \tag{B.1}$$

where $\alpha = \tan^{-1} \frac{y}{x_o - x} \approx \frac{y}{x_o - x}$, and $\alpha' \approx \tan^{-1} \frac{y'}{x_o} \approx \frac{y'}{x_o}$

Therefore we have .

$$\sec^2 \gamma = 1 + \frac{\left(-z_o + \epsilon y' + z\right)^2}{\rho_r^2 (\pi - 2\alpha - 2\alpha' - 2\theta)^2} . \tag{B.2}$$

Substituting,

$$\rho_l^2 = \rho_r^2 + \frac{\left(-z_o + \epsilon y' + z\right)^2}{\left(\pi - 2\alpha - 2\alpha' - 2\theta\right)^2} . \tag{B.3}$$

As is readily seen in Fig. 3, $\rho_r = \dfrac{L}{2\cos(\theta' + a)}$, where $L = \dfrac{x_o - x}{\cos a}$.

Therefore we obtain the relation

$$\rho_r = \frac{(x_o - x)\sec(\theta' + a)\sec a'}{2} \quad . \tag{B.4}$$

The entire expression for the true radius of the trajectory becomes

$$\rho_1 = \left[\frac{(x_o - x)^2 \sec^2(\theta' + a)\sec^2 a}{4} + \frac{(z_o + \epsilon y' + z)^2}{(\pi - 2a - 2a' - 2\theta')^2}\right]^{1/2} \quad . \tag{B.5}$$

The apparent radius ρ is calculated assuming all mesons originated from the center of the target (i.e. $x = y = z = 0$). One employs the relation $\rho = \dfrac{x_o}{2}\sec\theta' \sec\gamma_o$, where $\gamma_o = \tan^{-1}\dfrac{2z_o}{\pi x_o}$. One then obtains the following equations:

$$\rho\cos\gamma_o = \frac{x_o}{2}\sec\theta'; \quad \rho\sin\gamma_o\cos\theta' = \frac{z_o}{\pi} \quad . \tag{B.6}$$

Rewriting Eq. (B.5),

$$\rho_1 = \left[\frac{x_o^2\left(1 - \dfrac{x}{x_o}\right)^2 \sec^2(\theta' + a)\sec^2 a}{4} + \frac{z_o^2}{\pi^2}\left(\frac{1 + \dfrac{\epsilon y'}{z_o} + \dfrac{z}{z_o}}{1 - \dfrac{2\phi}{\pi}}\right)^2\right]^{1/2} , \tag{B.7}$$

where $\phi = a + a' + \theta'$.

We wish to expand Eq. (B.7) through small quantities of the third order.

Now $\sec(\theta' + a) = \dfrac{1}{\cos(\theta' + a)} = \dfrac{1}{\cos\theta'\cos a - \sin\theta'\sin a}$

$$= \frac{\sec\theta'}{\left(1 - \dfrac{a^2}{2} - \theta' a + \cdots\right)} \quad .$$

Therefore, $\sec^2(\theta' + a)\sec^2 a \approx \sec^2\theta'(1 + 2a^2 + 2\theta' a)$. (B.8)

Substituting in Eq. (B. 7),

$$\rho_1 \approx \left[x_o^2 \left(1 - \frac{2x}{x_o} + \frac{x^2}{x_o^2} \right) \sec^2 \theta' \, (1 + 2a^2 + 2\theta' a) \right. \tag{B.9}$$

$$+ \frac{z_o^2}{\pi^2} \left(1 + \frac{2\epsilon y'}{z_o} + \frac{2z}{z_o} + \frac{2\epsilon y' z}{z_o^2} + \frac{\epsilon^2 y'^2}{z_o^2} + \frac{z^2}{z_o^2} \right)$$

$$\left. \left(1 + \frac{4\phi}{\pi} + \frac{12\phi^2}{\pi^2} + \frac{32\phi^3}{\pi^3} \right) \right]^{1/2}$$

Employing the relations of Eq. (B. 6), one obtains

$$\rho_1 \approx \left[\rho^2 \cos^2 \gamma_o \left(1 - \frac{2x}{x_o} + \frac{x^2}{x_o^2} \right) \left(1 + 2a^2 + 2\theta' a \right) + \rho^2 \sin^2 \gamma_o \right.$$

$$\left(1 - \theta'^2 \right) \left(1 + \frac{2\epsilon y'}{z_o} + \frac{2z}{z_o} + \frac{2\epsilon y' z}{z_o^2} + \frac{\epsilon^2 y'^2}{z_o^2} + \frac{z^2}{z_o^2} \right)$$

$$\left. \left(1 + \frac{4\phi}{\pi} + \frac{12\phi^2}{\pi^2} + \cdots \right) \right]^{1/2}$$

$$\approx \rho \left[1 + \cos^2 \gamma_o \left(- \frac{2x}{x_o} + \frac{x^2}{x_o^2} + 2a^2 + 2\theta' a - \frac{4x a^2}{x_o} - \frac{4x\theta' a}{x_o} \right) \right. \tag{B.10}$$

$$+ \sin^2 \gamma_o \left(\frac{2\epsilon y'}{z_o} + \frac{2z}{z_o} + \frac{2\epsilon y' z}{z_o^2} + \frac{z^2}{z_o^2} + \frac{4\phi}{\pi} \right.$$

$$\left. \left. + \frac{8z\phi}{\pi z_o} + \frac{4\phi z^2}{\pi z_o^2} \right) \right]^{1/2} .$$

We are interested in the quantity $\langle \rho_1^{\eta} \rangle$. Therefore we raise the above expression to the η^{th} power, and expand still further. Since

$$\sin^2 \gamma_o \approx \frac{4z_o^2}{\pi^2 x_o^2} \quad \text{and} \quad \cos^2 \gamma_o = 1 - \frac{4z_o^2}{\pi^2 x_o^2},$$ we have

$$\rho_1^{\eta} \approx \rho^{\eta} \left[1 - \frac{2x}{x_o} + \frac{x^2}{x_o^2} + \frac{2y^2}{x_o^2} + \frac{4xy^2}{x_o^3} + \frac{2\theta' y}{x_o} + \frac{2\theta' yx}{x_o^2} - \frac{4xy^2}{x_o^3} \right.$$

$$- \frac{4x\theta' y}{x_o^2} + \frac{8x z_o^2}{\pi^2 x_o^3} + \frac{8 z_o \epsilon y'}{\pi^2 x_o^2} + \frac{8 z z_o}{\pi^2 x_o^2} + \frac{8\epsilon y' z}{\pi^2 x_o^2}$$

$$\left. + \frac{4z^2}{\pi^2 x_o^2} + \frac{16 (z_o + z)^2 \phi}{\pi^3 x_o^2} \right]^{\eta/2} \qquad \text{(B.11)}$$

Therefore, from the binomial theorem;

$$\rho_1^{\eta} \approx \rho^{\eta} \left\{ 1 + \frac{\eta}{2} \left[- \frac{2x}{x_o} + \frac{x^2}{x_o^2} + \text{- - - -} + \frac{4z^2}{\pi^2 x_o^2} + \frac{16 (z_o + z)^2 \phi}{\pi^3 x_o^2} \right] \right.$$

$$+ \frac{\eta (\eta - 2)}{8} \left[\frac{4x^2}{x_o^2} - \frac{4x^3}{x_o^3} - \frac{8xy^2}{x_o^3} - \frac{8xy\theta'}{x_o^2} - \frac{32 xz z_o}{\pi^2 x_o^3} \right.$$

$$\left. \left. - \frac{16 xz^2}{\pi^2 x_o^3} \right] + \frac{\eta (\eta - 2) (\eta - 4)}{48} \left[\frac{8x^3}{x_o^3} \right] \right\}. \qquad \text{(B.12)}$$

Collecting terms of different orders, and averaging, we finally get

$$\rho_1^{\eta} \approx \rho^{\eta} \left[1 - \eta \frac{\langle x \rangle}{x_o} + \frac{\eta(\eta-1)\langle x^2 \rangle}{2 x_o^2} + \frac{\eta \langle y^2 \rangle}{x_o^2} + \frac{\eta \langle y\, \theta' \rangle}{x_o} \right.$$

$$+ \frac{4\eta z_o \langle z \rangle}{\pi^2 x_o^2} + \frac{2\eta \langle z^2 \rangle}{\pi^2 x_o^2} + \frac{8\eta \langle (z_o + z)^2 (\theta' + y/x_o + y'/x_o) \rangle}{\pi^3 x_o^2}$$

$$+ \frac{4\eta z_o^2 \langle x \rangle}{\pi^2 x_o^3} - \frac{\eta(\eta-1)\langle x\, y\, \theta' \rangle}{x_o^2} + \frac{4\eta z_o \epsilon \langle y' \rangle}{\pi^2 x_o^2}$$

$$+ \frac{4\eta \epsilon \langle y' z \rangle}{\pi^2 x_o^2} - \frac{\eta(\eta-2)\langle x y^2 \rangle}{x_o^3} - \frac{2\eta(\eta-2)\langle x z^2 \rangle}{\pi^2 x_o^3}$$

$$\left. - \frac{4\eta(\eta-2) z_o \langle x z \rangle}{\pi^2 x_o^3} - \frac{\eta(\eta-1)(\eta-2)\langle x^3 \rangle}{6 x_o^3} \right] \qquad (3.17)$$

C. Statistical Calculation of the Mass Ratio

1. The Mean Value of $R_1 p^{-q}$

Let $U(p_1, p)\, dp_1$ be the probability that the true momentum lies between p_1 and $p_1 + dp_1$ when the apparent momentum is p. Let $V(R_1, p_1)\, dR_1$ be the probability that the observed track length lies between R_1 and $R_1 + dR_1$ when the momentum is p_1. Finally, let $W(p)\, dp$ be the fraction of the measured values of the apparent momentum that lie between p and $p + dp$. Therefore we may write in the usual manner

$$\left\langle R_1 p^{-q} \right\rangle = \int_p \int_{p_1} \int_{R_1} R_1 p^{-q}\ W(p)\ U(p_1, p)\ V(R_1, p_1)\ dR_1\, dp_1\, dp \quad . \tag{5.2}$$

Integrating first with respect to R_1, we have

$$\int_{R_1} R_1\, V(R_1, p)\, dR_1 = R(1 + \tau), \tag{4.24}$$

where τ is insensitive to the velocity of the meson. [See Eq. (4.18) for the definition of τ]. We have the ideal range-momentum relation,

$$R = C_o\, M^{1 - q_o}\, p_1^{\,q_o} \quad ,$$

where M is the mass of the particle expressed in units of the proton mass and q_o is the true value of the exponent of the range-momentum equation. Because of the Lewis Effect, q_o differs in principle from the q obtained by the proton range-energy data by $\approx p_1 \dfrac{d\tau_1}{dp_1}$ ($\approx 0.01\%$ in this experiment). Therefore, continuing with the integration,

$$\left\langle R_1 p^{-q} \right\rangle = C_o (1 + \tau)\, M^{1 - q_o} \int_p \int_{p_1} p^{-q}\, W(p)\, p_1^{\,q_o}\, U(p_1, p)\, dp_1, dp \quad . \tag{C.1}$$

But

$$\int_{p_1} p_1^{\,q_o}\, U(p_1, p)\, dp_o = p^{\,q_o} (1 + \omega_q) \quad . \tag{3.16}$$

Hence for the integration over the third variable, p, we have:

$$\left\langle R_1 p^{-q} \right\rangle = C_o (1+\tau)\ 1+\omega_q\ M^{1-q_o} \int_p p^{q_o - q} W(p)\, dp \quad . \tag{C.2}$$

Let $p = \langle p \rangle + \delta p$. Then

$$p^{q_o - q} = \langle p \rangle^{q_o - q} \left[1 + \frac{\delta p}{\langle p \rangle}\right]^{q_o - q} = \langle p \rangle^{q_o - q} \left[1 + \frac{p - \langle p \rangle}{\langle p \rangle}\right]^{q_o - q} . \tag{C.3}$$

Substituting and expanding,

$$\left\langle R_1 p^{-q} \right\rangle = C_o M^{1-q_o} \langle p \rangle^{q_o - q} \left[1 + \omega_q + \tau + \frac{(q_o - q)(q_o - q - 1)}{2} \frac{\sigma_p^2}{\langle p^2 \rangle} + \ldots\right] .$$

But $(q_o - q)(q_o - q - 1) \approx q - q_o$ since $|q_o - q| \ll 1$. Therefore

$$\left\langle R_1 p^{-q} \right\rangle \approx C_o M^{1-q_o} \langle p \rangle^{q_o - q} \left[1 + \omega_q + \tau + \frac{(q - q_o)}{2} \frac{\sigma_p^2}{\langle p \rangle^2}\right], \tag{5.3}$$

where $\sigma_p^2 = \int (p - \bar{p})^2\ W(p)\, dp$; and τ and ω_q are both $\ll 1$.

Since the sign in $(q_o - q)$ is unknown, we choose $\langle q_o - q \rangle = 0$

2. The variance of $R_1 p^{-q}$.

The variance is defined as

$$\sigma^2 = \left\langle R_1^2\ p^{-2q} \right\rangle - \left\langle R_1 p^{-q} \right\rangle^2 \quad . \tag{C.5}$$

From Eq. (5.3) we obtain

$$\left\langle R_1 p^{-q} \right\rangle^2 = C_o^2 M^{2-2q_o} \langle p \rangle^{2q_o - 2q} \left[1 + 2\omega_q + 2\tau + (q - q_o) \frac{\sigma_p^2}{\langle p \rangle^2} + \ldots\right] .$$

(C.6)

As before, one has

$$\left\langle R_1^2\, p^{3q} \right\rangle = \int_p \int_{p_1} \int_{R_1} R_1^2\, p^{-2q}\, W(p)\, U(p_1, p)\, V(R_1, p_1)\, dR_1\, dp_1\, dp \qquad (C.7)$$

$$\text{Let } R_1 = \langle R_1 \rangle + \delta R_1 = \langle R_1 \rangle \left(1 + \frac{\delta R_1}{R_1}\right) = \langle R_1 \rangle \left(1 + \frac{R_1 - R_1}{R_1}\right)$$

But

$$\langle R_1 \rangle = R(1+\tau) = C_o M^{1-q_o}\, p_1^{q_o}\, (1+\tau)$$

Therefore, we have

$$\left\langle R_1^2\, p^{-2q} \right\rangle = C_o^2\, M^{2-2q_o}\, (1+\tau)^2 \left(1 + \frac{\sigma_R^2}{\langle R_1 \rangle^2}\right) \int\int p^{-2q}\, p_1^{-2q_o}\, W(p)\, U(p_1, p)\, dp\, dp_1 \qquad (C.8)$$

From previous discussions, (see Appendix B), one can write

$$\int p_1^{2q_o}\, W(p_1, p)\, dp_1 = p^{2q_o} \left(1 + \omega_{2q}\right) . \qquad (C.9)$$

Substituting within the integral, one obtains

$$\begin{aligned}
\left\langle R_1^2\, p^{-2q} \right\rangle &= C_o^2\, M^{2-2q_o}\, (1+\tau)^2 \left(1 + \frac{\sigma_R^2}{R_1^2}\right)\left(1 + \omega_{2q}\right) \int_p p^{2q_o - 2q}\, W(p)\, dp \\
&= C_o^2\, M^{2-2q_o} \left(1 + \frac{\sigma_R^2}{\langle R_1 \rangle}\right) \left(1 + \omega_{2q}\right) \left[1 + (q - q_o)\, \frac{\sigma_p^2}{\langle p \rangle^2}\right] \langle p \rangle^{2q_o - 2q} \\
&= C_o^2\, M^{2-2q_o} \left[1 + 2\tau + \frac{\sigma_R^2}{\langle R_1 \rangle^2} + \omega_{2q} + (q - q_o)\, \frac{\sigma_p^2}{\langle p \rangle^2}\right] \langle p \rangle^{2q_o - 2q} .
\end{aligned} \qquad (C.10)$$

Substituting in the definition of the variance,

$$\sigma^2 \equiv \left\langle R_1^2\, p^{-2q} \right\rangle - \left\langle R_1\, p^{-q} \right\rangle^2 = C_o^2\, M^{2-2q_o} \langle p \rangle^{2q_o - 2q} \left[\omega_{2q} - 2\omega_q + \frac{\sigma_R^2}{\langle R_1 \rangle^2} \right] \tag{C.11}$$

From Eqs. (2.9), (3.16), and (4.24), we have:

$$C_o^2\, M^{2-2q_o} \langle p \rangle^{2q_o} = \langle R_1 \rangle^2 \left[1 - 2\omega_q - 2\tau \right] . \tag{C.12}$$

Substituting in our expression for the variance (Eq. C.11) and neglecting second-order terms in ω_q and τ, we get

$$\sigma^2 \approx \langle p \rangle^{2q} \left[\sigma_R^2 + R_1^2 \left(\omega_{2q} - 2\omega_q \right) \right] . \tag{5.4}$$

3. The Mass Ratio

If we use the average value of the observed quantity $R_1\, p^{-q}$ instead of $R\, p_1^{-q}$, it leads to an apparent mass ratio a', defined by

$$a' = \frac{\left\langle R_{1\pi}\, p_\pi^{-q} \right\rangle}{\left\langle R_{1\mu}\, p_\mu^{-q} \right\rangle} . \tag{5.1}$$

The true mass ratio is expressed by

$$a = \frac{\left\langle R_\pi\, p_{1\pi}^{-q} \right\rangle}{\left\langle R_\mu\, p_{1\mu}^{-q} \right\rangle} . \tag{C.13}$$

Employing Eq. (5.3),

$$a'^{1-q} = a^{1-q_o} \left[\frac{\langle p_\pi \rangle}{\langle p_\mu \rangle} \right]^{q_o - q} \left[\frac{1 + \tau_{1\pi} + \omega_{q_\pi}}{1 + \tau_{1\mu} + \omega_{q_\mu}} \right] \tag{C.14}$$

We assume $\langle s - s_o \rangle = 0$ since we do not know the sign of the uncertainty in the shrinkage factor. Therefore $\tau_{2\pi} = \tau_{2\mu} = 0$. Similarly $\langle q - q_o \rangle$ is set = 0 .

Therefore,

$$a'^{1-q} \approx a^{1-q_o} \left[1 + \left(\tau_{1\pi} - \tau_{1\mu}\right) + \left(\omega_{q_\pi} - \omega_{q_\mu}\right)\left[\frac{\langle p_\pi \rangle}{\langle p_\mu \rangle}\right]\right]^{q_o - q} \quad . \tag{C.15}$$

Let us define r so that

$$\frac{\langle p_\pi \rangle}{\langle p_\mu \rangle} \equiv a\,(1 + r) \quad , \quad r \ll 1 \quad . \tag{5.5}$$

Substituting,

$$\begin{aligned} a'^{1-q} &\approx a^{1-q_o}\left[1 + \left(\tau_{1\pi} - \tau_{1\mu}\right) + \left(\omega_{q_\pi} - \omega_{q_\mu}\right)\right]\left[a\,(1 + r)\right]^{q_o - q} \\ &\approx a^{1-q}\left[1 + \left(\tau_{1\pi} - \tau_{1\mu}\right) + \left(\omega_{q_\pi} - \omega_{q_\mu}\right)\right] \quad . \end{aligned} \tag{C.16}$$

Therefore, we obtain

$$a = a'\left[1 + \frac{\tau_{1\pi} - \tau_{1\mu}}{q - 1} + \frac{\omega_{q_\pi} - \omega_{q_\mu}}{q - 1}\right] \quad . \tag{5.6}$$

4. The Statistical Uncertainty in the Mass Ratio.

From Eqs. (C. 4), (C. 13), and (5. 5) we have

$$a = a'\,(1 + r)^{\frac{q_o - q}{1 - q}}\left[1 + \frac{\left(\tau_\pi - \tau_\mu\right)}{q - 1} + \frac{\left(\omega_{q_\pi} - \omega_{q_\mu}\right)}{q - 1} + \frac{q - q_o}{2\,(1 - q)}\left(\frac{\sigma_{p_\pi}^2}{\langle p_\pi \rangle^2} - \frac{\sigma_{p_\mu}^2}{\langle p_\mu \rangle^2}\right)\right] \tag{C.17}$$

Recalling that $\tau = \tau_1 + \tau_2$, where $\tau_1 = \frac{1}{612\ M\ \ell n\ 3780\ \beta^2}$ and $\tau_2 = \frac{S - S_o}{S_o} \langle \sin^2 \gamma_1 \rangle$, and defining the uncertainties in q and s as σ_q and σ_s, respectively, one obtains

$$\frac{\sigma_a^2}{a^2} = \frac{\sigma_{a'}^2}{a'^2} + \frac{\sigma_q^2}{4\,(q-1)^2}\left(\frac{\sigma_{p_\pi}^2}{\langle p_\pi \rangle^2} - \frac{\sigma_{p_\mu}^2}{\langle p_\mu \rangle^2} - 2r\right)^2 \qquad \text{(C.18)}$$

$$+ \frac{\sigma_s^2}{(q-1)^2}\left(\langle \sin^2 \gamma_{1\pi} \rangle - \langle \sin^2 \gamma_{1\mu} \rangle\right)^2,$$

where σ_a^2 and $\sigma_{a'}^2$ are the statistical uncertainties in the true and apparent mass ratios, respectively.

If there are n_π observations of $R_{1\pi}\, p_\pi^{-q}$ and n_μ observations of $R_{1\mu}\, p_\mu^{-q}$, the statistical uncertainty in the mass ratio can be expressed as

$$\sigma_a^2 = \frac{a^2}{(q-1)^2}\left[\frac{\sigma_\pi^2}{n_\pi \langle R_{1\pi}\, p_\pi^{-q} \rangle^2} + \frac{\sigma_\mu^2}{n_\mu \langle R_{1\mu}\, p_\mu^{-q} \rangle^2}\right.$$

$$+ \frac{\sigma_q^2}{4}\left(\frac{\sigma_{p_\pi}^2}{\langle p_\pi \rangle^2} - \frac{\sigma_{p_\mu}^2}{\langle p_\mu \rangle^2} - 2r\right)^2$$

$$\left. + \frac{\sigma_s^2}{S^2}\left(\langle \sin^2 \gamma_{1\pi} \rangle - \langle \sin^2 \gamma_{1\mu} \rangle\right)^2\right]. \qquad \text{(5.7)}$$

D. Dynamics of π - μ Decay

One assumes the decay scheme $\pi \rightarrow \mu + \nu$, where ν represents a neutral particle, presumably a neutrino. For a pion decaying while at rest, one can write the relativistic conservation-of-energy and momentum equations as follows:

$$m_\pi c^2 = \sqrt{p_\mu^2 + m_\mu^2 c^4} + \sqrt{p_\nu^2 c^2 + m_\nu^2 c^4} \quad ; \tag{6.1}$$

$$p_\mu = p_\nu \, . \tag{6.2}$$

1. Mass of Neutrino

For simplicity let $m_\pi / m_\mu = a$ and $m_\nu / m_\mu = \beta$.

Also let $p_\mu = p_o$, the full decay momentum.

Substituting the momentum equation in the energy expression, and performing the algebra, we have

$$\frac{m_\pi}{m_\mu} = a = \sqrt{\left(\frac{p_o}{m_\mu c}\right)^2 + 1} + \sqrt{\left(\frac{p_o}{m_\mu c}\right)^2 + \beta^2} \, . \tag{D.1}$$

Transposing and squaring both sides of Eq. (D.1), we have

$$a^2 - 2a\sqrt{\left(\frac{p_o}{m_\mu c}\right)^2 + 1} + 1 + \left(\frac{p_o}{m_\mu c}\right)^2 = \left(\frac{p_o}{m_\mu c}\right)^2 + \beta^2 \, . \tag{D.2}$$

Therefore,

$$a^2 + 1 - \beta^2 = 2a\sqrt{1 + \left(\frac{p_o}{m_\mu c}\right)^2} \, . \tag{D.3}$$

Solving for β^2, we get

$$\beta^2 = a^2 + 1 - 2a\sqrt{1 + \left(\frac{p_o}{m_\mu c}\right)^2} \quad . \tag{D.4}$$

or

$$m_\nu = m_\mu \left[a^2 + 1 - 2a\sqrt{1 + \left(\frac{p_o}{m_\mu c}\right)^2} \right]^{1/2} \quad . \tag{6.3}$$

2. Pion-Muon Mass Difference

If one now assumes $m_\nu = 0$, we have from Eq. (6.3)

$$a^2 + 1 = 2a\sqrt{1 + \left(p_o/m_\mu c\right)^2} \quad . \tag{D.5}$$

Squaring once again,

$$\left(a^2 + 1\right)^2 = 4a^2 + \frac{4a^2 p_o^2}{m_\mu^2 c^2} \tag{D.6}$$

or

$$\left(a^2 - 1\right)^2 = \frac{4a^2 p_o^2}{m_\mu^2 c^2} \tag{D.7}$$

Therefore,

$$\left(a + 1\right)\left(a - 1\right) = \frac{2a\, p_o}{m_\mu c} \tag{D.8}$$

Since we have $a = m_\pi / m_\mu$, we can write

$$\left(m_\pi - m_\mu\right) c^2 = \frac{2a}{a+1} \; p_o c \; . \tag{6.4}$$

3. Mass of Muon

Under the assumption that $m_\nu = 0$, we can also solve Eq. (6.3) for the mass of the μ-meson. Consequently,

$$m_\mu c^2 = \frac{2a}{a^2 - 1} \; p_o c \; . \tag{6.6}$$

4. Kinetic Energy of Muon from Pion Decaying at Rest

The quantity T_o will refer to the kinetic energy of the μ-meson at the time of creation. Rewriting the conservation equations in terms of the kinetic energy T_o, we have

$$m_\pi c^2 = m_\mu c^2 + T_o + m_\nu c^2 + T_\nu$$

$$= m_\mu c^2 + T_o + \sqrt{p_o^2 c^2 + m_\nu c^4} \; , \tag{D.9}$$

since $p_\nu = p_o$. Continuing,

$$m_\pi c^2 = m_\mu c^2 + T_o + \sqrt{m_\mu^2 c^4 + 2m_\mu c^2 \; T_o + T_o^2 + m_\nu^2 c^4} \; . \tag{D.10}$$

Or, transposing and squaring,

$$\left[\left(m_\pi - m_\mu\right) c^2 - T_o \right]^2 = m_\mu^2 c^4 + m_\nu^2 c^4 + 2m_\mu c^2 \; T_o + T_o^2 \tag{D.11}$$

Expanding, and substituting $a = m_\pi/m_\mu$, one obtains

$$(a-1)^2 - \frac{2\,T_o}{m_\mu c^2}(a-1) + \frac{T_o^2}{\left(m_\mu c^2\right)^2} = 1 + \frac{2\,T_o}{m_\mu c^2} + \beta^2 + \frac{T_o^2}{\left(m_\mu c^2\right)^2} . \tag{D.12}$$

Solving for T_o,

$$T_o = m_\mu c^2 \left[\frac{(a-1)^2 - \beta^2}{2a} \right] . \tag{D.13}$$

Substituting the expression for $m_\mu c^2$ as given in Eq. (6.6) and letting $\beta = 0$,

$$T_o = \left[\frac{2a}{a^2-1}\, p_o c\right]\left[\frac{(a-1)^2}{2a}\right] \tag{D.14}$$

or,

$$T_o = \frac{a-1}{a+1}\, p_o c . \tag{6.7a}$$

If one now solves for $p_o c$ in Eq. (6.6) and replaces m_μ with m_π/a, one obtains the alternate expression

$$T_o = \frac{(a-1)^2}{2a^2}\, m_\pi c^2 . \tag{6.7b}$$

E. Correction to Mean Range of Mu-Completes

It can easily be shown geometrically that the probability of a particle's remaining within the emulsion is approximately equal to $t/2R$ if $R > t$, where t is the thickness of the emulsion and R is the residual range of the particle within the emulsion. If one assumes that the tracks of the monoenergetic particles are straight, all tracks originating from a point will lie on a sphere of surface area equal to $4\pi R^2$. If the tracks are then presumed to originate at any depth within the emulsion, the area of the surface subtended by the emulsion is equal to $2\pi Rt$. Therefore the probability of remaining within the emulsion becomes

$$\frac{2\pi Rt}{4\pi R^2} = \frac{t}{2R} \quad .$$

Let R_μ be the calculated mean range of the μ-completes. Analytically one has

$$\langle R_\mu \rangle = \frac{\int R\, N(R)\, dR}{\int N(R)\, dR} \quad . \tag{E.1}$$

Assuming a Gaussian range-distribution function, and introducing the probability factor, one can write

$$\langle R_\mu \rangle = \frac{\int_R e^{-\frac{(R - \langle R_o \rangle)^2}{2\sigma_{R_o}^2}} R\, dR}{\int_R e^{-\frac{(R - \langle R_o \rangle)^2}{2\sigma_{R_o}^2}} dR} \equiv \frac{I_1}{I_2} \quad , \tag{E.2}$$

where $\sigma_{R_o}^2$ is the true variance of the range distribution, and $\langle R_o \rangle$ is the true mean.

Integrating the numerator, one obtains

$$I_1 = \sqrt{2\pi}\ \sigma_{R_o} \quad . \tag{E.3}$$

To evaluate I_2, let $R = \langle R_o \rangle + \epsilon$. Therefore $dR = d\epsilon$.

Substituting,

$$I_2 = \frac{1}{\langle R_o \rangle} \frac{\int_e^{\infty} \frac{\epsilon^2}{2\sigma_{R_o}^2} d\epsilon}{1 + \epsilon / \langle R_o \rangle} \qquad \text{(E. 4)}$$

Expanding Eq. (E. 4),

$$I_2 \approx \frac{1}{\langle R_o \rangle} \int \left(1 - \frac{\epsilon}{\langle R_o \rangle} + \frac{\epsilon^2}{\langle R_o \rangle^2} - \frac{\epsilon^3}{\langle R_o \rangle^3} + \cdots\right) e^{-\frac{\epsilon^2}{2\sigma_{R_o}^2}} d\epsilon \quad . \qquad \text{(E. 5)}$$

Integrating,

$$I_2 \approx \frac{\sqrt{2\pi}\ \sigma_{R_o}}{\langle R_o \rangle} \left(1 + \frac{\sigma_o^2}{\langle R_o \rangle^2} + \frac{3\sigma_o^4}{\langle R_o \rangle^4} + \cdots\right) . \qquad \text{(E. 6)}$$

Therefore,

$$\langle R_\mu \rangle = \frac{I_1}{I_2} \approx \frac{\langle R_o \rangle}{1 + \frac{\sigma_{R_o}^2}{\langle R_o \rangle^2} + \frac{3\sigma_{R_o}^4}{\langle R_o \rangle^4}} \approx \langle R_o \rangle \left(1 - \frac{\sigma_{R_o}^2}{\langle R_o \rangle^2} - \frac{2\sigma_{R_o}^4}{\langle R_o \rangle^4} + \cdots\right) \qquad \text{(E. 7)}$$

As σ_{R_o} is unknown, we wish to replace it by the experimental estimate of the straggling, $\sigma_{R_\mu}^2$. Let

$$\sigma_{R_\mu}^2 = \frac{\int \left(R - \langle R_\mu \rangle\right)^2 \frac{e^{-\frac{\left(R - \langle R_o \rangle\right)^2}{2\sigma_{R_o}^2}}}{R} dR}{I_2} \equiv \frac{I_3}{I_2} \quad . \qquad \text{(E. 8)}$$

Now let $\langle R_\mu \rangle = \langle R_o \rangle + \delta = \langle R_o \rangle \left(1 + \frac{\delta}{\langle R_o \rangle}\right)$. Therefore $R - \langle R_\mu \rangle = \epsilon - \delta$.

Substituting,

$$I_3 = \int \frac{(\epsilon - \delta)^2 \; e^{-\frac{\epsilon^2}{2\sigma_{R_o}^2}} \; d\epsilon}{\langle R_o \rangle + \epsilon} \quad . \tag{E.9}$$

Expanding,

$$I_3 \approx \frac{1}{\langle R_o \rangle} \int e^{-\frac{\epsilon^2}{2\sigma_{R_o}^2}} \left(1 - \frac{\epsilon}{\langle R_o \rangle} + \frac{\epsilon^2}{\langle R_o \rangle^2} - \frac{\epsilon^3}{\langle R_o \rangle^4} + \cdots\right)\left(\epsilon^2 - 2\delta\epsilon + \delta^2\right) d\epsilon \tag{E.10}$$

All odd powers in the integrand may be dropped, since they integrate out to zero. Therefore, collecting the remaining terms and integrating,

$$I_3 \approx \frac{\sqrt{2\pi}\,\sigma_{R_o}}{\langle R_o \rangle} \left[\delta^2 + \left(1 + \frac{\delta}{\langle R_o \rangle}\right)^2 \sigma_{R_o}^2 + 3\left(\frac{\delta^2}{\langle R_o \rangle^4} + \frac{2\delta}{\langle R_o \rangle^3} + \frac{1}{\langle R_o \rangle^2}\right) \sigma_{R_o}^4\right] . \tag{E.11}$$

Substituting and performing the algebra, one obtains

$$\sigma_{R_\mu}^2 = \frac{I_3}{I_2} \approx \delta^2 + \sigma_{R_o}^2 \left(1 + \frac{2\delta}{\langle R_o \rangle}\right) + \frac{2\sigma_{R_o}^4}{\langle R_o \rangle^2} \left(1 + \frac{2\delta}{\langle R_o \rangle}\right) . \tag{E.12}$$

From Eq. (E. 7) we have, to the second order of small quantities,

$$\langle R_\mu \rangle \approx \langle R_o \rangle \left(1 - \frac{\sigma_{R_o}^2}{R_o^2}\right) , \tag{E.13}$$

or

$$\langle R_o \rangle \approx \langle R_\mu \rangle + \frac{\sigma_{R_o}^2}{\langle R_o \rangle} \approx \langle R_\mu \rangle + \frac{\sigma_{R_\mu}^2}{\langle R_o \rangle + 2\delta} - \frac{\delta^2}{\langle R_o \rangle} \quad . \tag{E.14}$$

But by definition, $\langle R_o \rangle = \langle R_\mu \rangle - \delta$; therefore

$$\langle R_o \rangle \approx \langle R_\mu \rangle + \frac{\sigma_{R_\mu}^2}{\langle R_\mu \rangle}(1 - \delta) - \frac{\delta^2}{\langle R_\mu \rangle} . \qquad (E.15)$$

As $\delta^2 << \sigma_{R_\mu}^2$ and $\delta << 1$, we finally obtain

$$\langle R_o \rangle \approx \langle R_\mu \rangle + \frac{\sigma_{R_\mu}^2}{\langle R_\mu \rangle} . \qquad (8.1)$$

F. The Propagation of Errors

The π/μ mass ratio a is determined solely from Run I with an uncertainty expressed by Eq. (5.7). The relative magnitudes of the terms contributing to the total error in a are such that uncertainties introduced by the σ_s^2 and σ_q^2 terms are essentially negligible. Therefore, in the following discussion, those terms which are functions of σ_s^2 and σ_q^2 will be omitted for the purpose of simplicity.

Unlike the case of a, all other experimental values are averaged over both Runs I and II. Since the individual means obtained from each of the runs are not completely independent of one another, the usual simple averaging procedure is no longer valid. It is therefore necessary to express all the pertinent equations of Sec. VIA in terms of directly observable and independent parameters.

The following detailed analysis gives a sample of the procedure employed in obtaining final mean values for the meson masses and their related quantities, T_o and p_o.

In Run I, the absolute momentum p_o is determined from the relation

$$(p_o)_I \left[\frac{\langle R_o \rangle}{\langle R_{1\mu}\, p_\mu^{-q} \rangle}\right]^{1/q} \left[1 + \frac{\tau_\mu - \tau_o}{q} + \frac{\omega_{q_\mu}}{q}\right] . \qquad (6.10)$$

In Run II,

$$\left(p_o\right)_{II} = \left[\frac{\left\langle R_o' \right\rangle}{a^{q-1}\left\langle R'_{1\pi}\ p'^{-q}_{\pi} \right\rangle}\right]^{1/q} \left[1 + \frac{\tau'_{\pi} - \tau'_{o}}{q} + \frac{\omega'_{q_\pi}}{q}\right] . \qquad (6.12)$$

As the terms in τ and ω_q are quite small, they can be neglected in the present discussion. The primed measurable quantities refer to Run II; the unprimed to Run I. It is to be noted in Eq. (6.12) that $\left(p_o\right)_{II}$ is a function of a which has been determined from Run I. Since

$$a = \left[\frac{\left\langle R_{1\pi}\ p_{\pi}^{-q} \right\rangle}{\left\langle R_{1\mu}\ p_{\mu}^{-q} \right\rangle}\right]^{\frac{1}{1-q}} , \qquad (5.1)$$

we may rewrite Eq. (6.12) as follows:

$$\left(p_o\right)_{II} = \left[\frac{\left\langle R_o' \right\rangle}{\left\langle R'_{1\pi}\ p'^{-q}_{\pi} \right\rangle}\right]^{1/q} \left[\frac{\left\langle R_{1\pi}\ p_{\pi}^{-q} \right\rangle}{\left\langle R_{1\mu}\ p_{\mu}^{-q} \right\rangle}\right]^{1/q} . \qquad (F.1)$$

We shall choose the calculation of the pion-meson mass difference to serve as a typical example of the general averaging procedure followed.

$$\left(m_{\pi} - m_{\mu}\right) c^2 = \frac{2a}{a+1}\ p_o\, c . \qquad (6.4)$$

For simplicity of notation, let $\lambda = \left(m_{\pi} - m_{\mu}\right) c^2$, $\left\langle K_{\pi} \right\rangle = \left\langle R_{1\pi}\ p_{\pi}^{-q} \right\rangle$, and $\left\langle K_{\mu} \right\rangle = \left\langle R_{1\mu}\ p_{\mu}^{-q} \right\rangle$. For Runs I and II, we may write Eq. (6.4) in terms of observable quantities as follows:

$$\lambda_I = \frac{2c \left[\frac{\langle K_\pi \rangle}{\langle K_\mu \rangle}\right]^{\frac{1}{1-q}} \cdot \left[\frac{\langle R_o \rangle}{\langle K_\mu \rangle}\right]^{\frac{1}{q}}}{\left[\frac{\langle K_\pi \rangle}{\langle K_\mu \rangle}\right]^{\frac{1}{1-q}} + 1} \qquad \text{(F. 2a)}$$

$$\lambda_{II} = \frac{2c \left[\frac{\langle K_\pi \rangle}{\langle K_\mu \rangle}\right]^{\frac{1}{q(1-q)}} \cdot \left[\frac{\langle R_\sigma' \rangle}{\langle K_\pi' \rangle}\right]^{\frac{1}{q}}}{\left[\frac{\langle K_\pi \rangle}{\langle K_\mu \rangle}\right]^{\frac{1}{1-q}} + 1} \qquad \text{(F. 2b)}$$

Differentiating, one obtains the following partial derivatives:

Run I	Run II
$\frac{\partial \lambda_I}{\partial \langle K_\pi \rangle} = \frac{\lambda_I}{(1+\alpha)(1-q)\langle K_\pi \rangle}$	$\frac{\partial \lambda_{II}}{\partial \langle K_\pi \rangle} = \frac{\lambda_{II}(1+\alpha-q\alpha)}{q(1-q)(\alpha+1)\langle K_\pi \rangle}$
$\frac{\partial \lambda_I}{\partial \langle K_\mu \rangle} = -\frac{\lambda_I}{q(1-q)(1+\alpha)\langle K_\mu \rangle}$	$\frac{\partial \lambda_{II}}{\partial \langle K_\mu \rangle} = -\frac{\lambda_{II}(1+\alpha-q\alpha)}{q(1-q)(\alpha+1)\langle K_\mu \rangle}$

Run I (Cont.)

$$\frac{\partial \lambda_I}{\partial \langle R_o \rangle} = \frac{\lambda_I}{q\langle R_o \rangle}$$

$$\frac{\partial \lambda_I}{\partial H} = \frac{\lambda_I}{H}$$

Run II (Cont.)

$$\frac{\partial \lambda_{II}}{\partial \langle K_\pi' \rangle} = -\frac{\lambda_{II}}{q\langle K_\pi' \rangle}$$

$$\frac{\partial \lambda_{II}}{\partial R_o'} = \frac{\lambda_{II}}{q\langle R_o' \rangle}$$

$$\frac{\partial \lambda_{II}}{\partial H'} = \frac{\lambda_{II}}{H'} \qquad \text{(F.3)}$$

where $\frac{\partial \lambda_I}{\partial H}$ and $\frac{\partial \lambda_{II}}{\partial H'}$ reflect the errors in $(p_o)_I$ and $(p_o)_{II}$, respectively, introduced by uncertainties in the absolute values of the magnetic fields, H and H'.

Let

$$\langle \lambda \rangle = A\lambda_I + (1 - A)\lambda_{II} \qquad \text{(F.4)}$$

where A and (1-A) represent the averaging weights of the two measurements λ_I and λ_{II}, respectively.

Differentiating Eq. (F.4)

$$\Delta\langle\lambda\rangle = A\left(\frac{\partial\lambda_I}{\partial\langle K_\pi\rangle}\Delta\langle K_\pi\rangle + \frac{\partial\lambda_I}{\partial\langle K_\mu\rangle}\Delta\langle K_\mu\rangle + \frac{\partial\lambda_I}{\partial\langle R_o\rangle}\Delta\langle R_o\rangle + \frac{\partial\lambda_I}{\partial H}\Delta H\right)$$

$$+(1-A)\left(\frac{\partial\lambda_{II}}{\partial\langle K_\pi\rangle}\Delta\langle K_\pi\rangle + \frac{\partial\lambda_{II}}{\partial\langle K_\mu\rangle}\Delta\langle K_\mu\rangle + \frac{\partial\lambda_{II}}{\partial\langle K_\pi'\rangle}\Delta\langle K_\pi'\rangle + \frac{\partial\lambda_{II}}{\partial\langle R_o'\rangle}\Delta\langle R_o'\rangle\right.$$

$$\left. + \frac{\partial\lambda_{II}}{\partial H'}\Delta H'\right) \qquad (F.5)$$

$$= A\left[\frac{\partial\lambda_I}{\partial\langle K_\pi\rangle} - \frac{\partial\lambda_{II}}{\partial\langle K_\pi\rangle}\right]\Delta K_\pi + A\left[\frac{\partial\lambda_I}{\partial\langle K_\mu\rangle} - \frac{\partial\lambda_{II}}{\partial\langle K_\mu\rangle}\right]\Delta K_\mu \qquad (F.6)$$

$$+ A\frac{\partial\lambda_I}{\partial\langle R_o\rangle}\Delta\langle R_o\rangle + A\frac{\partial\lambda_I}{\partial H}\Delta H + \frac{\partial\lambda_{II}}{\partial\langle K_\pi\rangle}\Delta\langle K_\pi\rangle + \frac{\partial\lambda_{II}}{\partial\langle K_\mu\rangle}\Delta\langle K_\mu\rangle$$

$$+(1-A)\left[\frac{\partial\lambda_{II}}{\partial K_\pi'}\Delta\langle K_\pi'\rangle + \frac{\partial\lambda_{II}}{\partial\langle R_o'\rangle}\Delta\langle R_o'\rangle + \frac{\partial\lambda_{II}}{\partial H'}\Delta H'\right]$$

Substituting the derivatives of Eq. (F.3) in Eq. (F.6), we have

$$\Delta\langle\lambda\rangle = A\left[\frac{\lambda_I}{(1+a)(1-q)} - \frac{\lambda_{II}(1+a-qa)}{q(1-q)(a+1)}\right]\frac{\Delta\langle K_\pi\rangle}{\langle K_\pi\rangle} \qquad (F.7)$$

$$+A\left[-\frac{\lambda_I(1+a-qa)}{q(1+a)(1-q)} + \frac{\lambda_{II}(1+a-qa)}{q(1+a)(1-q)}\right]\frac{\Delta\langle K_\mu\rangle}{\langle K_\mu\rangle}$$

$$+\frac{A\lambda_I}{q}\frac{\Delta\langle R_o\rangle}{\langle R_o\rangle} + A\lambda\frac{\Delta H}{H} + \frac{\lambda_{II}(1+a-qa)}{q(1-q)(1+a)}\frac{\Delta\langle K_\pi\rangle}{\langle K_\pi\rangle} \qquad \text{(F.7 cont.)}$$

$$-\frac{\lambda_{II}(1+a-qa)}{q(1-q)(1+a)}\frac{\Delta\langle K_\mu\rangle}{\langle K_\mu\rangle} - \frac{(1-A)\lambda_I}{q}\frac{\Delta\langle K_\pi'\rangle}{\langle K_\pi'\rangle}$$

$$+(1-A)\frac{\lambda_{II}}{q}\frac{\Delta\langle R_o'\rangle}{\langle R_o'\rangle} + (1-A)\lambda\frac{\Delta H'}{H'}.$$

Now assume $\lambda_I \approx \lambda_{II} \approx \langle\lambda\rangle$. Therefore, collecting terms, we have

$$\frac{\Delta\langle\lambda\rangle}{\langle\lambda\rangle} \approx \frac{[A(q-1)(a+1)+(1-q)a+1]}{q(1-q)(1+a)}\frac{\Delta\langle K_\pi\rangle}{\langle K_\pi\rangle}$$

$$-\frac{1+(1-q)a}{q(1-q)(1+a)}\frac{\Delta\langle K_\mu\rangle}{\langle K_\mu\rangle} - \frac{(1-A)}{q}\frac{\Delta\langle K_\pi'\rangle}{\langle K_\pi'\rangle}$$

$$+\frac{(1-A)}{q}\frac{\Delta\langle R_o'\rangle}{\langle R_o'\rangle} + (1-A)\frac{\Delta H'}{H'} + \frac{A}{q}\frac{\Delta\langle R_o\rangle}{\langle R_o\rangle}$$

$$+A\frac{\Delta H}{H}. \qquad \text{(F.8)}$$

If one now squares Eq. (F.8) and takes mean values, the various cross-product terms average out to zero and we get

$$\overline{\left(\frac{\Delta\langle\lambda\rangle}{\langle\lambda\rangle}\right)^2} = \frac{\left[A\,(q-1)(a+1) + (1-q)\,a + 1\right]}{q\,(1-q)(1+a)} \overline{\left(\frac{\Delta\langle K_\pi\rangle}{\langle K_\pi\rangle}\right)^2}$$

$$+ \left[\frac{1 + (1-q)\,a}{q\,(1-q)\,(a+1)}\right]^2 \overline{\left(\frac{\Delta\langle K_\mu\rangle}{\langle K_\mu\rangle}\right)^2} + \frac{A^2}{q^2} \overline{\left[\frac{\Delta\langle R_o\rangle}{\langle R_o\rangle}\right]^2}$$

$$+ \frac{(1-A)^2}{q^2} \overline{\left(\frac{\Delta\langle R_o'\rangle}{R_o'}\right)^2} + \frac{(1-A)^2}{q^2} \overline{\left(\frac{\Delta\langle K'_\pi\rangle}{\langle K_\pi'\rangle}\right)^2}$$

$$+ A^2 \overline{\left(\frac{\Delta H}{H}\right)^2} + (1-A)^2 \overline{\left(\frac{\Delta H'}{H'}\right)^2} . \qquad \text{(F.9)}$$

Furthermore, if we now replace $\overline{\left(\frac{\Delta\langle K_\pi\rangle}{\langle K_\pi\rangle}\right)^2}$ by the experimental variance $\frac{\sigma_\pi^2}{n_\pi \langle K_\pi\rangle^2}$ and the other terms with their corresponding experimental variances, and let

$$a = \frac{1}{q^2} \overline{\left(\frac{\sigma_{R_o}^2}{n_o \langle R_o\rangle^2}\right)}, \qquad b = \frac{1}{q^2} \overline{\left(\frac{\sigma_{R_o'}^2}{n_o' \langle R_o'\rangle^2}\right)},$$

$$c = \frac{1}{q^2} \overline{\left(\frac{\sigma_{\pi'}^2}{n_{\pi'} \langle K_{\pi'}\rangle^2}\right)}, \qquad d = \overline{\left(\frac{\Delta H}{H}\right)^2},$$

$$e = \overline{\left(\frac{\Delta H'}{H'}\right)^2} \quad , \qquad f = \frac{1}{q^2 (1-q)^2 (a+1)^2} \overline{\left(\frac{\sigma_\pi^2}{n_\pi K_\pi^2}\right)}$$

and $$g = \frac{\left[1 + (1-q)\, a\right]^2}{q^2 (1-q)^2 (a+1)^2} \overline{\left(\frac{\sigma_\mu^2}{n_\mu \langle K_\mu \rangle^2}\right)} \quad ,$$

we can write,

$$\overline{\left(\frac{\Delta\langle\lambda\rangle}{\langle\lambda\rangle}\right)^2} = A^2 (a+d) + (1-A)^2 (b+c+e) + \left[A(q-1)(a+1) + (1-q)\, a + 1\right]^2 f + g \quad . \qquad \text{(F.10)}$$

Now $\overline{\left(\frac{\sigma_\pi^2}{n_\pi \langle K_\pi \rangle^2}\right)^2}$, $\overline{\left(\frac{\sigma_\pi'^2}{n_\pi' \langle K_\pi' \rangle^2}\right)}$, etc. represent the mean-square percentage errors or variances in the quantities $\langle K_\pi \rangle$, $\langle K_\pi' \rangle$, etc., for Runs I and II. Since both the runs are comprised of several plates each, these mean-square percentage errors are evaluated from a weighted average of the variances of the individual plates.

Applying the Principle of Least Squares, one differentiates Eq. (F.10) with respect to A and sets the derivative equal to zero to find the minimum error in $\langle\lambda\rangle$.

$$\frac{\partial}{\partial A}\overline{\left(\frac{\Delta\langle\lambda\rangle}{\langle\lambda\rangle}\right)^2} = A\,(a + d) - (1 - A)(b + c + e) + (q - 1)(a + 1) f \left[A (q - 1)(a + 1) + (1 - q) a + 1\right] = 0.$$

Therefore

$$A (a + d + b + c + e) - (b + c + e) + Af (q - 1)^2 (a + 1)^2 + f (q - 1)(a + 1)\left[(1 - q) a + 1\right] = 0 \quad . \tag{F.11}$$

Solving for A, one has

$$A = \frac{b + c + e - (q - 1)(a + 1)\left[(1 - q) a + 1\right] f}{a + d + b + c + e + (q - 1)^2 (a + 1)^2 f} \quad . \tag{F.12}$$

Having obtained this value for A, one then inserts it in Eq. (F. 4) to give $\langle\lambda\rangle$ and in Eq. (F. 9) to obtain an estimate of the error, $\Delta\langle\lambda\rangle$.

ACKNOWLEDGMENTS

The author is indebted to Dr. Walter H. Barkas for his constant guidance and invaluable assistance at all stages of the study. Dr. Barkas developed much of the theory of the experiment and contributed numerous ideas and suggestions regarding experimental procedures.

Miss Frances M. Smith has been an amiable and active partner in all phases of the work; much of the success of the experiment is due to her.

Dr. Robert L. Thornton's continued interest in the program is gratefully acknowledged.

Mrs. Thomas Griswold has been an excellent and very patient assistant in the laboratory during the many months of tedious microscope scanning, also performing a large share of the lengthy calculations. Mr. Evan Bailey entered into the discussions of some of the statistical problems and helped with the early calculations. The apparatus was constructed by Mr. Wallace Conover with the assistance of Mr. James McFaden and Mr. E. Bailey. The Computing Group, under the direction of Mr. John Killeen, assisted in some of the calculations. The cyclotron crew, under the supervision of Mr. James Vale, were most cooperative during the cyclotron bombardments. The necessary magnetic measuring equipment was provided by Mr. Duane Sewell. Mr. Albert Oliver helped process the nuclear emulsions.

The memory of the late Dr. Eugene Gardner was with us at all times. The earlier work and ideas of Dr. Gardner and Dr. C. M. G. Lattes laid the foundation of the present study.

TABLE I.

SUMMARY OF MESON MASS MEASUREMENTS WITH COSMIC RAYS

Author	Year	Reference	Particle Type	Mass Values	Method and Comments [CC - Cloud Chamber, NE - Nuclear Emulsion]
Corson and Brode (and others)	1938	4	μ^+, μ^-	200 ± 50	CC; Hρ vs. specific ionization (i)
Wheeler and Ladenburg	1941	6	μ^+, μ^-	~180	Summary of all meson mass measurements up to 1941; range-momentum relations
Nielsen and W. M. Powell	1943	78	μ^+, μ^-	~200	CC; Hρ vs. i
Hughes	1946	79	μ^+, μ^-	~200	CC; Hρ vs. R, i; reported spectrum of mass values 30-340 m_o
Fretter	1946	7	μ^+, μ^-	202 ± 5	CC; Hρ vs. R; first of more accurate determinations, showed unique mass value for penetrating component of cosmic rays
Lattes, Occhialini, and C. F. Powell	1948	17	π^+/μ^+	1.65± 0.11	NE; grain count vs. R; mass normalization
Goldschmidt-Clermont, et al	1948	80	π^+, π^- μ^+, μ^-	272 ± 12 202 ± 8	NE; scattering vs. R

TABLE I.

SUMMARY OF MESON MASS MEASUREMENTS WITH COSMIC RAYS (CONT.)

Author	Year	Reference	Particle Type	Mass Values	Method and Comments [CC - Cloud Chamber, NE - Nuclear Emulsion]
Lattimore	1948	81	π^-	290 ± 80	NE; scattering vs. R
Brown et al.	1949	82	π/μ	1.33 ± 0.05	NE; grain count vs. R
	1950	18	π^+, π^-	290 ± 20	
Brode	1949	9	μ^+, μ^-	212 ± 5	New statistical analysis of data of Ref. 7
Leighton, Anderson, and Serif	1949	27	μ^+	217 ± 4	CC; end point of $\mu^+ \rightarrow \beta^+ + 2\nu$ decay
Retallack and Brode	1949	10	μ^+, μ^-	215 ± 4	CC; $H\rho$ vs R
Brode	1949	8	μ^+, μ^-	215 ± 2	Weighted mean including data of Refs. 7, 10
Barbour	1950	83	π^+, π^-	270 ± 20	NE; $H\rho$ vs R
			μ^+, μ^-	226 ± 15	
Franzinetti	1950	84	π^+	281 ± 7	NE; $H\rho$ vs R
			π^-	288 ± 13	
			μ^+	217 ± 4	
Camerini et al.	1950	85	π^+, π^-	283 ± 7	NE; grain count vs. scattering angle

TABLE I

SUMMARY OF MESON MASS MEASUREMENTS WITH COSMIC RAYS (CONT.)

Author	Year	Reference	Particle Type	Mass Values	Method and Comments [CC - Cloud Chamber, NE - Nuclear Emulsion]
Merkle, Goldwasser, and Brode	1950	11	μ^+, μ^-	196 ± 3	CC; Hρ vs R
Carlson, Hooper, and King	1950	26	π^o	295 ± 20	NE; Doppler shift spectrum of γ-rays in cosmic ray stars
Nonnemaker and Street	1951	86	μ^+, μ^-	220 ± 12	CC; Hρ vs R
Ascoli	1953	87	μ^+, μ^-	207.4 ± 2.4	CC; Hρ vs R

TABLE II

SUMMARY OF MASS MEASUREMENTS WITH ARTIFICIALLY PRODUCED MESONS

Author	Year	Reference	Particle Type	Mass Values	Method and Comments [CC - Cloud Chamber, NE - Nuclear Emulsion]
E. Gardner and Lattes	1948	19	π^-	313 ± 16	NE; Hρ vs R
Barkas, E. Gardner, and Lattes	1948	88	π^- μ^-	~305 ~202	NE; Hρ vs. grain count
Van Rossum	1949	89	π^-	280 ± 15	NE; Hρ vs. grain count
Bishop	1949	20	π^+ π^- μ^+ π/μ	~286 ~285 ~216 1.32 ± 0.01	NE; Hρ vs R
Smith et al.	1950	21	π^+, π^- μ^+	276 ± 6 210 ± 4	NE; Hρ vs R
Bowker	1950	90	π^-	264 +26 -22	NE; Hρ vs grain count
Lederman, Tinlot, and Booth	1951	23	$\pi^- - \mu^-$	66 ± 3	CC; Decay in flight, $\pi^- \rightarrow \mu^- + \nu$

TABLE II (CONT.)

SUMMARY OF MASS MEASUREMENTS WITH ARTIFICIALLY PRODUCED MESONS

Author	Year	Reference	Particle Type	Mass Values	Method and Comments [CC - Cloud Chamber, NE - Nuclear Emulsion]
Panofsky, Aamodt, and Hadley	1951	24	π^-	275.2 ± 2.5	Gamma Ray Spectrometer; $\pi^- + p \rightarrow n + \gamma$
			$\pi^- - \pi^0$	10.6 ± 2.0	Doppler Shift Spectrum, $\pi^- + p \rightarrow n + \pi^0$
Barkas, Smith, and E. Gardner	1951	40	π^+	277.4 ± 1.1	NE; Hρ vs R; Mass Normalization-Proton-Pion Comparison. Background Contamination.
				276.1 ± 1.3	
Cartwright	1951	33	π^+	275.1 ± 2.5	NE; $p + p \rightarrow \pi^+ + d$
Sagane, W. L. Gardner, and Hubbard	1951	31	μ^+	212.0 ± 5.0	Spiral Orbit Spectrometer; $\mu^+ \rightarrow \beta^+ + 2\nu$ end point
Birnbaum, Smith, and Barkas	1951	91	π^+/μ^+	1.318 ± .004	NE;
			$\pi^+ - \mu^+$	66.46 ± 0.16	Dynamics of $\pi^+ \rightarrow \mu^+ + \nu$;
			π^+	276.1 ± 2.3	Preliminary Results of Present Experiment
			μ^+	209.6 ± 2.4	
W. M. Powell	1951	92	$\pi^+ - \mu^+$	63.0 ± 2.0	CC; $\pi^+ \rightarrow \mu^+ + \nu$ Decay
Peterson, Iloff, and Sherman	1951	34	π^+	279.0 ± 1.5	NE; $p + p \rightarrow \pi^+ + d$

TABLE II (CONT.)

SUMMARY OF MASS MEASUREMENTS WITH ARTIFICIALLY PRODUCED MESONS

Author	Year	Reference	Particle Type	Mass Values		Method and Comments [CC - Cloud Chamber, NE - Nuclear Emulsion]
Crowe and Panofsky	1952	93	π^-	278.0	±2.5	Corrections to data of Ref. 24 due to ionization losses in converter.
Crowe	1952	25	π^-	273.5	±0.5	Gamma ray spectrometer; $\pi^- + p \rightarrow n + \gamma$
Chinowsky, Sachs, and Steinberger	1953	94	$\pi^- - \pi_o$	8.8	±0.6	Angular correlation of γ-ray pairs from decay of π^o produced by $\pi^- + p \rightarrow \pi^o + n$
Smith, Birnbaum, and Barkas	1953	41	π^+	273.4	±0.2	NE; Hρ vs R; Mass Normalization; proton-pion comparison
			π^-	272.5	±0.3	
Smith	1953	42	π^+	273.3	±0.2	Same data as Ref. 41 statistical corrections; correction[95] to stopping power formula due to sign of charge
			π^-/π^+			
Present Study Final Results (Values in parenthesis assume $m_\nu = 0$)	1953	-	π^+/μ^+	1.321	±0.002	NE; Hρ vs R; Mass Normalization; pion-meson comparison
			$\pi^+ - \mu^+$	(66.41	±0.07)	Dynamics of $\pi^+ \rightarrow \mu^+ + \nu^+$; decay momentum and mass ratio
			π^+	(273.5	±1.2)	Mass ratio and mass difference
			μ^+	(207.1	±1.1)	
			μ^+	206.9	±0.4	Mass ratio and π^+ mass from Ref.42
			μ^+	(206.9	±0.2)	Mass difference and π^+ mass from Ref.42

TABLE III UCRL-2522

MAGNETIC RIGIDITY CALCULATION -θ' = 0 AT DETECTOR
RUN I
(Explanation of symbols at end of table)

r	H	$\int_{r_1}^{r_1+x_o} Hr\,dr$	$\int_{r_1}^{r_1+x_o} Hr\,dr \Big/ 2r_1+x_o \; (\equiv A)$	sec γ_o	A sec γ_o	A sec γ_o	$r_1 + x_o$
inches	gauss	gauss -in^2	gauss -in		gauss -in	gauss-mm	mm
73.0	14250	10402 x10^2	7125	1.0412	7419	1884 x10^2	1866.9
74.0	14241	20941	14245	1.0098	14385	3654	1892.3
75.0	14230	31613	21360	1.0043	21452	5449	1917.7
76.0	14223	42423	28472	1.0024	28540	7249	1943.1
77.0	14214	53368	35578	1.0016	35635	9051	1968.5
78.0	14206	64448	42681	1.0011	42728	10853	1993.9
79.0	14198	75665	49779	1.0008	49819	12654	2019.3
80.0	14179	87008	56868	1.0006	56902	14453	2044.7

r = Cyclotron radius

r_1 = Radial distance from the center of the cyclotron to the center of the target = 72.5 inches

x_o = Distance between center of target and point at which trajectory crosses x-axis at detector. The x-axis is coincident with the median line of the target-detector assembly.

γ_o = Nominal inclination angle between actual orbit and median plane of cyclotron

θ = See Fig. 3 for definition.

TABLE IV

MAGNETIC RIGIDITY CALCULATION - $\theta' = 0$ AT DETECTOR

RUN II

(Explanation of symbols at end of Table 4)

r	H	$\int_{r_1}^{r_1+x_o} Hr\,dr$	$\frac{\int_{r_1}^{r_1+x_o} Hr\,dr}{2r_1+x_o} \equiv A$	sec γ_o	A sec γ_o	A sec γ_o	$r_1 + x_o$
inches	gauss	gauss-in^2	gauss-in		gauss-in	gauss-mm	mm
73.5	14238						
		10465x10^2	7119	1.1081	7889	2003 x10^2	1879.6
74.5	14229						
		21066	14233	1.0281	14633	3717	1905.0
75.5	14220						
		31802	21343	1.0126	21612	5489	1930.4
76.5	14211						
		42673	28449	1.0071	28651	7277	1955.8
77.5	14205						
		53682	35551	1.0045	35711	9071	1981.2
78.5	14196						
		64826	42649	1.0032	42785	10867	2006.6
79.5	14182						
		76100	49739	1.0023	49853	12663	2032.0
80.5	14163						
		87502	56819	1.0018	56922	14458	2057.4

r_1 = 73.0 inches

TABLE V

MEAN VALUES OF VARIABLE QUANTITIES IN FINITE TARGET - DETECTOR CORRECTION TERM IN MOMENTUM CALCULATION

Quantity	Pions	Muons
$\langle x \rangle$	0	$\frac{N^+ - N^-}{N^+ + N^-} \quad \frac{ab}{a+b}$
$\langle y \rangle$	0	$\frac{ab}{a+b}$
$\langle z \rangle$	$c^2/3z_o \quad (z_o > c)$	$c^2/3z_o \quad (z_o > c)$
$\langle x^2 \rangle$	$a^2/3$	$\frac{a^2(a+3b)}{3(a+b)}$
$\langle y^2 \rangle$	$b^2/3$	$\frac{b^2(b+3a)}{3(a+b)}$
$\langle z^2 \rangle$	$c^2/3$	$c^2/3$
$\langle \theta' \rangle$	obs	obs
$\langle y' \rangle$	obs	obs
$\langle \theta'^2 \rangle$	obs	obs
$\langle y'^2 \rangle$	obs	obs
$\langle y\theta' \rangle$	0	$\frac{ab}{a+b} \langle \theta' \rangle$
$\langle z\theta' \rangle$	$c^2/3z_o \langle \theta' \rangle$	$c^2/3z_o \langle \theta' \rangle$
$\langle zy \rangle$	0	$\frac{c^2 ab}{3z_o(a+b)}$
$\langle zy' \rangle$	$c^2/3z_o \langle y' \rangle$	$c^2/3z_o \langle y' \rangle$
$\langle xy\theta' \rangle$	0	$\frac{N^+ - N^-}{N^+ + N^-} \frac{a^2 b^2}{(a+b)^2} \langle \theta' \rangle$
$\langle xz \rangle$	0	$\frac{N^+ - N^-}{N^+ + N^-} \frac{abc^2}{(a+b)3z_o}$
$\langle xz^2 \rangle$	0	$\frac{N^+ - N^-}{N^+ + N^-} \frac{abc^2}{3(a+b)}$
$\langle xy^2 \rangle$	0	$\frac{N^+ - N^-}{N^+ + N^-} \frac{ab^3(b+3a)}{3(a+b)^2}$
$\langle x^3 \rangle$	0	$\frac{N^+ - N^-}{N^+ + N^-} \frac{a^3 b}{a+b}$

TABLE VI

COMPOSITION OF ILFORD C-2 EMULSION

Element	gm/c.c.	M_i gm.	Z_i	N_i No.atoms/cc	$N_i Z_i$	$N_i Z_i^2$	$\frac{N_i Z_i^2}{M_i}$
Ag	1.85	107.9	47	1.113×10^{22}	4.85×10^{23}	2.46×10^{25}	2.28×10^{23}
Br	1.34	79.9	35	1.010	3.54	1.24	1.57
I	0.052	126.9	53	0.025	0.13	0.07	0.06
C	0.27	12.0	6	1.352	0.81	0.05	0.42
H	0.056	1.0	1	3.350	0.34	0.003	0.34
O	0.27	16.0	8	1.015	0.81	0.06	0.41
S	0.010	32.1	16	0.019	0.03	0.005	0.02
N	0.067	14.0	7	0.288	0.20	0.014	0.10
				Totals	1.07×10^{24}	3.90×10^{25}	5.20×10^{23}

TABLE VII.

PERTURBATION OF MAGNETIC FIELD BY SET SCREW ACTING AS MAGNETIC DIPOLE

$[H_o = 14216 \text{ gauss}]$

θ	H_T gauss	$H_T - H_o$ gauss	$2\cos^2\theta - \sin^2\theta$	I/r^3 gauss
0°	14252	36 ± 4	2.00	18.0± 2.0
$\pm 10^\circ$	14250	34 ± 4	1.91	17.8± 2.1
$\pm 20^\circ$	14244	28 ± 4	1.65	17.0± 2.4
$\pm 30^\circ$	14238	22 ± 4	1.25	17.6± 3.2
$\pm 40^\circ$	14227	11 ± 4	0.76	16.3± 5.3
$\pm 50^\circ$	14221	5 ± 4	0.24	20.8± 16.7
$\pm 55^\circ$	14216	0 ± 4	-0.01	- - -
$\pm 60^\circ$	14211	-5 ± 4	-0.25	20.0± 16.0

H_o Unperturbed magnetic field

r Distance from center of set screw to center of water sample in nuclear fluxmeter

θ Angle of rotation between the vector $\vec{r}$ and the direction of $\vec{H_o}$

I Total magnetic moment of set screw

$\langle I/r^3 \rangle = 17.6$ gauss

TABLE VIII.

SUMMARY OF MU-COMPLETE RANGE DISTRIBUTIONS

Plate No.	No. of Events	$\langle R_\mu \rangle$ Microns	$\sigma_{R_\mu}^2$ $(\text{Microns})^2$	$\langle R_o \rangle$ Microns	$\frac{\sigma_{R_\mu}}{\langle R_o \rangle}$	Normalizing Factor-600 Microns
22297	76	590.1	841.33	591.5	4.9%	1.015
23313	62	599.0	604.92	600.0	4.1	1.000
23315	25	608.8	650.00	609.9	4.2	0.982
25957	39	595.0	691.47	596.2	4.4	1.006
25958	77	593.9	860.09	595.3	4.9	1.009
25959s	31	597.6	703.33	598.8	4.4	1.002
25959b	56	592.3	685.53	593.5	4.4	1.011
25961	50	596.5	664.98	597.6	4.3	1.004
25967	53	596.8	1135.96	598.7	5.6	1.004
28848	26	598.2	454.04	599.0	3.6	1.002
28849	31	604.3	782.53	605.6	4.6	0.991
28853	32	592.2	713.35	593.4	4.5	1.011

$\langle R_\mu \rangle$ Observed mean range of μ-completes

$\sigma_{R_\mu}^2$ Variance of observed distribution of ranges

$\langle R_o \rangle$ Mean range of μ-completes corrected for probability, $t/2R_\mu$, of particle expending its entire energy within the emulsion of thickness t.

TABLE IX.

COMBINED RANGE DISTRIBUTION OF MU-COMPLETES
AND CHI-SQUARE TEST FOR NORMALITY

$[R_o = 600$ microns, $n_o = 558$ events, $\sigma_{R_o/R_o} = 4.5 \pm 0.1\%]$

R_i+5	ΔR	t	$\int_o^t \phi(t)dt$	A_{Left}	ΔA	f_n	f_o	$(f_o - f_n)^2$	$\frac{(f_o-f_n)^2}{f_n}$
525	- 75	- 2.76	- 0.4971	0.0029	0.0020	1	1		
535	- 65	- 2.39	- 0.4916	0.0084	0.0055	3	3	0	0
545	- 55	- 2.02	- 0.4783	0.0217	0.0133	7	8	1	0.143
555	- 45	- 1.65	- 0.4505	0.0495	0.0278	16	17	1	0.062
565	- 35	- 1.29	- 0.4015	0.0985	0.0490	27	26	1	0.037
575	- 25	- 0.92	- 0.3212	0.1788	0.0803	45	56	121	2.689
585	- 15	- 0.55	- 0.2088	0.2912	0.1124	63	45	324	5.143
595	- 5	- 0.18	- 0.0714	0.4286	0.1374	77	72	25	0.325
605	+ 5	+ 0.18	+ 0.0714	0.5714	0.1428	80	88	64	0.800
615	+ 15	+ 0.55	+ 0.2088	0.7088	0.1374	77	81	16	0.208
625	+ 25	+ 0.92	+ 0.3212	0.8212	0.1124	63	61	4	0.063
635	+ 35	+ 1.29	+ 0.4015	0.9015	0.0803	45	44	1	0.022
645	+ 45	+ 1.65	+ 0.4505	0.9505	0.0490	27	30	9	0.333
655	+ 55	+ 2.02	+ 0.4783	0.9783	0.0278	16	19	9	0.562
665	+ 65	+ 2.39	+ 0.4916	0.9916	0.0133	7	3	16	2.286
675	+ 75	+ 2.76	+ 0.4971	0.9971	0.0055	3	2		
685	+ 85	+ 3.12	+ 0.4991	0.9991	0.0020	1	1	0	0
695	+ 95	+ 3.49	+ 0.4998	0.9998	0.0007	0	1		

$$\chi^2 = \sum_n \frac{(f_o - f_n)^2}{f_n} = 12.673$$

No. of degrees of freedom = 15 - 3 = 12 Significance Level ≈ 0.4

R_i = Range value at center of interval

$\Delta R = 600 - (R_i + 5)$

$t = \Delta R / \sigma_{R_o}$

$\int_o^t \phi(t)\,dt$ = Area of normal curve from $o \rightarrow t$

$A_{Left} = .5000 + \int_o^t \phi(t)\,dt$

$\Delta A = (A_{Left})_{R_{i+1}} - (A_{Left})_{R_i}$

f_n = Expected no. of events for normal distribution

f_o = Observed number of events

TABLE X.

SAMPLE CALCULATIONS OF NORMALIZED RANGES, $R_{1\pi} p_{\pi}^{-q}$ AND $R_{1\mu} p_{\mu}^{-q}$

(Definition of symbols at end of table) - Plate No. 25959

Event No. & Type	x'	Δx"	y'	Δy"	d + Δx"	tan α'	α'	θ	θ - α'	tan(θ-α')	Δy" tan (θ-α')	R'
541π	17.043	5.816	15.275	1.514	178.749	+0.0085	+0.5°	+4.5°	+4.0°	+0.0699	+0.106	2020.355
545π	18.523	4.336	10.986	-2.775	177.269	-0.0156	-0.9	-10.4	-9.5°	-0.1673	+0.464	2019.233
546π	18.420	4.439	15.310	+1.549	177.372	+0.0087	+0.5	+2.5	+2.0	+0.0349	+0.054	2018.926
550π	18.627	4.232	8.424	-5.337	177.165	-0.0301	-1.7	-5.2	-3.5	-0.0612	+0.327	2018.992
551π	18.754	4.105	9.943	-3.818	177.038	-0.0216	-1.2	+1.9	+3.1	+0.0542	-0.207	2018.331
601μ	62.892	-2.174	8.549	-5.161	133.561	-0.0386	-2.2	+1.5	+3.7	+0.0647	-0.334	1974.727
603μ	63.153	-2.435	13.470	-0.240	133.300	-0.0018	-0.1	+4.5	+4.6	+0.0805	-0.019	1974.781
604μ	63.053	-2.335	12.349	-1.361	133.400	-0.0102	-0.6	-1.1	-0.5	-0.0087	-0.012	1974.912
606μ	63.309	-2.591	19.326	+5.616	133.144	+0.0422	+2.4	+13.2	+10.8	+0.1908	+1.071	1975.715
611μ	63.289	-2.571	10.727	-2.983	133.164	-0.0224	-1.3	-2.5	-1.2	-0.0210	+0.062	1974.726

TABLE X (CONT'D)

SAMPLE CALCULATIONS OF NORMALIZED RANGES, $R_{1\pi} p_{\pi}^{-q}$ AND $R_{1\mu} p_{\mu}^{-q}$
(Definition of symbols at end of table) - Plate No. 25959

Event No. & Type	A sec γ_o	$\theta' = \theta - 2\alpha'$	sec $(\theta - 2\alpha')$	p	log p	3.44 log p	$p^{3.44}$	R_1	$R_1 p^{-3.44}$
541π	12.758×10^5	+ 3.5°	1.0019	12.782×10^5	6.10661	21.00672	1.016×10^{21}	758.9	74.72×10^{-20}
545π	12.677	- 8.6	1.0114	12.821	6.10794	21.01131	1.026	729.3	71.05
546π	12.657	+ 1.5	1.0003	12.661	6.10246	20.99247	0.9828	702.0	71.43
550π	12.662	- 1.8	1.0005	12.668	6.10272	20.99335	0.9848	665.8	67.61
551π	12.615	+ 4.3	1.0028	12.650	6.10210	20.99123	0.9800	678.6	69.24
601μ	9.517	+ 5.9	1.0053	9.567	5.98078	20.57388	3.749×10^{20}	523.2	139.6
603μ	9.520	+ 4.7	1.0034	9.552	5.98009	20.57151	3.729	534.2	143.3
604μ	9.531	+ 0.1	1.0000	9.531	5.97914	20.56824	3.700	510.8	138.0
606μ	9.588	+ 8.4	1.0108	9.692	5.98641	20.59325	3.920	551.7	140.8
611μ	9.517	+ 0.1	1.0000	9.517	5.97850	20.56604	3.682	510.7	138.7

TABLE X. (CONT'D)

Definition of Symbols

x', y' = Coordinates of meson track at point of entry on emulsion surface (in millimeter units)

$\Delta x''$ = $x_f' - x'$; $\Delta y'' = y_f' - y'$ where x_f' , y_f' are the coordinates of the π or μ fiducial marks in the emulsion [pions: $(x_f', y_f') = (22.859, 13.761)$; muons: $(x_f' , y_f') = (60.718, 13.710)$]

d = distance along x-axis between center of target and fiducial mark ($d_\pi = 2014.433$ mm; $d_\mu = 1977.235$ mm)

θ, α', θ' = Defined in Fig. 3

R' = Cyclotron radius in mm. where orbit would cross x-axis in detector

$A \sec \gamma_o$ = Magnetic rigidity for $\theta' = \theta - 2\alpha' = 0$ as calculated in Tables IV and V, and read from Fig. 4. (in units of gauss - mm.)

p = Magnetic rigidity for $\theta' \neq o$. $p = A \sec \gamma_o \sec (\theta - 2\alpha')$ gauss - mm.

R = Measured range of meson track in microns.

TABLE XI

SUMMARY OF MEAN VALUES OF NORMALIZED RANGES AND MU-COMPLETE RANGES- RUNS I AND II

	Plate No.	$\langle R_{1\pi} p_\pi^{-q} \rangle$ x 10^{20}	n_π	$\frac{\sigma_\pi}{\langle R_{1\pi} p_\pi^{-q} \rangle}$	$\langle R_{1\mu} p_\mu^{-q} \rangle$ x 10^{20}	n_μ	$\frac{\sigma_\pi}{\langle R_{1\mu} p_\mu^{-q} \rangle}$	$\langle R_o \rangle$	n_o	$\frac{\sigma_{R_\mu}}{\langle R_o \rangle}$
Run I	25959	69.82±0.34	31	3.9±0.3 %	139.11±1.06	27	5.9±0.6 %	596.2±2.8	39	4.4±0.3 %
	25958	69.37±0.24	49	3.5±0.2	137.92±0.79	46	5.7±0.4	595.3±2.3	77	4.9±0.3
	25959	70.85±0.25	50	3.6±0.2	140.19±0.62	38	4.1±0.3	593.5±2.4	56	4.4±0.3
	25961	70.68±0.31	51	4.4±0.3	139.49±0.69	30	4.0±0.3	597.6±2.5	50	4.3±0.3
	25967	70.37±0.22	52	3.5±0.2	136.24±0.98	20	4.8±0.5	598.7±3.1	53	5.6±0.4
Run II	28848	70.84±0.22	69	3.8±0.2	———	—	———	599.0±2.8	26	3.6±0.3
	28849	72.48±0.22	71	3.7±0.2	———	—	———	605.6±3.3	31	4.6±0.4
	28853	70.74±0.24	78	4.5±0.2	———	—	———	593.4±3.1	32	4.5±0.4

$R_{1\pi}$, $R_{1\mu}$, and R_o in units of microns.

p_π and p_μ in units of gauss-mm.

TABLE XII.

CALCULATION OF PI - MU MASS RATIO - (Eq. 5.6)

Plate No	$R_{1\pi} p_\pi^{-q}$ x 10^{20}	$R_{1\mu} p_\mu^{-q}$ x 10^{20}	a'	$\omega_{q\pi}$ x 10^3	$\omega_{q\mu}$ x 10^3	$\frac{\omega_{q\pi} - \omega_{q\mu}}{q-1}$	$\frac{\tau_{1\pi} - \tau_{1\mu}}{q-1}$	$\frac{\Delta a}{a} \times 10^4$	$a = \frac{m_\pi}{m_\mu}$
25957	69.82	139.11	1.3264	+ 1.37	+1.78	$- 0.17 \times 10^{-3}$	$- 2.58 \times 10^{-4}$	- 4.26	1.3258
25958	69.37	137.92	1.3253	+ 1.45	- 1.38	+ 1.16	- 2.58	+ 9.01	1.3265
25959	70.85	140.19	1.3227	+ 1.39	+ 4.77	- 1.39	- 2.58	-16.48	1.3205
25961	70.68	139.49	1.3213	+ 1.36	- 0.53	+ 0.77	- 2.58	+ 5.16	1.3220
25967	70.37	136.24	1.3110	+ 1.53	+ 6.60	- 2.08	- 2.58	-23.38	1.3079

a' = apparent mass ratio; a = mass ratio corrected for finite target-detector and Lewis effects (Eq. 5.7)

Plate No	$\frac{\sigma_\pi^2}{n_\pi \langle R_{1\pi} p_\pi^{-q} \rangle^2}$	$\frac{\sigma_\mu^2}{n_\mu \langle R_{1\mu} p_\mu^{-q} \rangle^2}$	$\frac{\langle p_\pi \rangle}{\langle p_\mu \rangle}$	2 r x 10^2	$\frac{\sigma_{p_\pi}^2}{\langle p_\mu \rangle^2}$	$\frac{\sigma_{p_\mu}^2}{\langle p_\mu \rangle^2}$	A^2 x 10^5	B^2 x 10^8	C^2 x 10^8	Probable Error in a
25957	5.175×10^{-5}	13.005×10^{-5}	1.307	- 1.96	3.49×10^{-4}	0.92×10^{-4}	18.180	8.9	4.7	±0.0049
25958	2.452	7.312	I.3II	- 0.6I	0.90	I.4I	9.764	0.8	4.7	±0.0036
25959	2.610	4.365	1.331	+ 1.66	2.31	0.88	6.975	6.1	4.7	±0.0030
25961	4.162	5.400	1.300	- 3.03	10.80	1.09	9.562	22.0	4.7	±0.0031
25967	2.295	2.295	1.323	+ 0.45	0.71	3.01	13.950	0.5	4.7	±0.0043

Weighted Mean: a = 1.321±0.002

P. E. Internal Consistency = ±0.0017

P. E. External Consistency = ±0.0020

$$A^2 = \frac{\sigma_\pi^2}{n_\pi \langle R_{1\pi} p_\pi^{-q} \rangle^2} + \frac{\sigma_\mu^2}{n_\mu \langle R_{1\mu} p_\mu^{-q} \rangle^2}; \quad B^2 = \frac{\sigma_q^2}{4} \left(\frac{\sigma_{p_\pi}^2}{\langle p_\pi \rangle^2} - \frac{\sigma_{p_\mu}^2}{\langle p_\mu \rangle^2} - 2r \right)^2; \quad C^2 = \frac{\sigma_s^2}{S^2} \left[\langle \sin^2 \gamma_{1\pi} \rangle - \langle \sin^2 \gamma_{1\mu} \rangle \right]^2$$

TABLE XIII

CALCULATION OF ABSOLUTE DECAY MOMENTUM - RUN I - (Equation 6.10)

Plate No.	$\langle R_o \rangle$	$\langle R_{1\mu} p_\mu^{-q} \rangle \times 10^{20}$	$p_o' \times 10^{-5}$	$\frac{\omega_{q_\mu}}{q} \times 10^4$	$\frac{\tau_{1_\mu} - \tau_{1_o}}{q}$	$\frac{\Delta p_o}{p_o} \times 10^4$	$p_o \times 10^{-5}$
25957	596.2	139.11	9.9464	+ 7.30	0	+ 7.30	9.9537
25958	595.3	137.92	9.9670	- 5.66	0	- 5.66	9.9613
25959	593.5	140.19	9.9110	+19.5	0	+19.5	9.9303
25961	597.6	139.49	9.9452	- 2.17	0	- 2.17	9.9430
25967	598.7	136.24	10.0189	+ 27.0	0	+ 27.0	10.0458

p_o' = apparent value of absolute decay momentum in gauss-mm.

p_o = value of absolute decay momentum corrected for finite-target-and-detector and Lewis effects. (Eq. 6.11)

Plate No.	$\frac{\sigma_{R_o}^2}{n_o \langle R_o \rangle^2} \times 10^5$	$\frac{\sigma_\mu^2}{n_\mu \langle R_{1\mu} p_\mu^{-q} \rangle} 2 \times 10^5$	$p_\mu \times 10^{-5}$	$\frac{\sigma_{p_\mu}^2}{\langle p_\mu \rangle^2} \times 10^4$	$2\epsilon \times 10^2$	$E^2 \times 10^8$	$F^2 \times 10^8$	Statistical P.E. in p_o
25957	4.988	13.005	9.669	0.92	-5.64	71.32	4.73	$\pm 0.026 \times 10^5$
25958	3.152	7.152	9.689	1.41	-5.25	61.78	4.73	± 0.020
25959	3.475	4.365	9.576	0.88	-7.52	126.90	4.73	± 0.017
25961	3.724	5.400	9.688	1.09	-5.27	62.26	4.73	± 0.019
25967	5.980	11.655	9.622	3.01	-6.59	96.82	4.73	± 0.026

Run I - Weighted Mean = 9.958×10^5 gauss-mm. P.E. Internal Consistency = $\pm 0.0093 \times 10^5$

P.E. External Consistency = $\pm 0.0011 \times 10^5$

or $\langle p_o \rangle_I = 29.85 \pm 0.05$ Mev/c (adding error due to uncertainty in absolute value of magnetic field)

$$E^2 = \frac{\sigma_q^2}{4}\left(\frac{\sigma_p^2}{\langle p \rangle^2} + 2\epsilon\right)^2 \quad ; \quad F^2 = \frac{\sigma_s^2}{s^2}\left\langle \sin^2 \gamma_{1_\mu} \right\rangle - \left\langle \sin^2 \gamma_{1_o} \right\rangle^2$$

TABLE XIV.

CALCULATION OF ABSOLUTE DECAY MOMENTUM - RUN II - (Equation 6.12)

Plate No.	$\langle R_o \rangle$	$\langle R_{1\pi}\, p_\pi^{-q} \rangle \times 10^{20}$	a	$p_o' \times 10^{-5}$	$\frac{\omega_{q_\pi}}{q} \times 10^4$	$\frac{\tau_\pi - \tau_o}{q} \times 10^4$	$\frac{\Delta p_o}{p_o} \times 10^4$	$p_o \times 10^5$
28848	599.0	70.84	1.321	9.9473	+ 2.21	- 1.88	+ 0.33	9.9476
28849	605.6	72.48	1.321	9.9128	+ 0.81	- 1.88	- 1.07	9.9118
28853	593.4	70.74	1.321	9.9243	+ 1.71	- 1.88	- 0.17	9.9242

p_o' = apparent value of absolute decay momentum in gauss-mm.
p_o = value of absolute decay momentum corrected for finite target detector effects. (Equation 6.13)

Plate No.	$\frac{\sigma_{R_o}^2}{n_o \langle R_o \rangle^2} \times 10^6$	$\frac{\sigma_\pi^2}{n_\pi \langle R_{1\pi}\, p_\pi^{-q} \rangle^2} \times 10^6$	$p_\pi \times 10^{-5}$	$2\delta \times 10^2$	$\frac{\sigma_{p_\pi}^2}{\langle p_\pi \rangle^2} \times 10^5$	$G^2 \times 10^6$	$H^2 \times 10^7$	$J^2 \times 10^7$	Statistical P.E. in p_o
28848	48.67	21.42	12.693	6.34	3.14	70.09	9.04	1.89	$\pm 0.0164 \times 10^5$
28849	68.63	19.45	12.758	5.34	4.90	88.28	6.41	1.89	± 0.0183
28853	63.31	26.64	12.837	4.14	8.84	89.95	3.87	1.89	± 0.0185

Run II - Weighted Mean = 9.929×10^5 gauss-mm.

P.E. Internal Consistency = $\pm 0.010 \times 10^5$ gauss-mm. P.E. External Consistency = $\pm 0.007 \times 10^5$

or $\langle p_o \rangle_{II} = 29.77 \pm 0.05$ Mev/c (adding errors due to uncertainties in absolute value of magnetic field and in value of mass ratio, a).

$$G^2 = \frac{\sigma_{R_o}^2}{n_o \langle R_o \rangle^2} + \frac{\sigma_\pi^2}{n_\pi \langle R_{1\pi}\, p_\pi^{-q} \rangle^2} \; ; \; H^2 = \frac{\sigma_q^2}{4} \left(\frac{\sigma_{p_\pi}^2}{\langle p_\pi \rangle^2} + 2\delta \right)^2 \; ; \; J^2 = \frac{\sigma_s^2}{s^2} \left(\langle \sin^2 \gamma_{1\pi} \rangle - \langle \sin^2 \gamma_{1_o} \rangle \right)^2$$

UCRL-2522

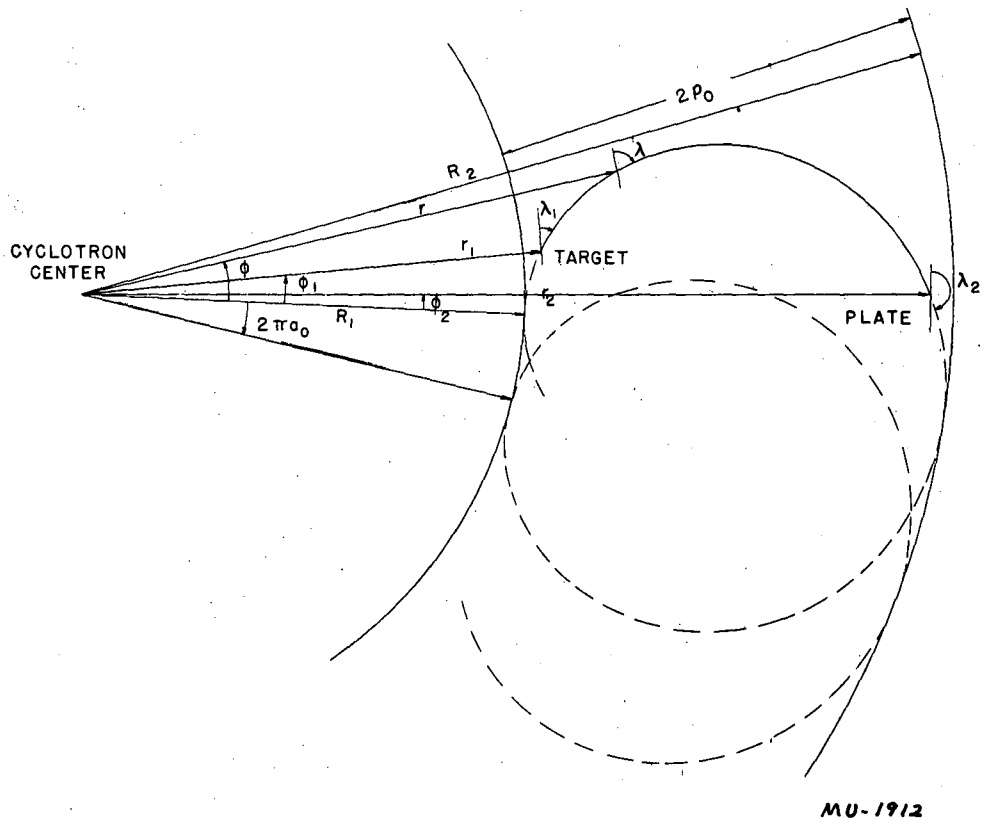

Fig. 1. Diagram illustrating the trochoidal type of orbit in the median plane followed by a charged particle in the radially decreasing magnetic field of the cyclotron.

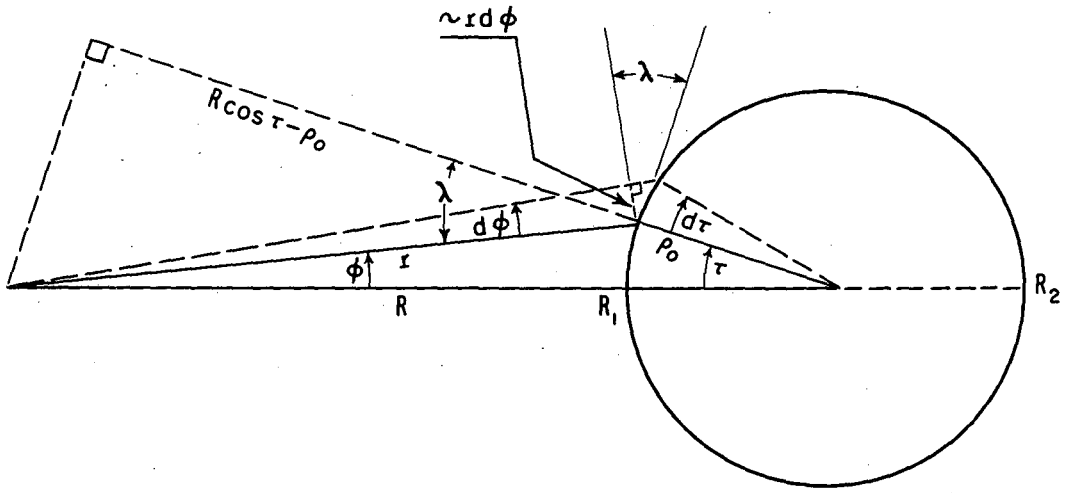

$$\rho_o = \frac{R_2 - R_1}{2} \qquad R = \frac{R_1 + R_2}{2}$$

$$r\,d\phi \approx \rho_o\,d\tau\,\cos\lambda$$

$$\cos\lambda = \frac{R\cos\tau - \rho_o}{r}$$

$$r\,d\phi \approx \frac{\rho_o}{r}(\cos\tau - \rho_o)\,d\tau$$

MU-7208

Fig. 2. Circular approximation to orbit in median plane followed by a charged particle. This figure gives an approximate geometrical relation necessary in the calculation of the momentum of the particle. (See Appendix A)

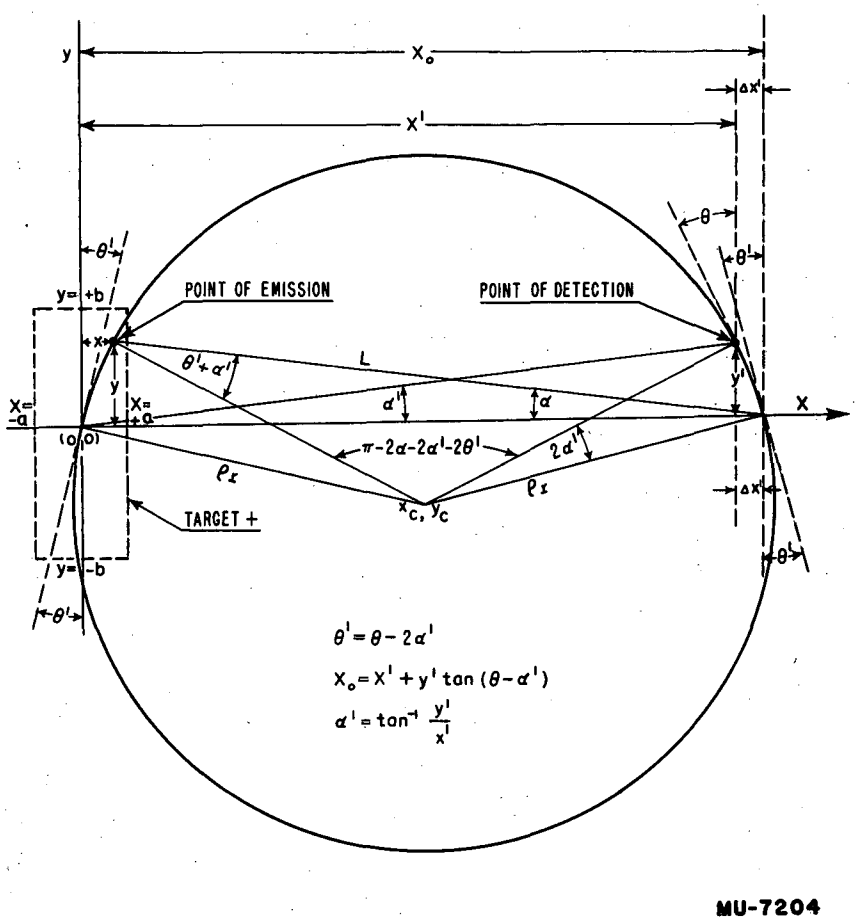

Fig. 3. Circular approximation to trajectory of meson leaving target at point (x, y) and entering detector at point (x', y'). This diagram shows all the pertinent geometrical parameters and relations required for the corrections to the momentum calculation owing to the finite size of the target and the finite area of the detector.

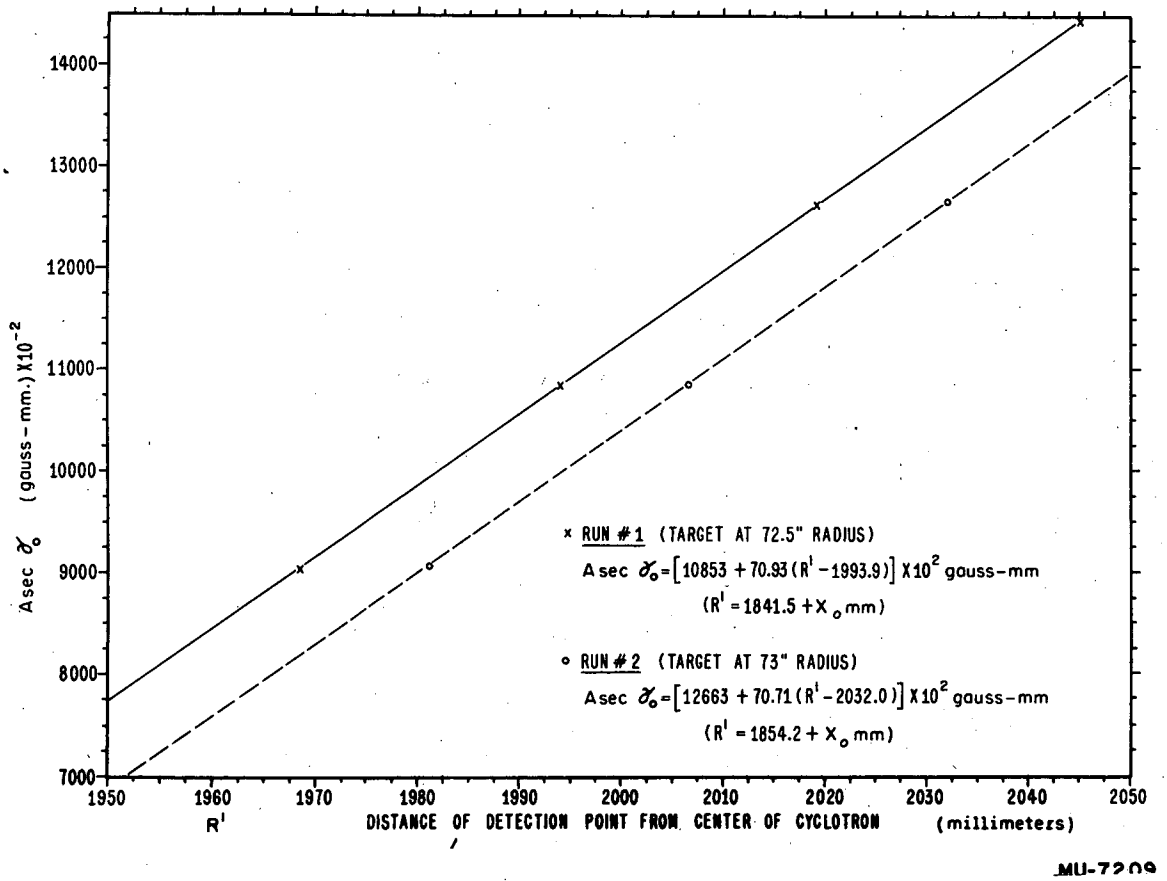

Fig. 4 Plot of the quantity $\dfrac{\sec \gamma_o \int_{r_1}^{r_1 + x_o} rH\, dr}{2 r_1 + x_o}$ vs.

dectector distance from center of cyclotron. (See Eq. 3.14.) Straight lines are fitted through the experimental points, simplifying the momentum calculations. $\left(R' \equiv r_1 + x_o.\right)$

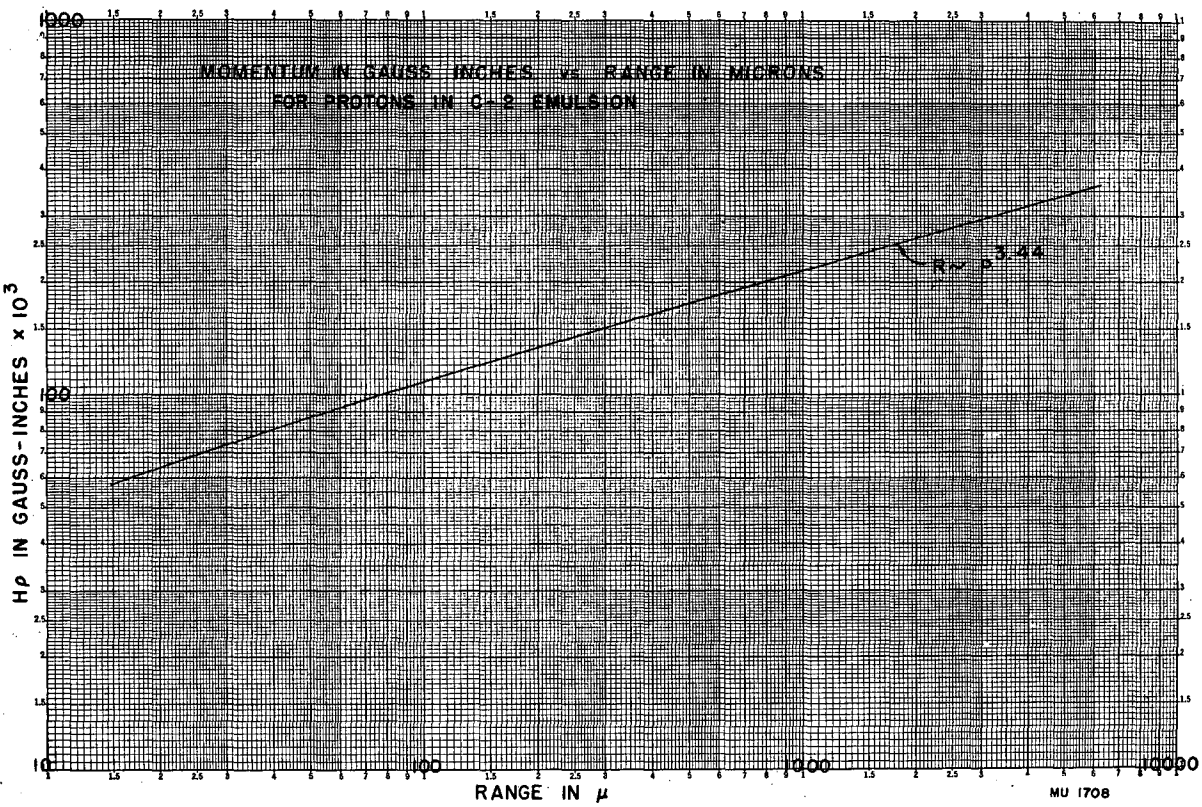

Fig. 5 The curve of log momentum vs. log range for protons in emulsion. Note how straight the line is for ranges above 1000 microns.

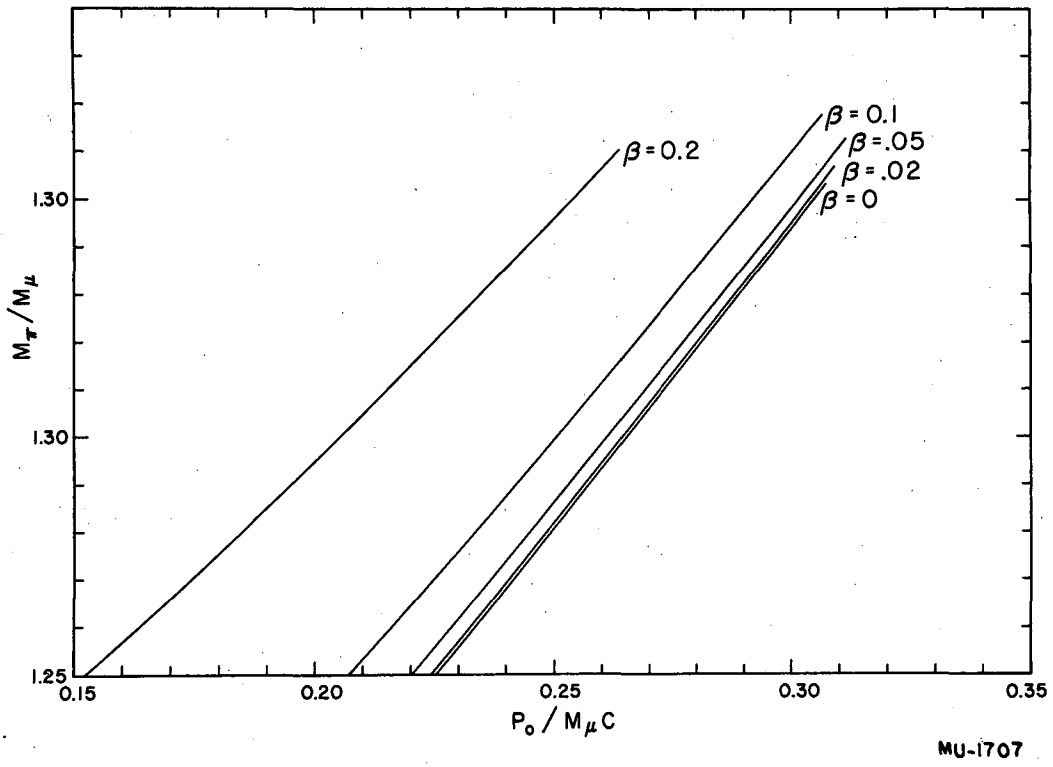

Fig. 6 The relation between the π- and μ-masses for various values of the neutral-particle mass ν as a function of the absolute decay momentum of the μ-meson. This family of curves shows the extreme sensitivity of the derived neutrino mass to slight variations of the π/μ mass ratio and the quantity $p_o/m_\mu c$.

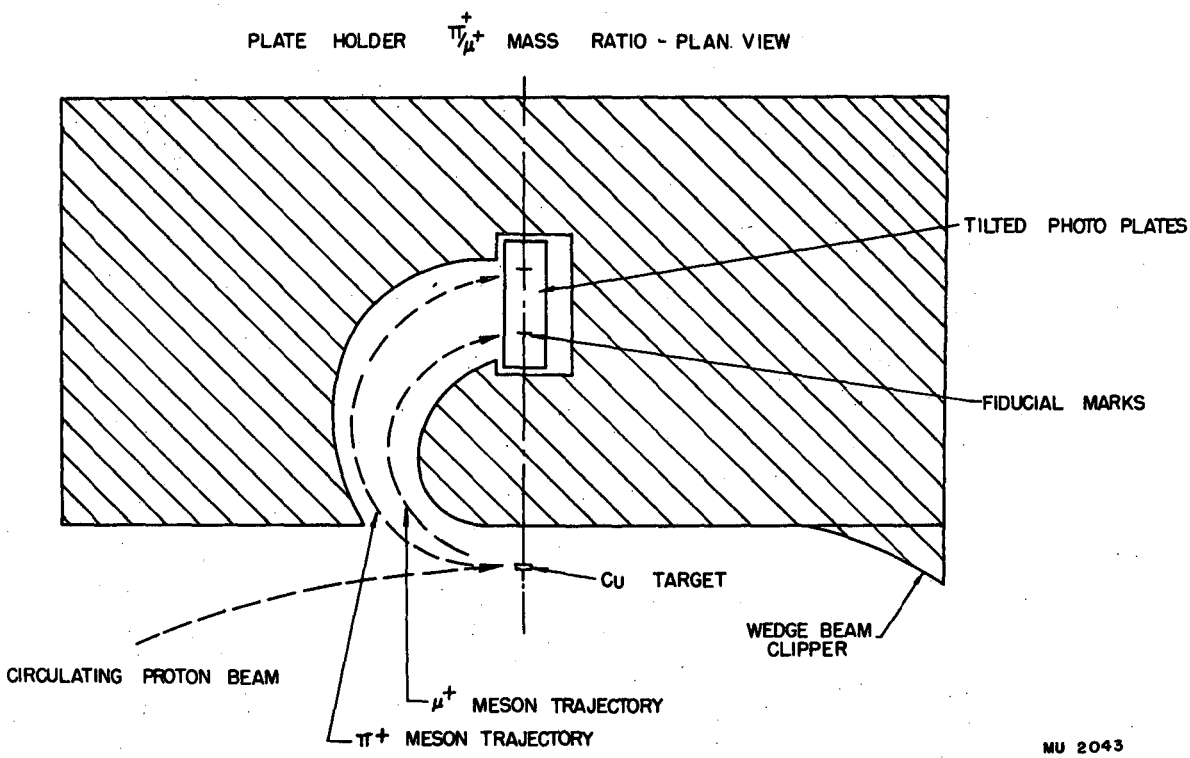

Fig. 7 Plan view of the experimental arrangement (Run I) inside the vacuum tank of the cyclotron. Typical pion and muon orbits are shown leaving the target and entering the emulsion detector.

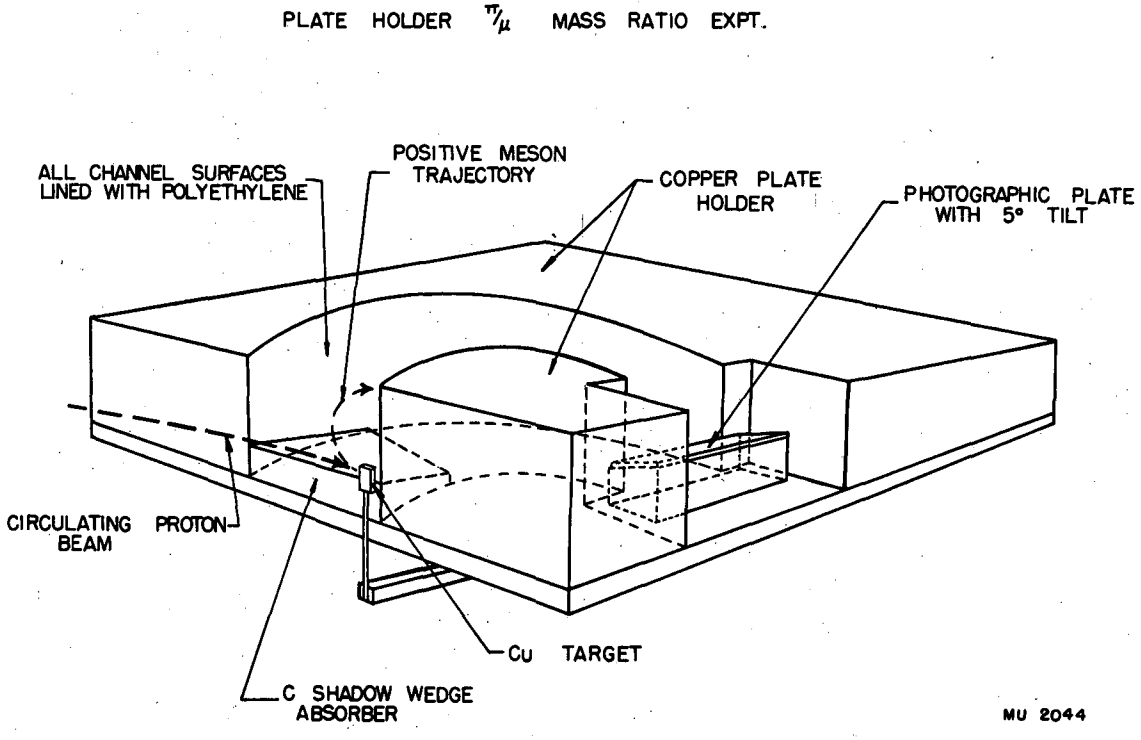

Fig. 8 Perspective view of the experimental apparatus of Run I; the target and detector assembly are rigidly mounted on a dural plate which is fixed in position on the proton probe cart.

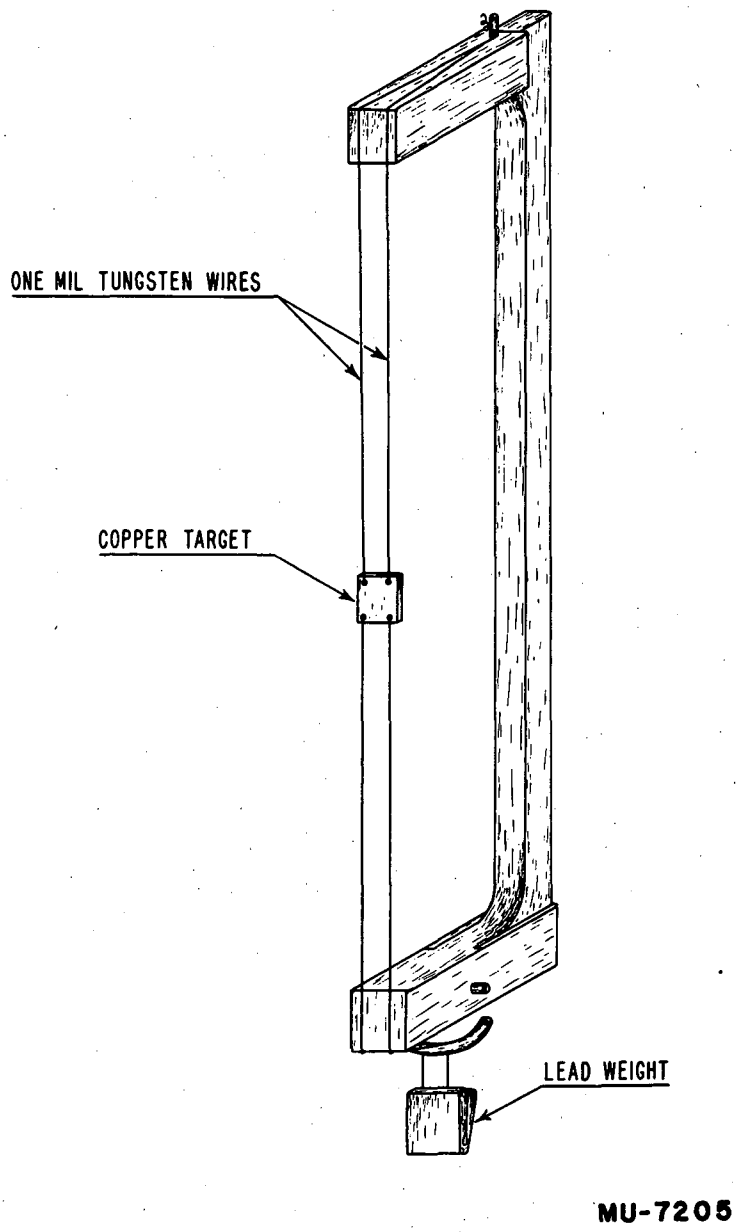

Fig. 9 Full-scale drawing of improved target holder of Run II. Background contamination at detector is reduced to zero.

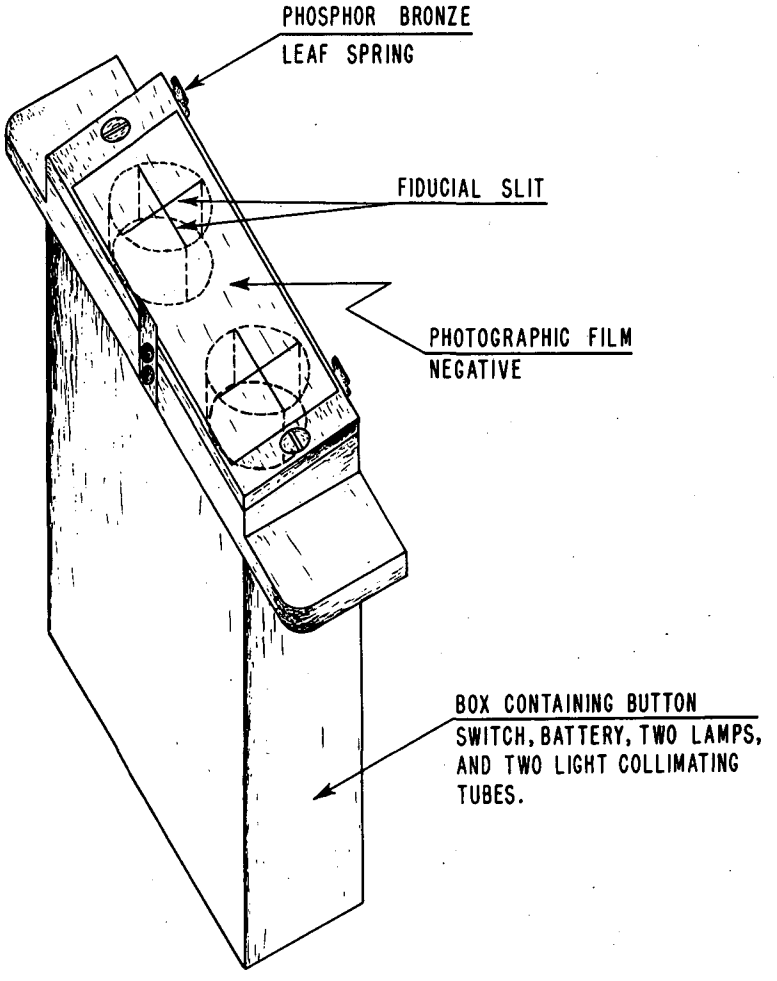

Fig. 10. Isometric full-scale sketch of plate holder. Fiducial slits were obtained by photographing a drawing of two sets of mutually perpendicular lines. The negative of this photograph is glass-backed and is cemented to the inclined brass surface. The nuclear emulsion detector is fixed in place on top of the film negative with the aid of the phosphor bronze leaf springs. A latent image of the fiducial lines is formed in the emulsion just prior to exposure within the cyclotron.

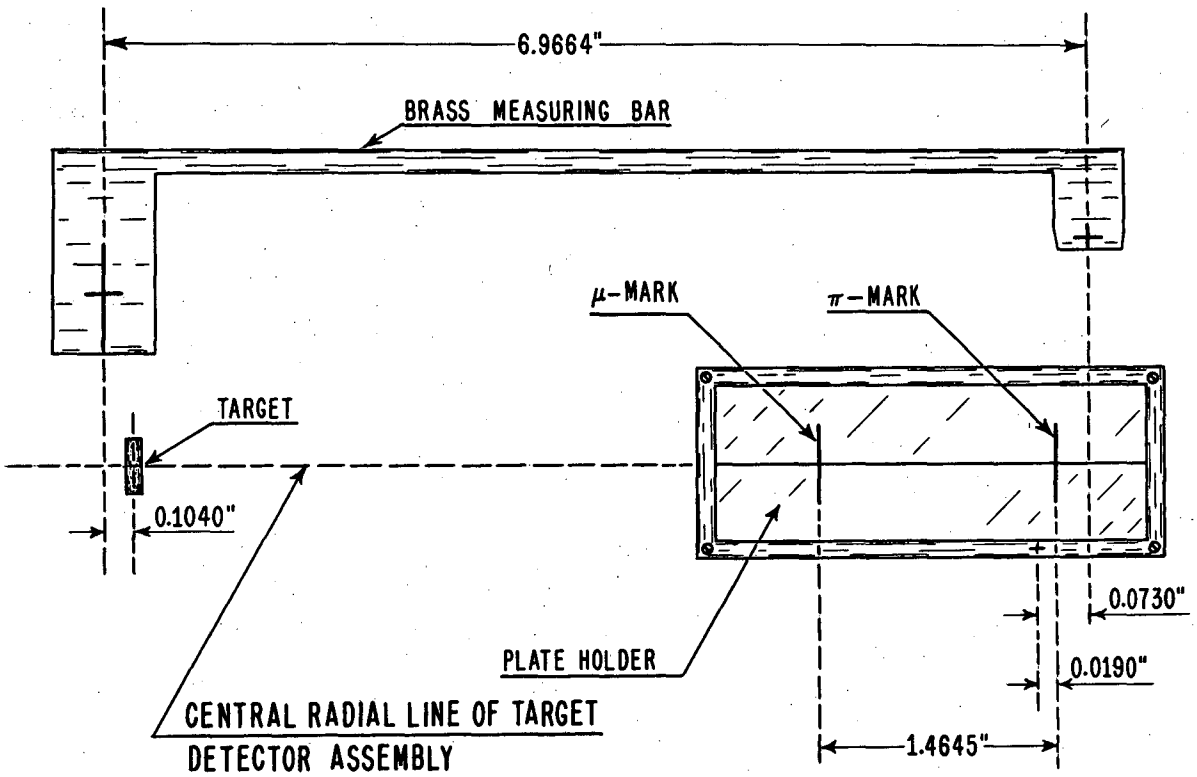

Fig. 11 Linear measurements of target-detector assembly taken during Run I. The measurements were obtained with the aid of a low-power microscope attached to a micrometer traveling in a direction parallel to that of the median line.

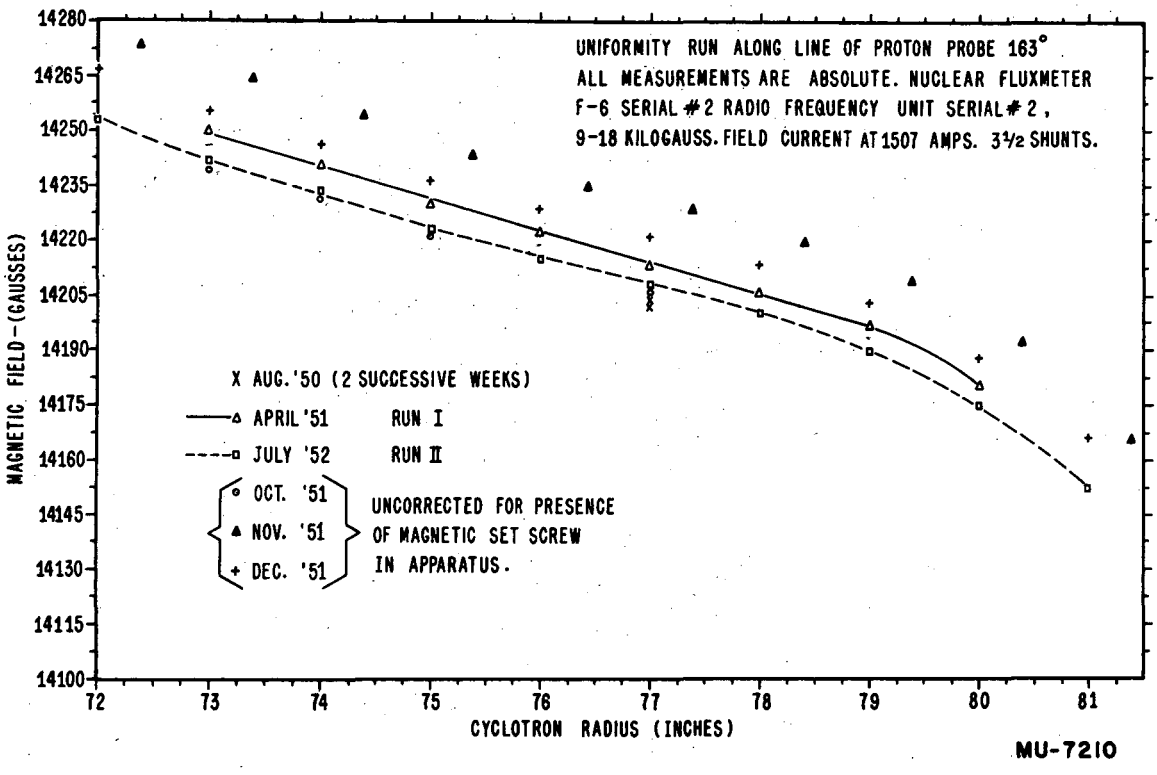

Fig. 12 Absolute measurements of the cyclotron magnetic field taken with the nuclear fluxmeter. Note the change in slope in the neighborhood of 80 inches.

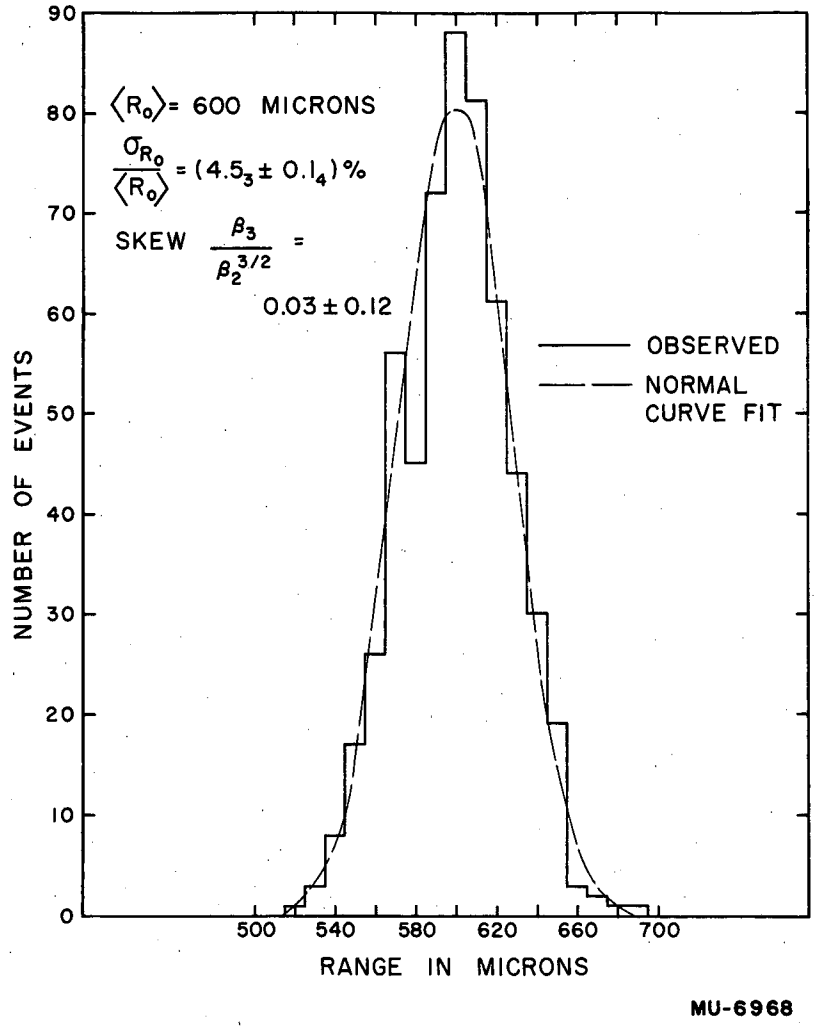

Fig. 13 Distribution of ranges of mu-completes: 558 events are taken from 12 plates and normalized to a mean range of 600 microns. A normal curve fit to the experimental data gives a χ^2-test significance level of ≈ 0.4.

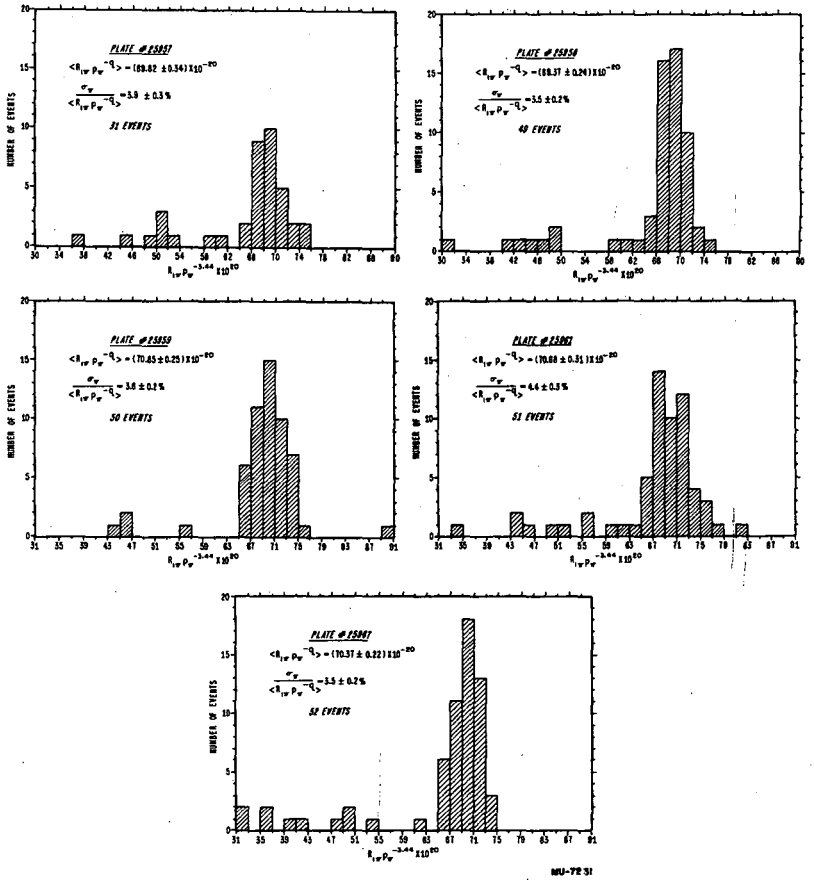

Fig. 14 Pion normalized-range distributions from the 5 plates of Run I. Note the small amount of background. Percentage variance slightly but not significantly lower than predicted value ($R_{l\pi}$ in units of microns, and p_π in gauss-mm.)

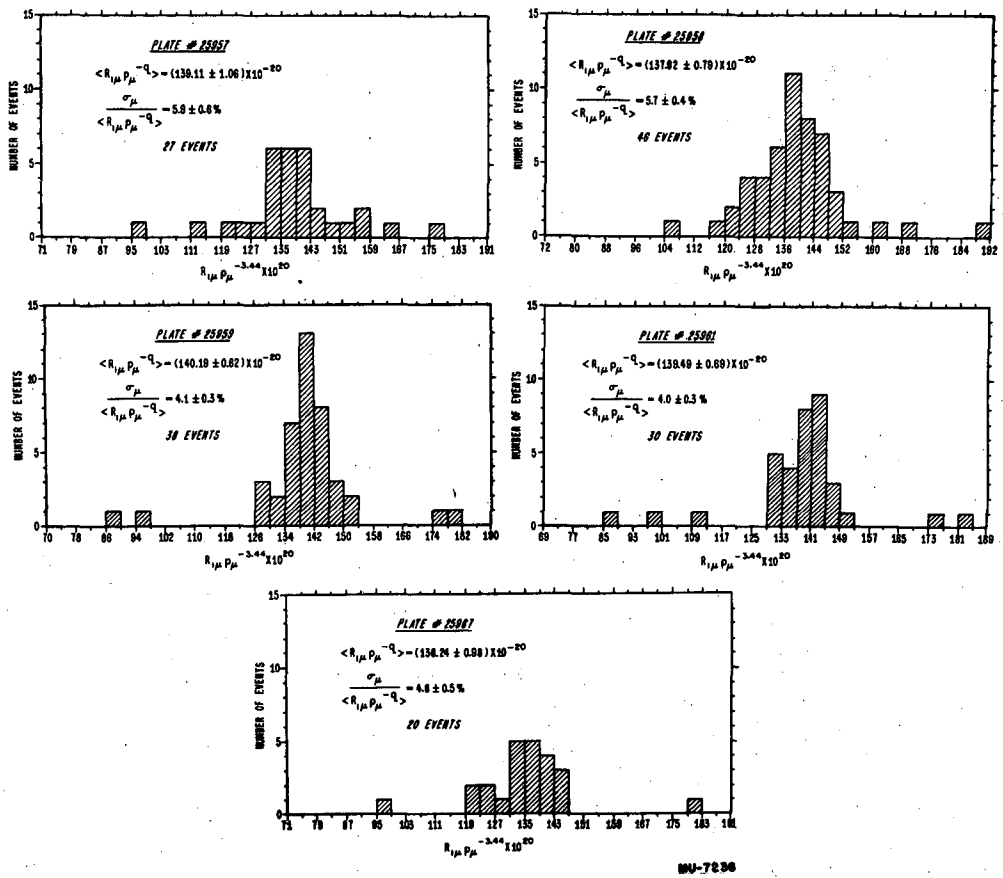

Fig. 15 Muon normalized-range distributions from 5 plates of Run I, showing some contamination. Average percentage variance just slightly higher than predicted value. ($R_{1\mu}$ in microns, p in gauss-mm.)

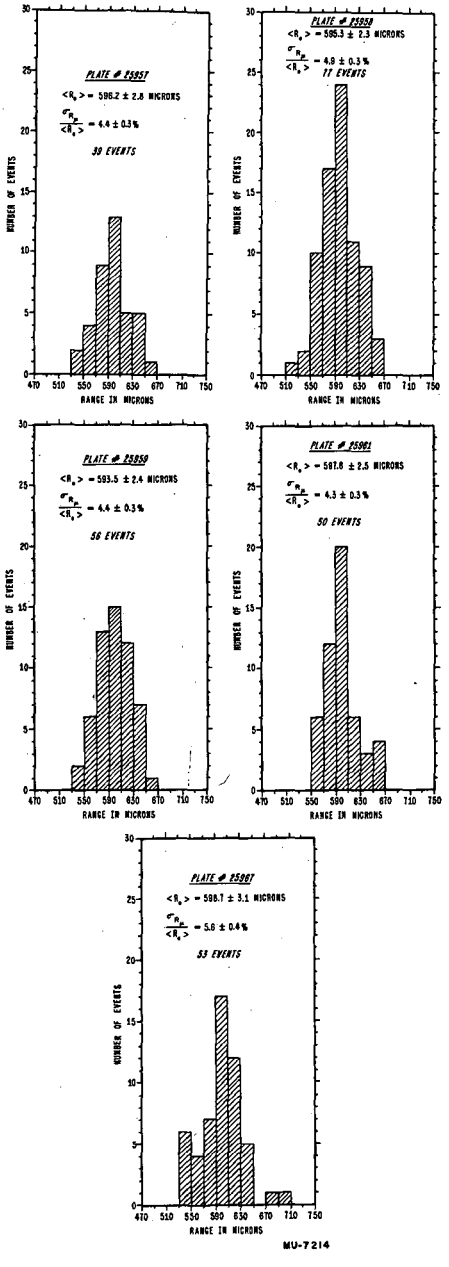

Fig. 16 Range distributions of mu-completes from five different plates - Run I.

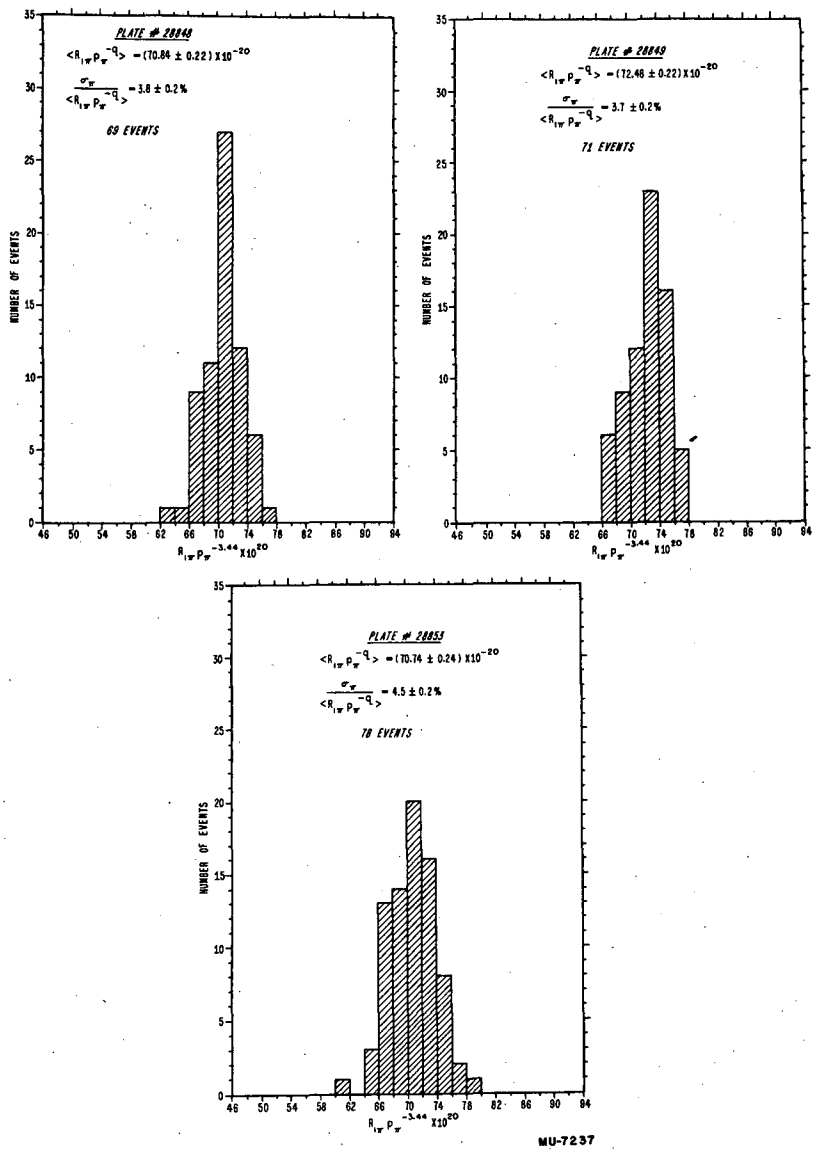

Fig. 17 Pion normalized-range distributions from the 3 plates of Run II. Note the complete absence of any apparent background. Average percentage variance in agreement with prediction. ($R_{1\pi}$ in microns, p in gauss-mm.)

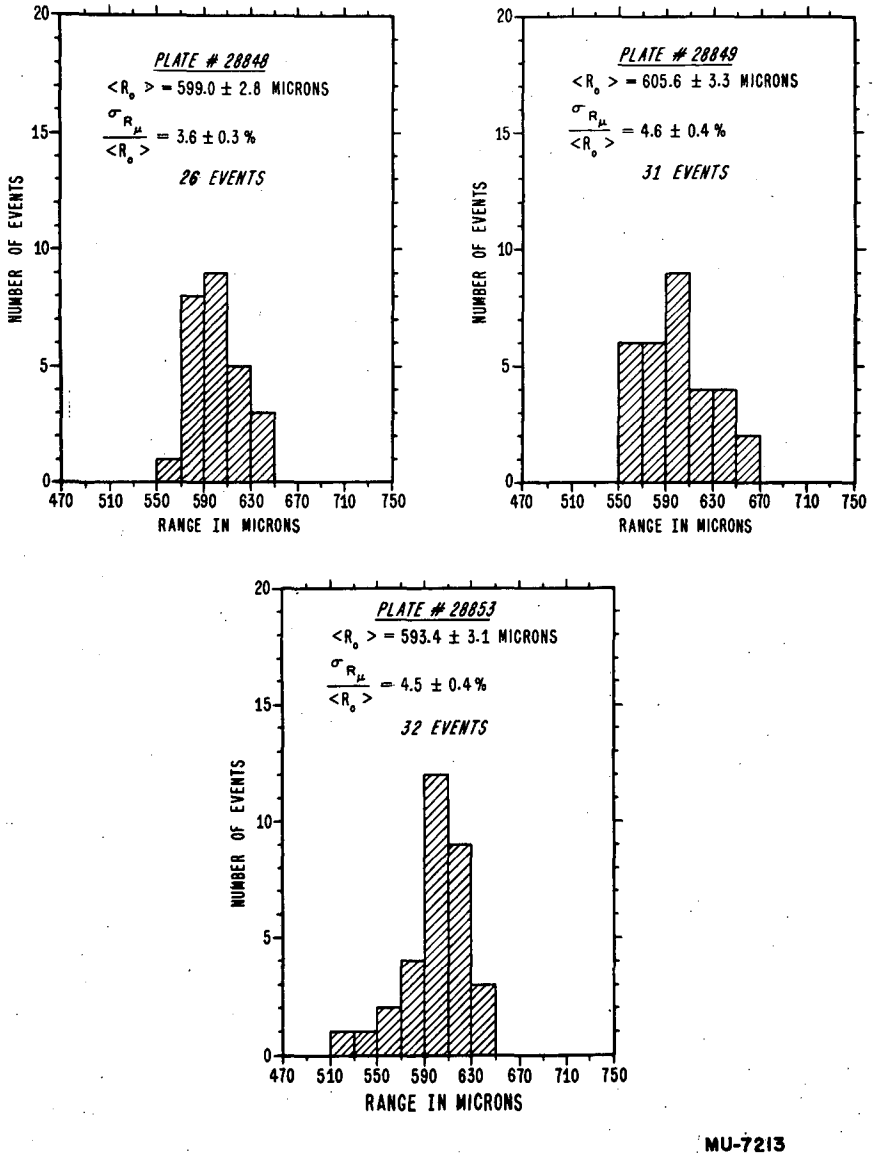

Fig. 18 Range distributions of mu-completes from the 3 plates of Run II.

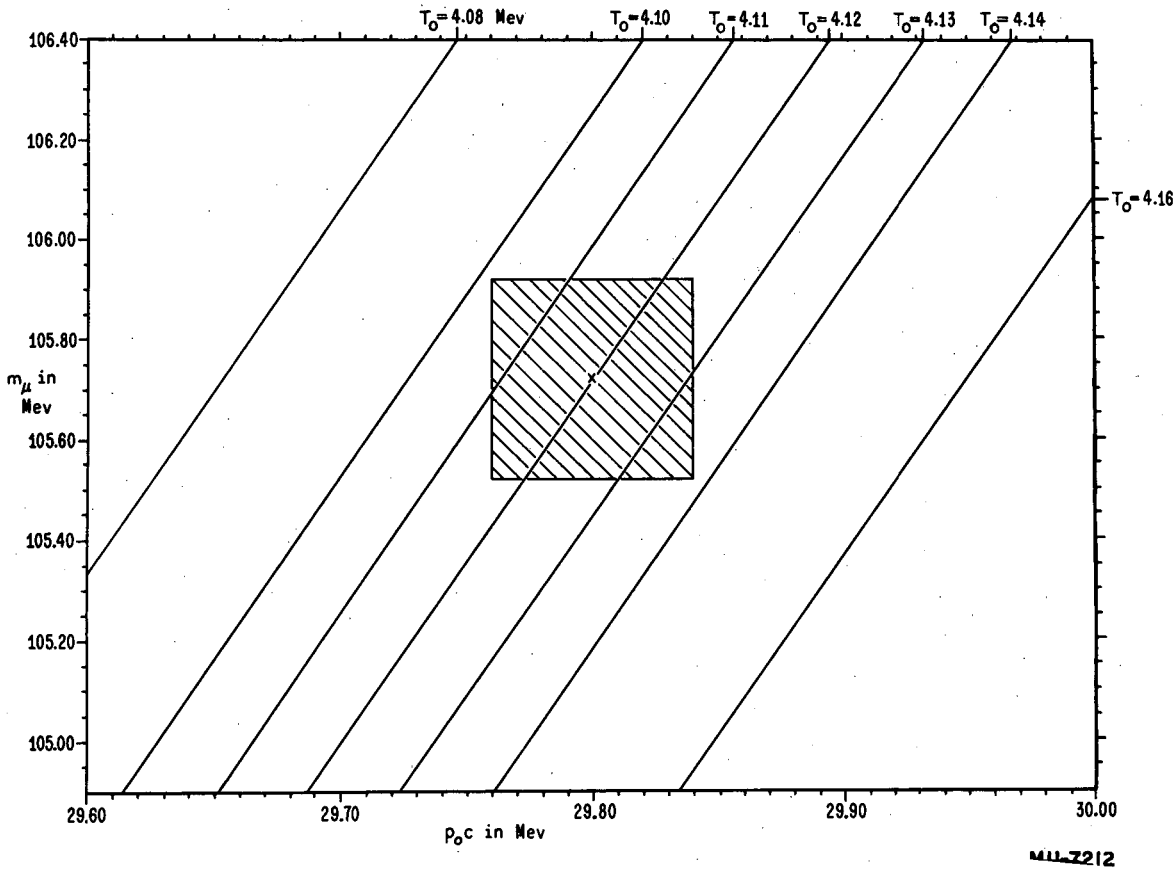

Fig. 19 Graphical solution to value of the absolute decay kinetic energy of the muon from the relativistic relation,

$$T_o = \sqrt{p_o^2 c^2 + m_\mu^2 c^4} - m_\mu c^2 \quad .$$

The hatched region represents the area subtended by the statistical probable errors in m_μ and p_o. The family of curves indicates a value of $T_o = 4.12 \pm 0.02$ Mev.

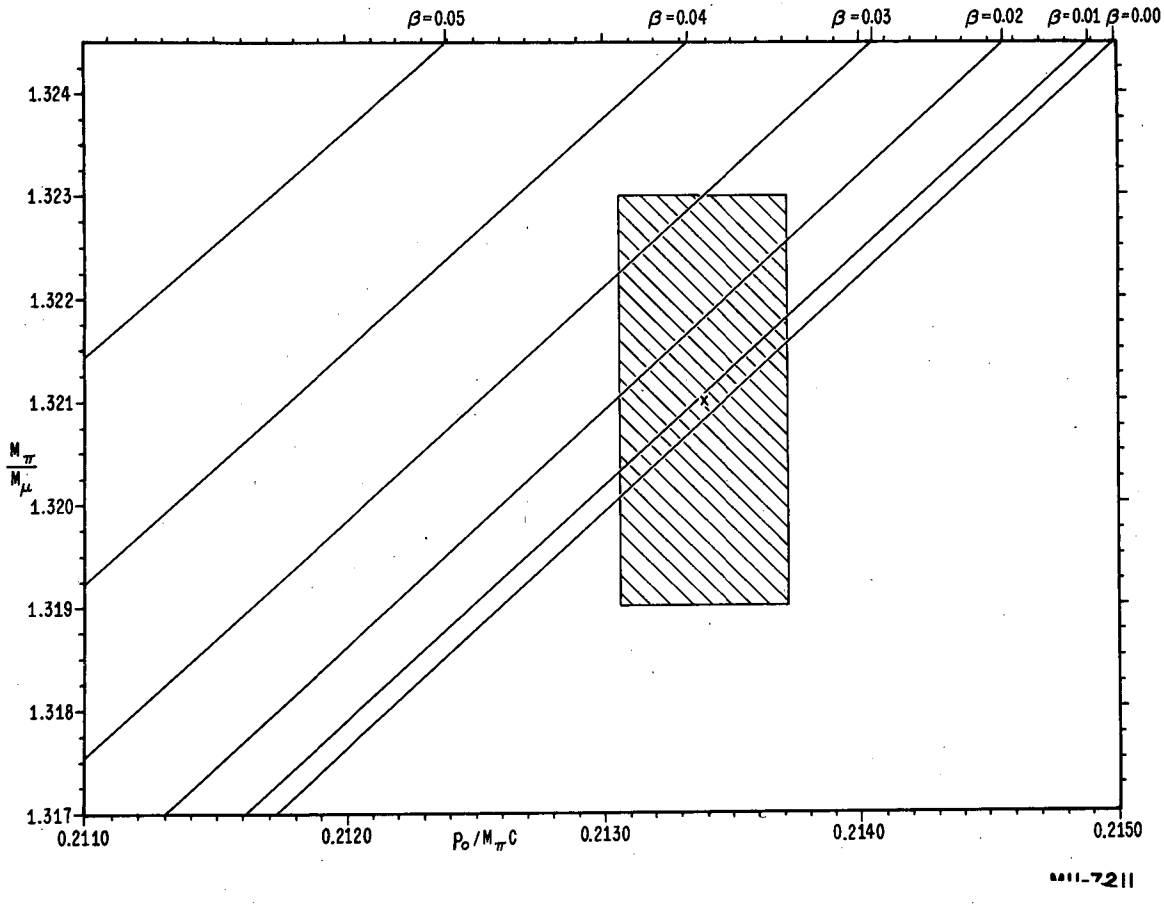

Fig. 20 Graphical solution to estimate of neutrino mass from Eq. 6.3. This essentially is an enlarged plot of Fig. 6. The hatched region represents the area subtended by the probable errors in the π/μ mass ratio and the quantity $p_o/m_\pi c$.
A probable upper limit of 6 to 7 m_o is indicated.
$(\beta = {}^{m_\nu}/_{m_\mu})$

REFERENCES

1. H. Yukawa, Proc. Phys.-Math. Soc., Japan 17, 48 (1935).
2. S. H. Neddermeyer and C. D. Anderson, Phys. Rev. 51, 884 (1937).
3. J. C. Street and E. C. Stevenson, Phys. Rev. 52, 1003 (1937).
4. D. R. Corson and R. B. Brode, Phys. Rev. 53, 215, 773 (1938).
5. R. E. Peierls, Reports on Progress of Physics, The Physical Society, (London) Vol. VI, 78 (1939).
6. J. A. Wheeler and R. Ladenburg, Phys. Rev. 60, 754 (1941).
7. W. B. Fretter, Phys. Rev. 70, 625 (1946).
8. R. B. Brode, Rev. Mod. Phys. 21, 37 (1949).
9. R. B. Brode, Phys. Rev. 75, 904 (1949).
10. J. G. Retallack and R. B. Brode, Phys. Rev. 75, 1716 (1949).
11. T. C. Merkle, E. L. Goldwasser, and R. B. Brode, Phys. Rev. 79, 926 (1950).
12. M. Conversi, E. Pancini, and O. Piccioni, Phys. Rev. 71, 209, (1947).
13. S. Sakata and T. Inoue, Prog. Theor. Phys. 1, 143 (1946).
14. Y. Tanakawa, Prog. Theor. Phys. 2, 220 (1947).
15. R. E. Marshak and H. A. Bethe, Phys. Rev. 72, 506, 1947).
16. C. M. G. Lattes, G. P. S. Occialini, and C. F. Powell, Nature 160, 453, 486 (1947).
17. C. M. G. Lattes, G. P. S. Occhialini, and C. F. Powell, Proc. Phys. Soc. London 61, 173 (1948).
18. C. F. Powell, Reports on Progress of Physics, The Physical Society, (London) Vol. XIII, 350 (1950), gives a brief summary of the various methods employed in direct measurements of the meson masses.
19. E. Gardner and C. M. G. Lattes, Science 107, 270, (1948).
20. A. S. Bishop, Phys. Rev. 75, 1468 (1949).
21. F. M. Smith, W. H. Barkas, A. S. Bishop, H. Bradner, and E. Gardner, Phys. Rev. 78, 86(A) (1950).
22. H. Bradner, Review of Work on Artificially Produced Mesons, UCRL-486 (1949).
23. L. Lederman, J. Tinlot, and E. T. Booth, Phys. Rev. 81, 281 (1951).
24. W. K. H. Panofsky, R. L. Aamodt, and J. Hadley, Phys. Rev. 81, 565 (1951).

25. K. M. Crowe, Precision Measurement of the Negative Pion Mass from its Radiative Absorption in Hydrogen, UCRL-2050 (1952). Also contains a summary of several theories of meson masses.
26. A. G. Carlson, J. E. Hooper, and D. T. King, Phil. Mag. 40, 1250 (1949).
27. R. B. Leighton, C. D. Anderson, and A. J. Seriff, Phys. Rev. 75, 1432 (1949).
28. A. Lagarrigue and C. Peyron, Comptes Rendus 233, 478 (1951).
29. J. H. Davies, W. O. Lock and H. Muirhead, Phil. Mag. 40, 1250 (1949).
30. H. J. Bramson, A. M. Seifert, and W. W. Havens, Jr., Phys. Rev. 88, 304 (1952).
31. R. Sagane, W. L. Gardner, and H. W. Hubbard, Phys. Rev. 82, 557 (1951).
32. H. W. Hubbard, Thesis, University of California (1952).
33. W. F. Cartwright, Phys. Rev. 82, 460 (1951).
34. V. Z. Peterson, E. Iloff, and D. Sherman, Phys. Rev. 81, 647 (1951).
35. J. Rainwater, Phys. Rev. 90, 349 (1953).
36. W. H. Barkas, Amer. Jour. of Phys. 20, 5 (1952).
37. P. E. Hodgson, Phil. Mag. 41, 725 (1950).
38. J. K. Bowker, J. R. Green, and W. H. Barkas, Phys. Rev. 81, 649 (1951).
39. W. H. Barkas, Proceedings of the Echo Lake Cosmic Ray Symposium, June 23, 1949.
40. W. H. Barkas, F. M. Smith, and E. Gardner, Phys. Rev. 82, 102 (1951).
41. F. S. Smith, W. Birnbaum, and W. H. Barkas, Phys. Rev. 91, 765 (1953).
42. F. M. Smith, Meson Mass Measurements II - On the Measurement of the Masses of the Charged Pions, UCRL-2371 (1954).
43. W. H. Barkas, Meson Mass Measurements I - Theory of the Mass Ratio Method, UCRL-2327 (1953).
44. C. O. O'Ceallaigh, Phil. Mag. 41, 838 (1950).
45. M. S. Livingston and H. H. Bethe, Rev. Mod. Phys. 9, 263 (1937).

46. W. E. Hazen, Phys. Rev. 67, 269 (1945).
47. R. H. Frost, Thesis, Univ. of Calif. (1947).
48. H. Bradner, F. M. Smith, W. H. Barkas, and A. S. Bishop, Phys. Rev. 77, 462 (1950).
49. E. Gardner, Private Communcation.
50. W. H. Barkas, Phys. Rev. 78, 90 (1950).
51. J. Thibaud, Phys. Rev. 45, 781 (1934).
52. W. Heitler, Quantum Theory of Radiation, p. 172, Oxford Press, 1944.
53. E. Fermi, Nuclear Physics, p. 36, Univ. of Chicago Press, Chicago, 1950.
54. M. J. Berger, Phys. Rev. 88, 59 (1952).
55. C. J. Bakker and E. Segrè, Phys. Rev. 81, 489 (1951).
56. L. Vigneron, Journ. de Physique 14, 145 (1953).
57. N. Bohr, Phil. Mag. 30, 581 (1915).
58. H. Cramer, Mathematical Methods of Statistics, Princeton University Press, Princeton, 1946.
59. H. W. Lewis, Phys. Rev. 85, 20 (1952).
60. J. Lindhard and M. Scharff, Dan. Mat. Phys. Medd. 27, No. 15 (1953).
61. L. Winand, Photographic Sensitivity, p. 288, Butterworths, London, 1951.
62. A. J. Oliver, Measurements of the Effects of Moisture in Nuclear Track Emulsion, UCRL-2176 (1953).
63. F. Bloch and A. Nordsieck, Phys. Rev. 52, 54 (1937).
64. H. Primakoff, Phys. Rev. 84, 1255 (1951).
65. Nakano, Nichimura, and Yamaguchi, Prog. Theor. Phys. 6, 1028 (1951).
66. T. Eguchi, Phys. Rev. 85, 943 (1952).
67. W. F. Fry, Phys. Rev. 91, 130 (1952).
68. G. C. Hanna and B. Pontecorvo, Phys. Rev. 75, 983 (1949).
69. S. C. Curran, J. Angus, and A. L. Cockeroff, Nature, 162, 302 (1948).
70. J. K. Bowker, Private Communication.
71. F. Bloch, W. W. Hansen, and M. Packard, Phys. Rev. 70, 474 (1946).
72. F. M. Smith, Private Communication.
73. A. M. Seifert, Private Communication to W. H. Barkas.
74. W. F. Fry and G. R. White, Phys. Rev. 90, 207 (1953).

75. P. G. Hoel, Introduction to Mathematical Statistics, p. 186, Wiley, New York, 1947.
76. R. T. Birge, Phys. Rev. 40, 207 (1932).
77. W. M. DuMond and E. R. Cohen, Rev. Mod. Phys. 25, 691 (1953).
78. C. E. Nielsen and W. M. Powell, Phys. Rev. 63, 384 (1943).
79. D. J. Hughes, Phys. Rev. 69, 371 (1946).
80. Goldschmidt-Clermont, King, Muirhead and Ritson, Proc. Roy. Soc. 61, 183 (1948).
81. S. Lattimore, Nature, 161, 518 (1948).
82. R. Brown, U. Camerini, P. H. Fowler, H. Muirhead, C. F. Powell and D. M. Ritson, Nature, 163, 82 (1949).
83. I. Barbour, Phys. Rev. 78, 518 (1950).
84. C. Franzinetti, Phil. Mag. 41, 86 (1950).
85. U. Camerini, P. H. Fowler, W. O. Lock, and H. Muirhead, Phil.Mag. 41, 413 (1950).
86. G. M. Nonnemaker and J. C. Street, Phys. Rev. 82, 564 (1951).
87. G. Ascoli, Phys. Rev. 90, 1079 (1953).
88. W. H. Barkas, E. Gardner and C. M. G. Lattes, Phys. Rev. 74, 1558A (1948).
89. L. Van Rossum, Comptes Rendus 228, 676 (1949).
90. J. K. Bowker, Phys. Rev. 78, 87A (1950).
91. W. Birnbaum, F. M. Smith, and W. H. Barkas, Phys. Rev. 83, 895A (1951).
92. W. M. Powell, Private Communication.
93. K. M. Crowe and W. K. H. Panofsky, Private Communication.
94. W. Chinowsky, A. Sachs, and J. Steinberger, Bull. Amer. Phys. Soc. 28, No. 6, 13 (1953).
95. E. Fermi - Private Communication to W. H. Barkas.